

Chasing Shadows: Identifying Undiscovered Exoplanets in Kepler's Historical Data

Author:

Stuart Smith

Supervisor:

Dr Andrew Rushby

April 2024



School of Natural Sciences

Birkbeck College, University of London

United Kingdom

2024

Declaration

The author attests that the content presented in this dissertation is original, and has not been previously submitted for a degree at this university or any other. Any contributions from external sources are duly acknowledged through proper referencing.

Author:

Stuart Smith

A handwritten signature in black ink, appearing to read "Stuart Smith".

Date:

Monday 22nd April 2024

School:

Birkbeck College, University of London

Acknowledgments

This dissertation could not have been completed without the guidance, support, knowledge and inspiration of Dr Andrew Rushby, to whom I am eternally grateful.

To Elijah, for encouraging me to leave the harbour.

"A ship in harbour is safe, but that is not what ships are built for" - John A Shedd

"Patterns make things easy" - Clews

Table of Contents

1. Introduction.....	1
1.1. Exoplanets.....	1
1.1.1. Current Exoplanet Catalogue.....	1
1.1.2. Detection Methods.....	2
1.1.2.1. Transit Detection.....	2
1.1.2.2. Radial Velocity Detection.....	6
1.1.2.2. Direct Imaging of Planetary Systems.....	7
1.1.2.4. Gravitational Microlensing.....	9
1.1.2.5. Astrometry.....	11
2. Wider Mission Context.....	11
3. Kepler/K2 Mission Context.....	13
4. Project Aims.....	16
5. Software Requirements.....	16
6. Data Validation: Confirmation of Known Exoplanets.....	18
7. Selection of Main Data Set.....	27
7.1. Selection of Data Subsample.....	28
8. Data Interrogation of Subsample A.....	34
8.1. Data Interrogation of Subsample B.....	37
9. Presentation of New Binary Star System.....	40
10. Presentation of New Exoplanet Candidates.....	48
11. Calculations of Stellar and Planetary Characteristics.....	55
12. Conclusion and Future Research Avenues.....	58
Research Acknowledgments.....	60
Bibliography.....	61

List of Tables and Figures

Chapter 1

Figure 1.1: A simplified diagram showing the mechanism of exoplanet transits.

Figure 1.2: The light curve generated by a Jupiter sized candidate around KIC 10723750.

Figure 1.3: A composite image of a gas giant companion orbiting 2M1207.

Figure 1.4: The first pictures release of an exoplanet imaged directly by the JWST.

Figure 1.5: A secondary spike caused by an exoplanet during a microlensing event.

Chapter 2

Table 1: An overview of space based exoplanet missions.

Chapter 3

Figure 3.1: Exoplanet detections, and their year of discovery.

Figure 3.2: The precision levels of the K2 mission, compared to its original state.

Chapter 6

Figure 6.1: Raw data for Kepler 757450 loaded into LcViewer.

Figure 6.2: Available detrend options for LcViewer.

Figure 6.3: Kepler 757450 data, once detrended

Figure 6.4: Signal finding setup.

Figure 6.5: Repeat Instance detection menu.

Figure 6.6: Phase fold setup.

Figure 6.7: Phase fold complete, instance generated, and candidate curve highlighted.

Chapter 7.1

Figure 7.1.1: The interface of LcSignalFinder, after the data set had been analysed.

Figure 7.1.2: All 25136 signals found, plotted for Object Size (R_{Earth}) vs Instances.

Figure 7.1.3: Filters available for data files from initial analysis.

Chapter 8

Figure 8.1: Data files from Subsample A plotted for Object Size (R_{Earth}) vs Signal Duration.

Figure 8.2: False positive event highlighted by software.

List of Figures Continued

Chapter 8

Figure 8.1.1: Data files from Subsample B plotted for Object Size (R_{Earth}) vs Signal Duration.

Figure 8.1.2: Unusual flux increases in the light curve of Star 2085565548335557504

Chapter 9

Figure 9.1: Map denoting the position of Star 2082110397465409792

Figure 9.2: The position of Star 2082110397465409792 in the Cygnus constellation

Figure 9.3: J/H/K and 3-Colour band imagery of 2MASS 20042333+4445313.

Figure 9.4: Detrended light curve of 2MASS 20042333+4445313.

Figure 9.5: Signal search in the light curve of 2MASS 20042333+4445313.

Figure 9.6: Stellar properties of 2MASS 20042333+4445313

Figure 9.7: Phase fold curve of Transit Event A

Figure 9.8: Phase fold curve of Transit Event B

Chapter 10

Figure 10.1: Map denoting the position of Star 2077415590199401728.

Figure 10.2: J/H/K and 3-Colour band imagery of Star 2077415590199401728.

Figure 10.3: Gaia imagery of Star 2077415590199401728 at a FOV of 28" x 23"

Figure 10.4: Gaia data for 2MASS 19345313+4129556.

Figure 10.5: Gaia data for Star 2077415590199401728.

Figure 10.6: Exoplanet transits in the light curve of Star 2077415590199401728.

Figure 10.7: Flux increase in the light curve of Star 2077415590199401728.

Figure 10.8: Secondary flux increase in the light curve of Star 2077415590199401728.

Figure 10.9: Forward scattering of light due to dust, in a light curve.

Figure 10.10: Flux increase in the light curve of KIC 11397541.

Abstract

The Kepler Space Telescope achieved remarkable success in both its original Kepler, and follow up K2 phases, detecting nearly 3000 exoplanets to date. However, due to the level of success, the vast amount of data generated by the telescope has yet to be fully analysed, and thus, this paper sets out to analyse available data sets in order to help add to the completeness of current archives, particularly those pertaining to exoplanets. This data set is refined through explicit criteria, to allow for the search of short-period exoplanets between $1 R_{\text{Earth}}$ and $2 R_{\text{Earth}}$ in size, in an effort to fill gaps in the current radius valley. This is an area between $1.5 R_{\text{Earth}}$ and $2 R_{\text{Earth}}$ where relatively few exoplanets are found due to an unknown physical constraint. KST mission specific context, and wider mission context is provided, as well as the reasoning behind the choices to analyse this specific data set. Exoplanet detection techniques are reviewed with Radial Velocity, Direct Imaging, Gravitational Microlensing, and Astrometry all discussed, with additional focus given to Transit Detection, as it was the primary detection method of the KST. This paper also presents the discovery of a new binary star system comprised of at least one M Dwarf star at $0.256 R_{\odot}$, and new exoplanet candidates at $2.267 R_{\text{Earth}}$ and $1.744 R_{\text{Earth}}$, orbiting a star at $0.617 M_{\odot}$. Future research avenues to confirm these discoveries are then outlined.

1. Introduction

Since their discovery in 1992 (*'Historic Timeline | Explore – Exoplanet Exploration: Planets Beyond our Solar System'*, 2024), our perception of exoplanets has continually evolved. This is particularly apparent in the last two decades, which have seen the first of a number of dedicated exoplanet hunting missions being launched. Within this paper, exoplanets and exoplanet missions are defined, plus contextualised within the wider research field, to aid understanding. This paper aims to search historical data releases from the Kepler Space Telescope, primarily to confirm the validity of findings, made by other research groups, but also in an effort to find planetary candidates that may not yet have come to our attention. These aims are explained in further detail in Section 4. Context for these findings in the wider setting is provided, and recommendations for future research laid out.

1.1. Exoplanets

From the Greek “Outside Wanderer”, exoplanets are exactly that; worlds that are detected outside our own Solar System. The term ‘Exoplanet’ is all encompassing. Small, Pluto-like objects will be classified alongside gas giants larger than Jupiter, so long as they meet the most basic of criteria: being outside our Solar System. Whilst planets are traditionally thought to orbit only stars, there is a subcategory of “Rogue Planets” that wander with a galactic, not stellar, orbit, and these too are classified under the umbrella of exoplanets should they be detected.

1.1.1. Current Exoplanet Catalogue

At the time of writing, there are 5612 confirmed exoplanets (*'Exoplanet Exploration: Planets Beyond our Solar System'*, 2024), with 1919 described as ‘Neptune-Like’, 1791 as Gas Giants, 1695 as ‘Super Earths’, 200 as ‘Terrestrial’, and the remaining 7 currently listed as ‘Unknown’. Given that 66% of exoplanets discovered so far are giant, gaseous bodies, a clear trend has been set - large bodies such as these are either easier to detect, or, that they are more prevalent in the universe should these 5612 confirmed exoplanets be representative over a larger scale. The majority of these exoplanets that have been detected however, are all in a very small area of the observable universe, thus what has been

currently observed may not be indicative of the real trend across the whole universe. It could be that the currently observed regions are just naturally prevalent in large, gaseous bodies, due to the availability of materials for the Star systems in their early evolution. An abundance of gas in these early stages allows for greater planetary sizes when considering, in this particular case, the formation of bodies primarily formed of gas.

1.1.2. Detection Methods

There are a variety of ways in which these bodies can be detected, with a range of benefits from each. The utilisation of these methods changes over time, with some becoming more prevalent once our capability to observe the universe with them improves. These methods are discussed further, below.

1.1.2.1. Transit Detection

A transit detection occurs when an exoplanet passes between its host star and the observer (whether that be an Earth based telescope, or one in orbit), and causes a measurable dim in the flux of the star. At the time of writing, 74% of known exoplanets have been observed in this manner. The process is identical to the way in which we can observe the terrestrial planets Mercury and Venus as they pass in front of the sun, and even some large scale scientific platforms such as the International Space Station. Whilst exoplanets are much further away, and their distance measured in Light Years rather than thousands of kilometres, the principal is the same. Should this dimming of the star's flux continue at regular intervals, it can be ascertained that the cause is likely an exoplanet completing its orbit around the observed star. At present, an exoplanet will need to transit across its host star a minimum of three times in order to be noted as a planetary candidate. There are other phenomena that can cause dimming, such as large exozodiacal or interstellar dust clouds, but these tend to have a decreased effect on the reduction in flux, and not have a uniform shape to their light curve. Transits are presented in light curves, with exoplanets typically showing a 'U' shaped dip in the flux levels. A visualisation of this process is seen below in Figure 1.1. The star's flux maintains a steady constant, until point 2, when the exoplanet crosses the star's threshold and begins to block a small percentage of

its light. This dip is recorded, and the level of light blocked remains constant until point 3, where the exoplanet completes its transit. At this stage, light from the star is no longer being blocked, and the light curve begins to record the star's flux at its original level. It should be noted however that Figure 1.1 (*'Exoplanet Diagrams: The transit method'*, 2015) is a simplified presentation of exoplanet detection through the transit method. There will be instances when multiple exoplanet transits happen simultaneously, or where other stellar objects (asteroids/comets/dust clouds etc.) may interfere with the light levels recorded. These instances may present themselves in a transit as smaller dips in the main flux decrease (in the case of multiple simultaneous planetary transits), or as uneven or irregular dips for other stellar objects.

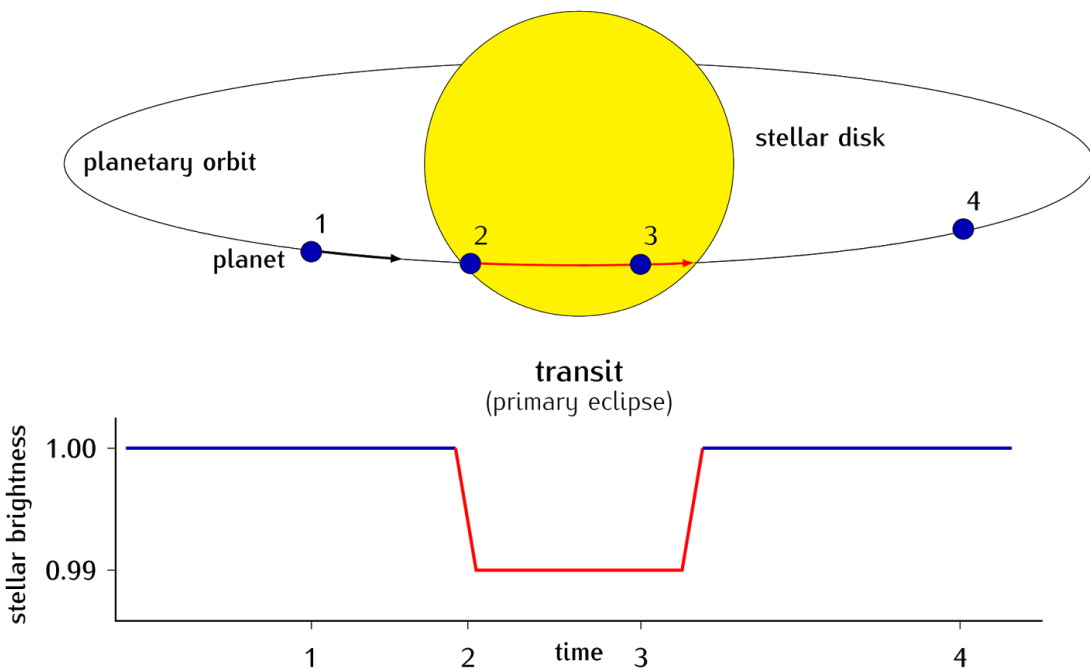


Figure 1.1: A simplified diagram showing the mechanism of exoplanet transits.

Compared to Figure 1.1, Figure 1.2 below shows the true light curve of a transiting Jupiter sized exoplanet. Whilst the line of best fit (in red) matches the simplified version in Figure 1.1, there is a noticeable level of noise and scattering of the data points, which shows the need for the deconvolution of the data for meaningful analysis.

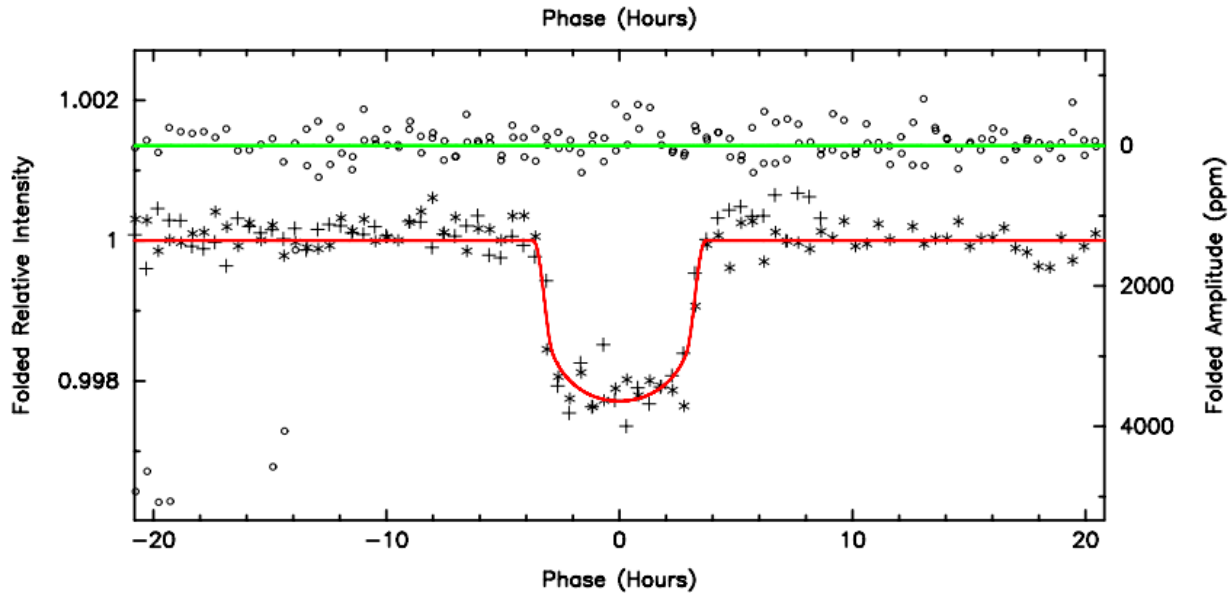


Figure 1.2: The light curve generated by a long-period Jupiter sized candidate around KIC 10723750 (Borucki et al., 2011).

A transit is useful in numerous ways. Not only does it provide the first clues to the presence of an exoplanet, when enough instances have been recorded and the exoplanet confirmed, it can help provide other useful data. Planetary radius is a key calculation that can be made, as the larger the planet, the more light it blocks from its host star. The reverse is true; small planets will block a much smaller amount of light, which by extension, can also make them harder to detect via transits. The orbit size can also be determined based on the amount of time between transit repetitions.

Atmospheric conditions on the exoplanet can also be determined via spectroscopy, should it possess one. As the transit occurs, some of the star's light will travel through the exoplanet's atmosphere, and this light will be dispersed in different manners ('*What's a transit? – Exoplanet Exploration: Planets Beyond our Solar System*', 2024) depending on what elements are present there. This can be used to determine its composition. If we are able to understand the composition of an atmosphere, we are then able to determine other factors such as habitability. To calculate habitability, we need to take into account orbit size, atmospheric conditions, the size of the exoplanet, temperature of the host star, and the temperature of the exoplanet's surface. An exoplanet that is primarily composed of gas is and far

from its star is unlikely to create conditions conducive to life, in the same way that a small, rocky world with a high surface temperature and orbiting both rapidly and very close to its host star would also struggle to support the breakout of life, or at least, life that has the potential to become advanced beyond a microbial stage. However, transits can highlight to us those worlds which are in their host star's habitable zone, of a good size, and have favourable surface and atmospheric conditions.

Transit detection is not without its limitations. It assumes that all exoplanets will have a ‘side on’ orbit to us as the observer, which is extremely unlikely to be the reality in almost every star system. In an instance where the orbit of an exoplanet is side-on to the observer, it will intercept the light reaching an observer from the host star that is being observed, and thus, transit across its face, and be recorded as a decrease in flux in a light curve. However, if due to unfavourable orientations in the observation it is determined we are observing a star ‘top down’ and from above, an orbiting exoplanet will never pass between the observation point and the star. Therefore, no starlight will be blocked, and no dip in flux ever recorded. The star may be listed as possessing no exoplanets, when in reality, it may hold any number of different worlds. Further, and as is currently the case, most transits detected come from exoplanets with very short orbital periods. Simply put, these exoplanets transit more regularly, and are therefore creating more repeat dips in their host star's light curve, and producing more data to be investigated and lead to their confirmation. If we investigate this issue in our own Solar System, Mercury has an orbital period of 88 days (*'Mercury: Facts - NASA Science'*, 2024) and would transit across the Sun readily for an observer, even during an observation period of one Earth year. Compared to Pluto with its orbit of 90,560 days (*'The Orbit of Pluto. How Long is a Year on Pluto? - Universe Today'*, 2017), not only will Mercury transit 1029 times before the first indication that Pluto is in the Solar System, the capability that we currently have means that our detection windows are not open long enough to ever record a Plutonian transit. As an example, the detection window for K2 was 83 consecutive days (*Howell et al., 2014*). Moreover, should we be in a position to record an exoplanet at such a distance from its host star, we would only detect it once, leaving it highly unlikely to be certified as an exoplanet rather than some other cosmic phenomena interfering with our observations.

Therefore, the number of exoplanets currently detected may only be a very small sample of the worlds that actually orbit around the stars we have investigated up to this time. Further, observations need to be continuous for the best results, which is resource intensive, and most readily available from space-based platforms, rather than Earth's surface observatories. Resultantly, missions are expensive to set up, launch, and run, should continuous observation be desired.

Whilst this paper will give particular focus to the space based Kepler and K2 missions, it should be noted that these are not the only missions involved with exoplanet transit detection. Table 1 expands on these missions, but the very first mission to undertake the search was COROT, a 30cm telescope launched by the ESA on the 27th December 2006 ('*ESA - COROT overview*', 2024). Whilst COROT may not have had prolific results on the scale of a mission such as Kepler, it did achieve some notable 'firsts', including 'COROT-Exo-7b' (Léger *et al.*, 2009), which was the first exoplanet detected to be of a similar size to Earth, rather than a large gas giant. Its radius was less than 2 times that of Earth ('*Exoplanet Exploration: Planets Beyond our Solar System CoRoT-7 b*', 2024).

1.1.2.2. Radial Velocity Detection

The traditional thought process that stars are the central object in a stellar system, and that planets orbit around them, is not entirely accurate. In-fact, stars and any planets they possess actually orbit around a common centre of mass known as a barycentre ('*What Is a Barycenter? | NASA Space Place*', 2020). Given that a star will have a much greater mass than any of its planets, it will be much, much closer to the barycentre, or in cases where the star is sufficiently dense, have the system's barycentre within it. As the star orbits around this point, spectrographic monitoring will show a redshift as it moves away from us, and a blueshift as it moves back towards us. Where spectrometers are sensitive enough, it becomes possible to measure slight variations, colloquially referred to as 'wobbles', in the levels of blueshift and redshift. When these wobbles occur in regular intervals, it can be determined that the star is being pulled out of alignment by an orbiting body. In instances where the detected body has a mass lower than $10 M_{Jup}$, it is most likely to be an exoplanet, and in

instances where the detected body has a mass more than this, it is likely to be another star ('Color-Shifting Stars: The Radial-Velocity... | The Planetary Society', 2020). Unlike transit detections, continuous monitoring is not required for best results, and as such, small scale observatories can be run on Earth with high accuracy. In the case of the EXPRES spectrograph at the Lowell Observatory, precision can be lower than 30cm/s^{-1} (Jurgenson et al., 2016) once noise from the observed star is accounted for. The method's success is clear as 19% of all exoplanets have been discovered with this method. It is best suited for finding large exoplanets, particularly gas giants, as they have a more discernible pulling effect on their host stars due to their higher masses. Smaller exoplanets are harder to find for the converse reason; their mass is so much smaller than the host star, that their presence has a minimal effect on the host star's orbit, and thus minimal ability to cause a wobble in the observed spectral signature. It should also be noted that those planets that are detected by radial velocity, are extremely unlikely to be candidates as the home of any form of life. They are simply too hot, and too close to their host stars to be survivable, and the very presence on such a large exoplanet at the centre of a system would be indicative of smaller, earth-like world's being ejected from any habitable orbit ('Color-Shifting Stars: The Radial-Velocity... | The Planetary Society', 2020).

1.1.2.3. Direct Imaging of Planetary Systems

As telescope capabilities improve, our ability to adapt missions to fulfil very specialised criteria also improves. One such improvement, and particularly in the case of the James Webb Space Telescope is the ability to take direct images. The process of taking photos of exoplanets is not entirely new; the SPHERE optic system at the European Southern Observatory has been capable of direct imaging since 2014, with particular capability being concentrated on bright stars that are "observed in the visible or near infrared" ('ESO - Instrument Description', 2021). However, due to the Earth's inherent infrared glow, the photos obtained by a system such as SPHERE are of limited quality. Even before this however, images were being taken of exoplanets, with Chauvin et al., (2004), presenting the case for a giant gas companion for the brown dwarf 2M1207, shown below in Figure 1.3.

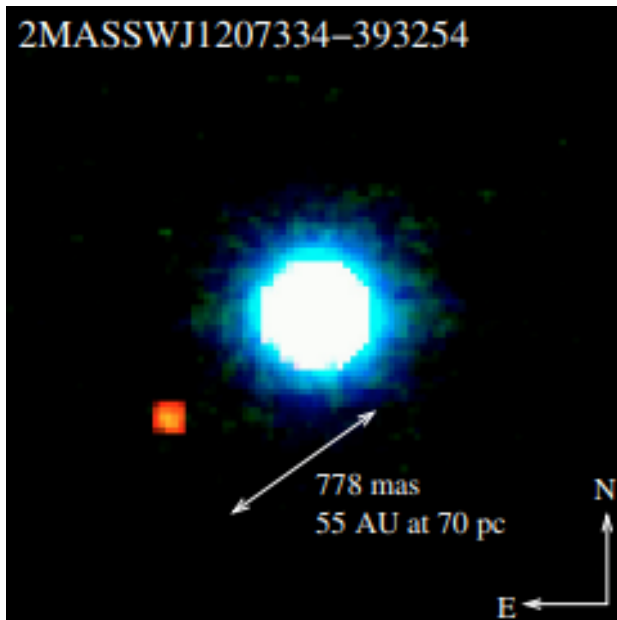


Figure 1.3: A composite image of a gas giant companion orbiting 2M1207 (Chauvin et al., 2004).

Telescopes such as James Webb, that are outside the confines of Earth's atmosphere, are now able to view star systems at greater infrared wavelengths ('NASA's Webb Takes Its First-Ever Direct Image of Distant World – James Webb Space Telescope', 2022), and thus conduct direct imaging at a much higher level of detail. Figure 1.4 below, shows the JWST's first direct image of an exoplanet (in this instance a large gas giant), around the star HIP 65426. It can be expected that observational capabilities will continue to improve, to the point where smaller, rocky worlds can be imaged, as opposed to the large self-luminous gas giants that currently make up the bulk of those exoplanets imaged and the processes behind taking such images are well laid out by Currie et al, (2023).

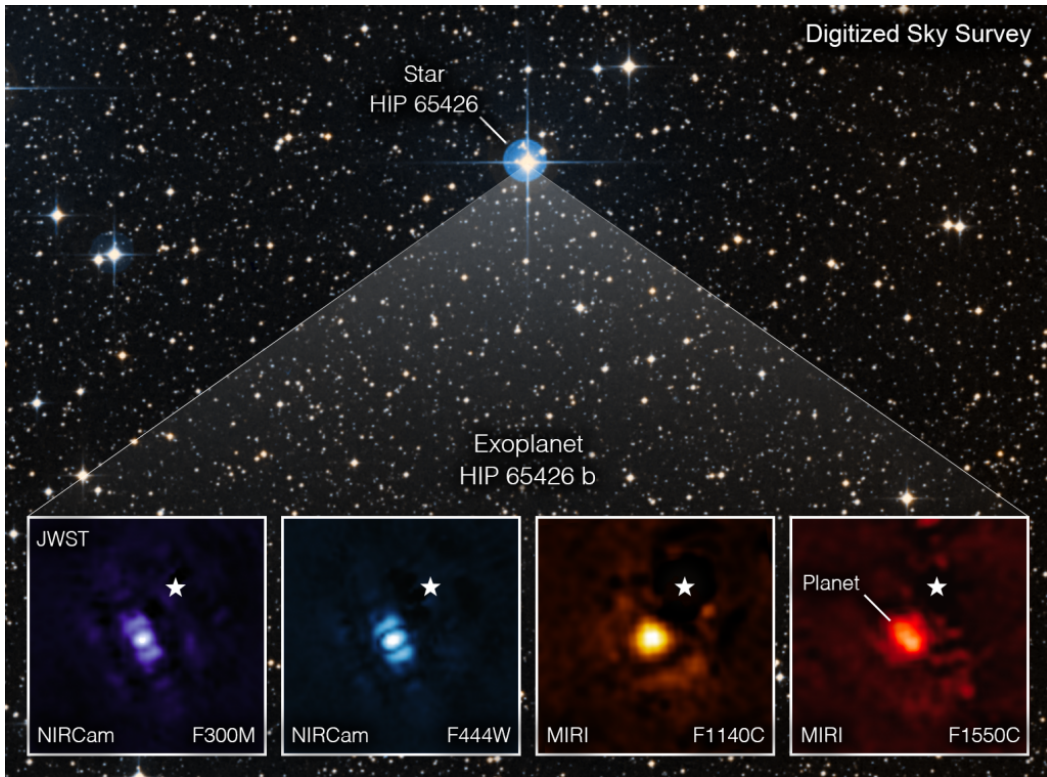


Figure 1.4: The first pictures release of an exoplanet imaged directly by the JWST. ('NASA's Webb Takes Its First-Ever Direct Image of Distant World – James Webb Space Telescope', 2022)

1.1.2.4. Gravitational Microlensing

Starlight does not always travel in straight lines. Sometimes, in specific conditions, it can be warped and bent by gravity. The primary effect of this is that gravity acts as a magnifying glass for the observer, by greatly increasing the light of distant objects. Typically, this happens between a foreground, and a distant star to the observer. As the two stars begin to align, light from the distant star is bent by the gravity of the foreground star, magnifying its light. This increase in brightness can be by as much as 1000 times ('Space-Warping Planets: The Microlensing Method | The Planetary Society', 2024), although this rate varies depending on the exact alignment of the observed objects. This increase in brightness allows for much easier observation of the distant star, although only for the short window for which the alignment lasts, which could be measured in periods of weeks or months. A secondary effect of gravitational microlensing is the concurrent ability to detect exoplanets in orbit

around the foreground star. Despite being to a smaller extent than that of a star, exoplanets still have a gravitational effect on the light waves of the background star. As this starlight is bent by the planet's gravity, it will produce a second, smaller spike in the brightness of the background object. Such an effect was captured by Beaulieu, J et al (2006), in their observations of the microlensing event of OGLE-2005-BLG-390, shown below in Figure 1.5;

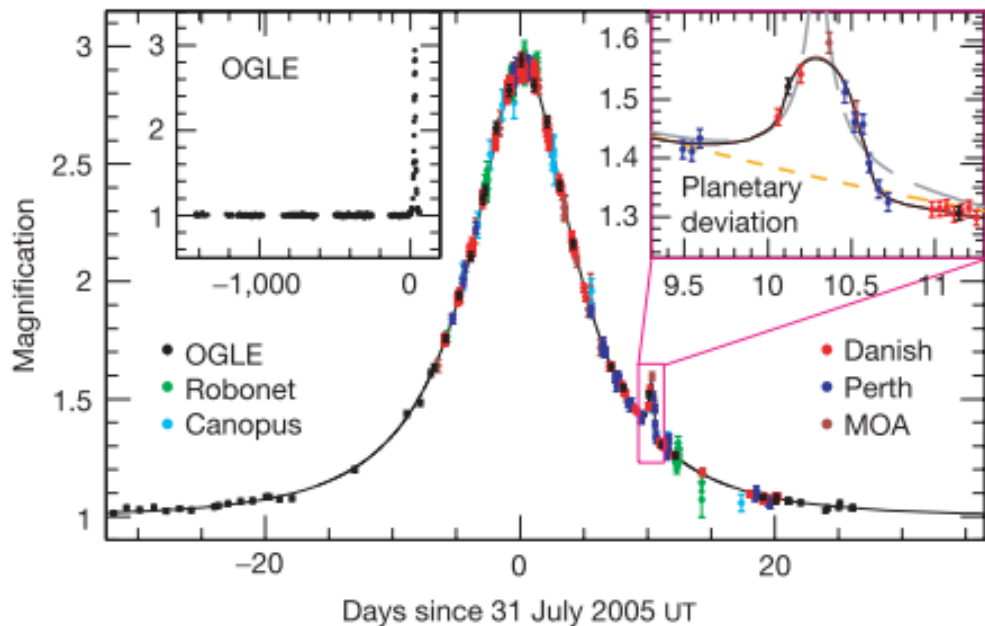


Figure 1.5: A secondary spike caused by an exoplanet during a microlensing event. (Beaulieu, J et al, 2006)

This event confirmed the presence of a $5.5M_{\text{Earth}}$ planet. Specific missions that will search for exoplanets using gravitational microlensing are now in advanced stages, with NASA's planned Nancy Grace Roman Space Telescope ('*Roman Space Telescope/NASA*', 2024) due to launch in 2026 (see Table 1), where it will use gravitational microlensing to survey the central region of the Milky Way.

1.1.2.5. Astrometry

Astrometry is the taking of precise measurements as to a star's position in the sky, and the oldest of all the listed detection methods. In a very similar way to radial velocity, a star's wobble can be determined to be the result of an unseen planetary companion tugging at its host star, and it is this wobble which astrometry looks to record. However, due to the incredibly small distances in the variance of a star's orbit, as a direct consequence of such wobbles, at the time of writing, only 3 exoplanets have been listed as discovered via astrometry. These are; DENIS-P J082303.1-491201b, (*Sahlmann et al., 2013*), GJ 896 Ab (*Curiel et al., 2022*), and HIP 66074b (*Sozzetti et al., 2023*). The latter of the three, was discovered via the Gaia Telescope. Gaia is a wide ranging mission, still active some ten years after its launch date on 19th December 2013 (*Prusti et al., 2016*). Primarily, the mission was focussed on the evolution of the galaxy, stellar formation and evolution, and binary star systems. However, Gaia was unique in that its instrumentation allowed the ability to conduct astrometry at an accuracy level (of micro-arcseconds), that has never been possible from ground-based telescopes. These accuracy levels allowed not only for the detection of exoplanets, but more crucially, some of their key properties, such as actual mass, as opposed to a roughly calculated lower limit mass (*Prusti et al., 2016*).

2. Wider Mission Context

The COROT telescope has already been discussed earlier in this paper, as has the Gaia Telescope, but these are not the only exoplanet missions to be launched, so it is advantageous to discuss these other missions too. Given the number of missions to discuss, Table 1 below has been provided to enable a clearer breakdown. This list is not exhaustive, and only presents those missions which are conducted from space. Earth based missions, such as the Next-Generation Transit Survey (NGTS), or Wide Angle Search for Planets (WASP) are not included, as they are too numerous (some 50+ missions) to cover meaningfully in the confines of this paper.

Table 1: An overview of space based exoplanet missions.

Mission Name	Mission Date	Mission Overview/Capabilities	Source
SWEEPS	2006 - 2006	7 Day monitoring window of the Galactic Bulge, using the Hubble Space Telescope. 16 Exoplanets discovered via transit detection.	(<i>Sahu et al., 2008</i>)
TESS	18.04.2018 - Present	“All-sky” survey, with goal to monitor 500,00 stars in an area 400x larger than Kepler. Focussed on the detection of Earth and “Super-Earth” sized exoplanets.	(‘ <i>TESS Mission Overview</i> ’, 2024)
CHEOPS	18.12.2019 - Present	High-precision observation of exoplanet size. Characterisation of stars already known to possess exoplanets.	(‘ <i>ESA - Cheops</i> ’, 2024)
JWST	25.12.2021 - Present	Coronagraphs enable direct imaging of star systems, spectrographs enable investigation of exoplanet atmospheres, and new detections are possible via Transit recording.	(‘ <i>Other Worlds - Webb/NASA</i> ’, 2024)
PLATO	2026 (Planned)	Characterisation of host stars, recording of exoplanets in habitable zone range of sun-like stars, search for exomoons and planetary rings.	(‘ <i>ESA - Plato</i> ’, 2024)
Nancy Grey Roman Space Telescope	2026 (Planned)	Microlensing survey and coronagraphs to enable direct imaging of mature gas giants. Also known as WFIRST.	(‘ <i>The Nancy Grace Roman Space Telescope</i> ’, 2024)
ARIEL	2029 (Planned)	Study of exoplanet atmospheres, including variations over time. Focus on rocky exoplanets, and gas giants.	(‘ <i>ESA - Ariel</i> ’, 2024)

3. Kepler/K2 Mission Context

On the 7th of March 2009, the Kepler Space Telescope (KST) was launched from Cape Canaveral. Whilst the date may have passed in obscurity for most of the world's populous, Kepler represented the first occasion for NASA in which a telescope had been specifically designed, built, and launched in our hunt for worlds outside of our own Solar System. It may not have been the very first exoplanet mission, given that the ESA's COROT had already been in service for around two and half years by KST's launch date, but it did herald in a new age of exploration with its advanced capabilities. Its primary goal was to survey designated regions of our night sky, looking for Earth sized exoplanets in and around the habitable zones (*Haas et al., 2010*) of their host stars, with its onboard photometer designed to measure the light coming from those stars. Whilst its influence was not immediate, nor publicly spectacular in the way of later missions such as JWST with its pictures of the cosmos, the time it spent collating data would soon come to fruition. The two spikes in Figure 3.1 ('*What's a transit? – Exoplanet Exploration: Planets Beyond our Solar System*', 2024) coincide with two large data releases from KST, with some 2000 combined exoplanets being discovered by the KST alone in these years. KST could simultaneously monitor 170,000 stars (*Haas et al., 2010*), and did so in a region of the Cygnus and Lyra constellations, due to the necessity of having a Field of View (FOV) that was outside of the ecliptic plane. In the ecliptic plane observations would be disturbed by the Sun, thereby limiting observational time. This did place a large limitation on the KST however, as this is a comparatively small area of the night sky that is being observed, and thus, the data collected and analysed from this area may not be indicative of the conditions elsewhere in the cosmos.

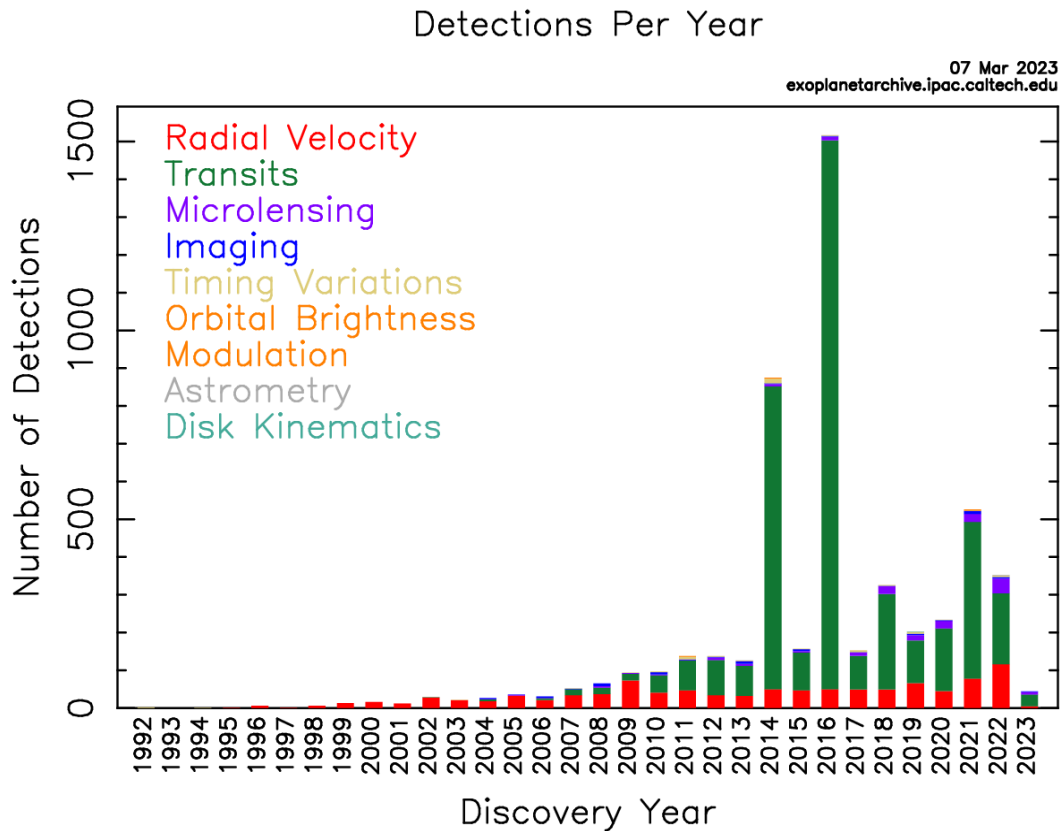


Figure 3.1: Exoplanet detections, and their year of discovery.

Whilst the mission began smoothly, by May of 2013, KST had begun to experience major technical issues, arising from two of its four reaction wheels failing. These were critical components that helped the KST maintain stable orientation in the X, Y, and Z axis. Two of these crucial components failing could have brought a premature end to the mission, as the telescope would not have been able to keep its orientation towards its primary targets of Cygnus and Lyra, and thus leading to a compromised ability to collect data in this area. To circumvent this issue, a secondary mission was proposed. This was to be called ‘K2’. K2 would function both as a way of extending the life of the KST, and as a way of gathering an entirely new set of observations from different regions of the night sky. Because of the reaction wheel failures, K2 was to be an ‘ecliptic-pointed mission’ (*Howell et al., 2014*), rather than being aimed at one specific area. This would allow KST to cover a much greater region of the observable universe than its original mission. These observations would be problematic though, as the telescope’s constant jittering from positional corrections meant the data would be dominated by noise (*Vanderburg and Johnson., 2014*). As a result of this, K2 would be operating at a greatly reduced level

of precision compared to the original KST mission, as shown below in Figure 3.2 (*Howell et al., 2014*). Further, by entering into the ecliptic plane, K2 would have reduced observational windows before interference from the Sun became too impeding.

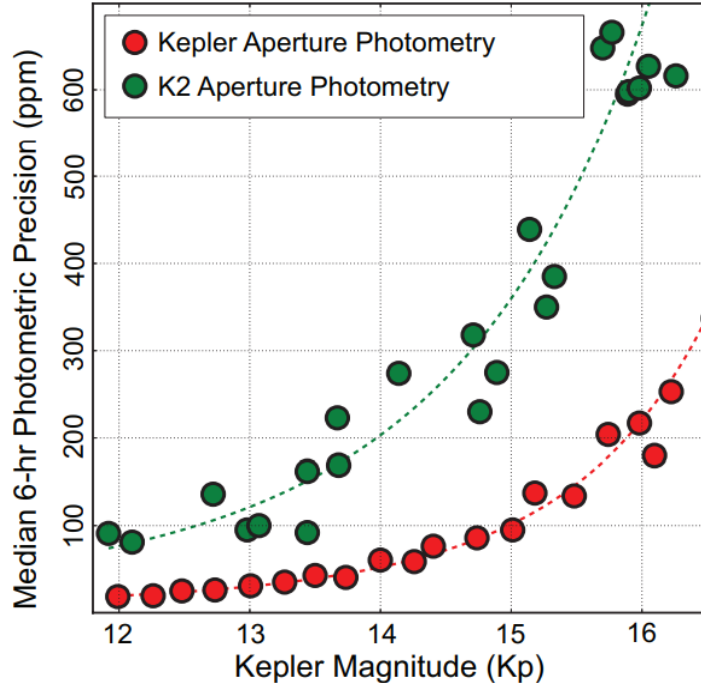


Figure 3.2: The precision levels of the K2 mission, compared to its original state.

Despite these challenges however, the second life gained through operating as K2, allowed the KST mission as a whole to continue for another 5 years, finally ceasing when its fuel tanks ran dry on November 15th 2018. The mission was a complete success, and whilst it may not have ended in the way intended, with its targets in Cygnus and Lyra long since left behind, these extra years provided so much data to search through, that for the most part, much of it has yet to be analysed. So far, from the data that has been analysed from KST in both its mission stages, there have been 2779 exoplanets discovered ('*NASA Exoplanet Archive*', 2024), confirming the resounding success of this mission.

4. Project Aims

Now that mission context has been provided, and detection techniques highlighted, it remains to discuss the specific objectives of this project, and the techniques used to facilitate the research involved. The vast amount of data collected by the KST (both in its primary mission, and later as K2), was released in multiple data packages, but given their size, these packages have not been fully analysed, and it can therefore be assumed that large swathes of this data may still contain signals that identify new stellar objects, and appropriately, exoplanets. At present these candidates remain obscured in the data releases. To contextualise the extent to which data analysis has not been conducted on the KST mission, the particular data directory used in this paper possessed a total of 412,219 data files (*'lctools - Kepler Bonus Light Curve Directories'*, 2024), split between 42 data releases, and was just one of the three available directories. Combined, the directories totalled some 1,189,900 files. Therefore this project attempts to analyse a specific subsample in one such data release from this directory, in order to try and identify any such exoplanet candidates (particularly short-period exoplanets), that may be contained there. These subsamples would be selected via appropriate criteria (see Section 7.1), to compress a chosen bulk data release (10,000 data files) into a manageable size, which could then be analysed in a realistic timeframe and practical manner. LcTools was selected for data analysis, because of its ease of use and open source nature, with further details in Section 5. Further, the results of this data interrogation are discussed, and potential future research avenues highlighted, in Sections 8 through 10, and Section 12 respectively.

5. Software Requirements.

Due to time constraints, primarily regarding the learning of an entire coding language in order to facilitate data analysis, this project desired a software that had minimal requirement for coding, and was ‘Windows’ based not only for ease of use, but for computational efficiency, due to the author’s prior experience in a Windows based computing environment. The sourcing of such a software package was made easier thanks to the MAST data sets, where packages and pipelines related to the Kepler, K2, and TESS missions were readily available (*‘RELATED SOFTWARE | MAST’*, 2024). On

review of the available packages, ‘LcTools’ was selected due to its fulfilment of the project criteria. Whilst in-depth functionality would take time to acquire, critical functions such as detrending curves, and searching light curves for signals could be mastered in a short time frame, with an intuitive User Interface (UI) making this process simpler. The package was also ‘Windows’ based, and required no coding knowledge to get started. A crucial advantage of the package was its comprehensive user guide, which greatly reduced the time taken to understand key aspects of the software and greatly facilitated more advanced use of its system. Further, the applications within LcTools were not specialised in a particular task, rather, they allowed for a more complete and holistic analysis of the data input to them, due to how they were subdivided. The LcTools package (*Schmitt and Vanderburg, 2021*) is broken into a number of smaller applications, namely;

LcViewer: Viewing and detrending light curves

LcSignalFinder: For the detection and recording of TTV associated signals

LcGenerator: Creation of light curve files for use in LcViewer/LcSignalFinder

LcReporter: Generation of Excel reports for signals recorded

All of the above software applications were used throughout this project, with a particular focus on LcViewer, and LcSignalFinder. It was recognised early that LcViewer uses the Barycentric Julian Date on the horizontal axis, although the means of converting this into Terrestrial Time were beyond the scope of this research. This posed no significant issues throughout the research, although it did mean that it was not possible to date the findings of Section 9 and Section 10 beyond a rudimentary timeframe (the original Kepler mission) due to their positioning within the Cygnus Constellation (Figure 9.2 and Figure D.8).

6. Data Validation: Confirmation of Known Exoplanets

With an appropriate software package having been selected, it was desirable to both confirm its validity, and that the results from previous searches could be replicated, thereby confirming that the methodology behind the data analysis was also sound. To do this, three confirmed exoplanets and a false positive event were selected from the Exoplanet archive database ('*NASA Exoplanet Archive*', 2024) and their Kepler ID's cross-referenced within the star files of LcTools ('*lctools - Kepler Bonus Star List Files*', 2024), in order to locate their light curves. In this particular instance, the light curve for the star Kepler 75 was selected, as it is known to host at least one exoplanet; Kepler 75b, and has similar characteristics to our own Sun. Kepler 75, or by its alternate names, KOI-889/KIC 757450 (*Hébrard et al.*, 2013), is a main sequence star, both a little cooler and a little smaller than our own Sun at 5330K ($\pm 120\text{K}$) and $0.88\text{M}_{\text{Sun}}$ ($\pm 0.06\text{M}_{\text{Sun}}$) (*Hébrard et al.*, 2013), respectively. However, these variances are not so drastic as to render its comparison to the Sun unrealistic. Once a Kepler data file has been loaded, in this instance the light curve for Kepler 75, LcViewer displays the raw data output, as shown below in Figure 6.1. Given that the data is of limited use in this format, the immediate step required is to detrend it. LcViewer has a dedicated tool for this, and the detrend can be entirely customised for different parameters. The detrend menu is easily located through either the drop down menu in the softwares toolbar, or via the keyboard shortcut 'SHIFT + D'. For the first data manipulations, the detrend settings were left as standard, as recommended in the LcTools User Guide. This is beneficial, as it allows any user to gain familiarity with the software before in-depth analysis begins.

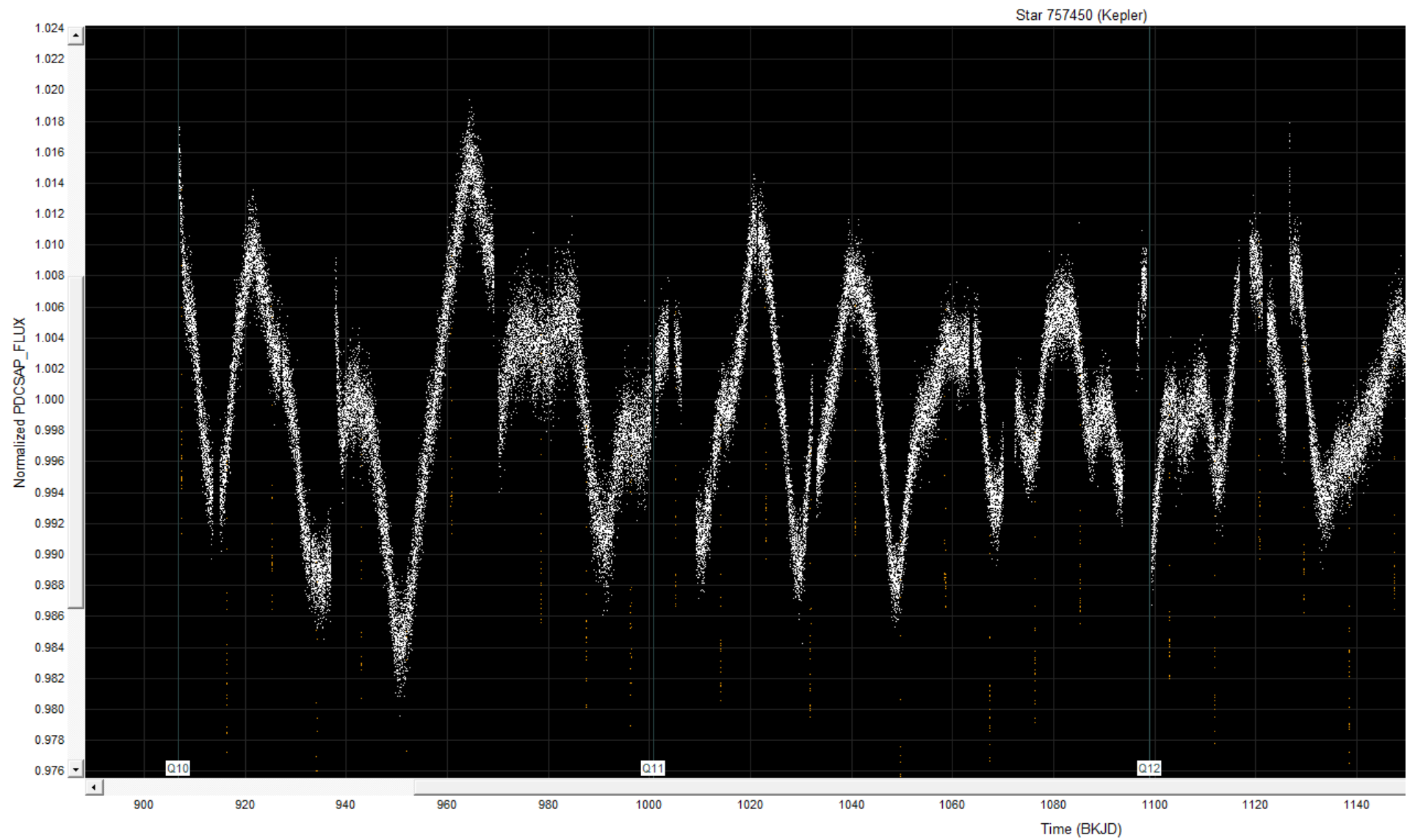


Figure 6.1: Raw data for Kepler 757450 loaded into LcViewer.

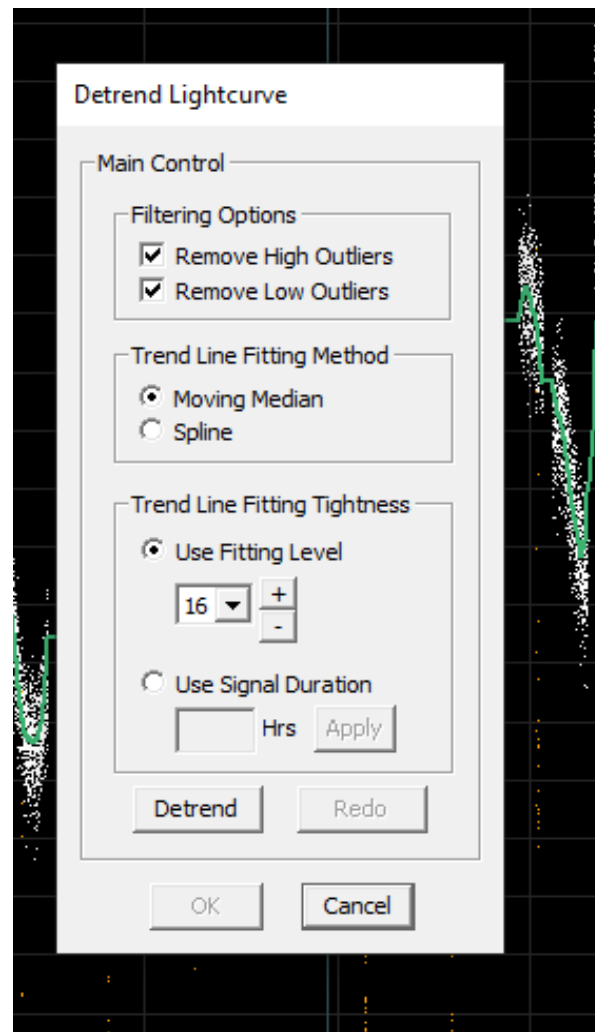


Figure 6.2: Available detrend options for LcViewer.

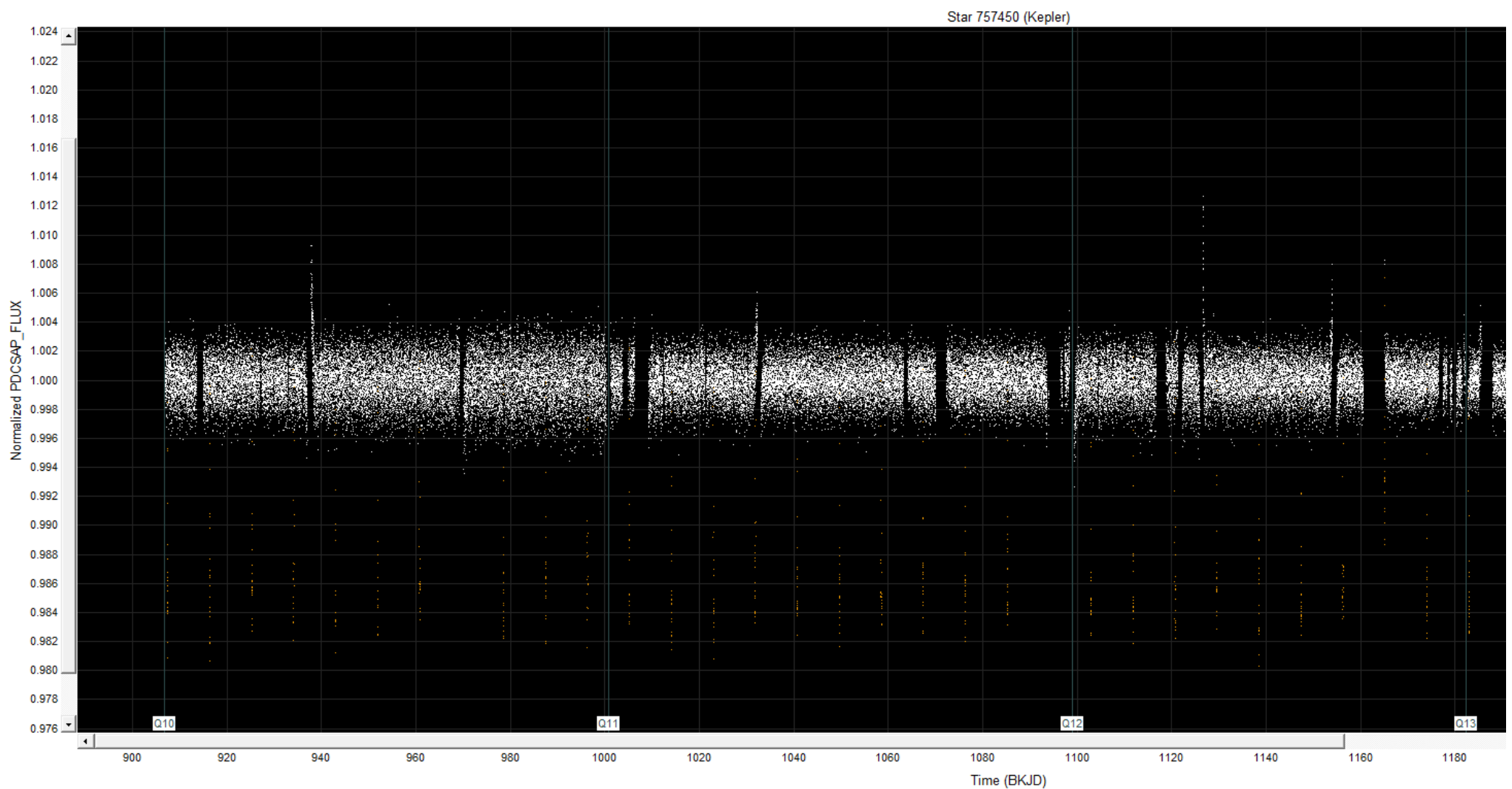


Figure 6.3: Kepler 757450 data, once detrended

Once data has been detrended, it becomes possible to use the software to look for repeat signals, which again, has entirely modifiable criteria. For this example, the minimum possible values were selected; $0.5 R_{\text{Earth}}$, Minimum period of 0.1 Days, and a minimum duration of 0.5 Hours. This casts the widest possible net for potential targets, and allows for a good baseline recording to be taken. If no signals are found with such minimal requirements, then it can be assumed that more targeted searches of the same data file, with stricter requirements, would also be unlikely to find a candidate signal, given that a baseline wide search would reveal even the slightest hint of a transit.

Minimum instances of target can also be amended, and for this validation test, a value of ‘2’ was selected. This means that the signal must be identified at least twice, for the software to count its inclusion. This helps ensure a minimum level of robustness of the data, as it therefore will not highlight every single dip in flux as a candidate object. This also greatly reduces the time taken to manually verify highlighted signals, as there are fewer to validate. However, setting a search up in this way does lead to an interesting constraint. Whilst not the case for the light curve of Kepler 75, by discounting single instance events there raises the possibility that a single transit event (by a long-period transiting body) will not be detected. Exoplanets with long-period orbits are particularly hard to find, as they typically fall beyond normal observation windows. If using a theoretical example of an exoplanet which has an orbit equivalent to 20 Earth years, and was detected on the first day of KST’s scientific operation (12th May 2009, (*Haas et al., 2010*)), then this exoplanet will simply have not been observed again, as insufficient time has passed. Given that the KST mission has since ended, and outside of stringent follow up from succeeding missions or detection through other means such as direct imaging (see Section 1.1.2.2), this particular exoplanet would not be observed again. Consequently, exoplanets with longer orbits remain elusive. However, in the case of Kepler 75, where LcViewer is being set up in a manner to enable the interrogation of the presence of a known exoplanet, a search value of two detection instances suffices. Figure 6.4 shows this step in greater detail, highlighting the options available to the user.

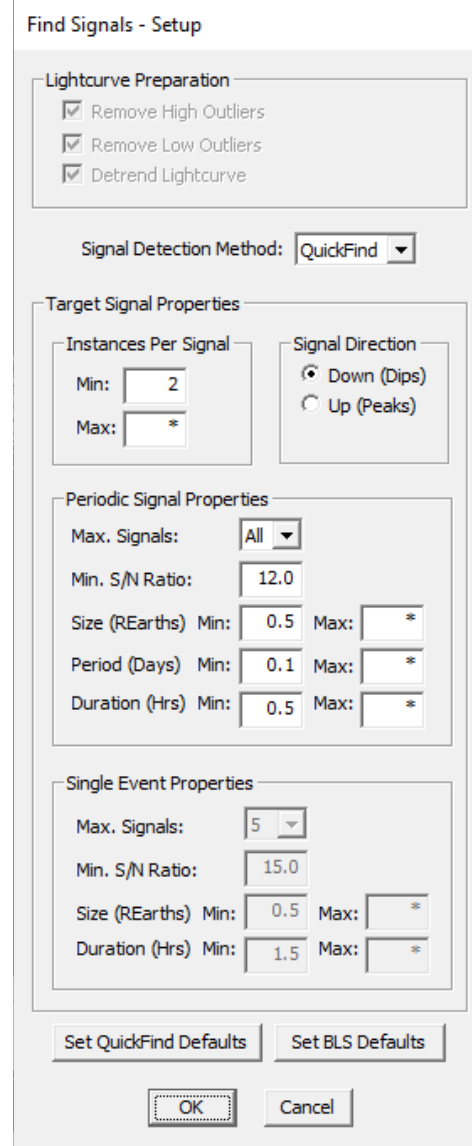


Figure 6.4: Signal finding setup.

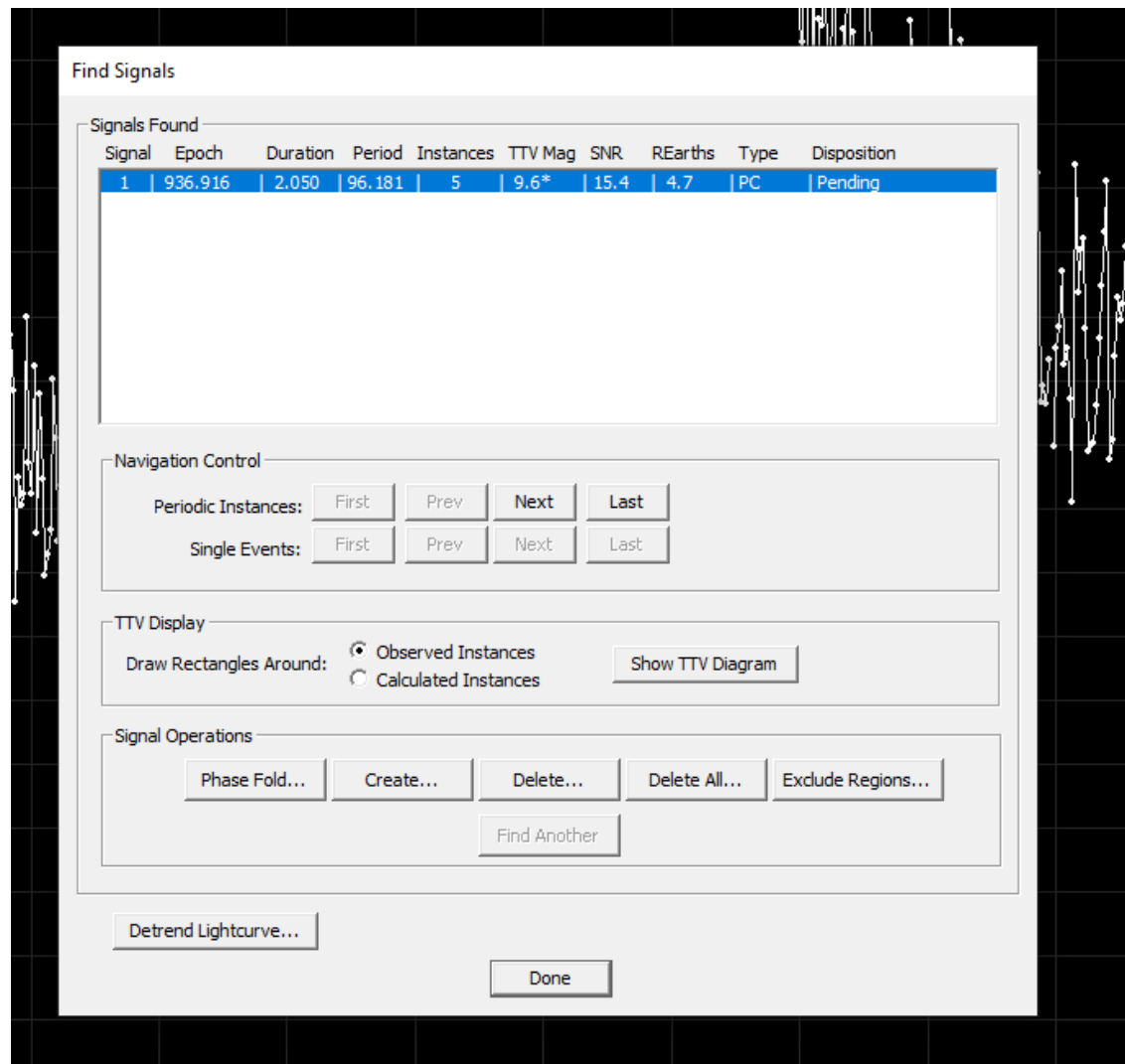


Figure 6.5: Repeat Instance detection menu.

Should any signals be found, the software enables the user to set up a phase fold. A phase fold is a process in which all data points from the entire light curve are time shifted ('phased') into a single period, highlighting any subtleties that might occur in brightness variations (*'Light Curves, Periods, and Phase'*, 2024). LcViewer again makes this stage definable for the users individual requirements.

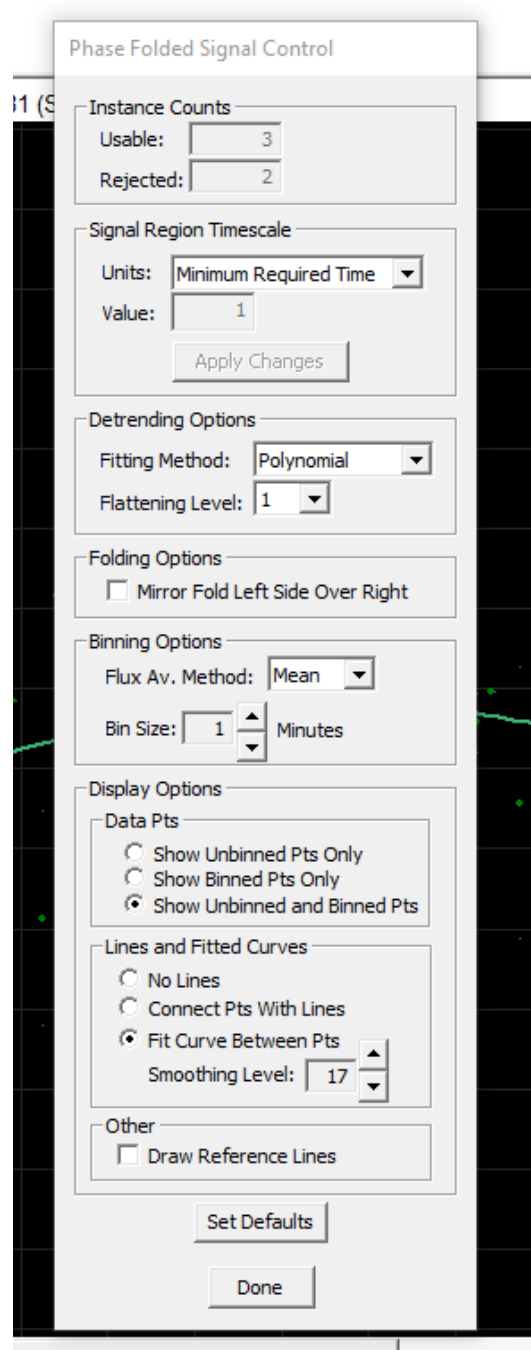


Figure 6.6: Phase fold setup

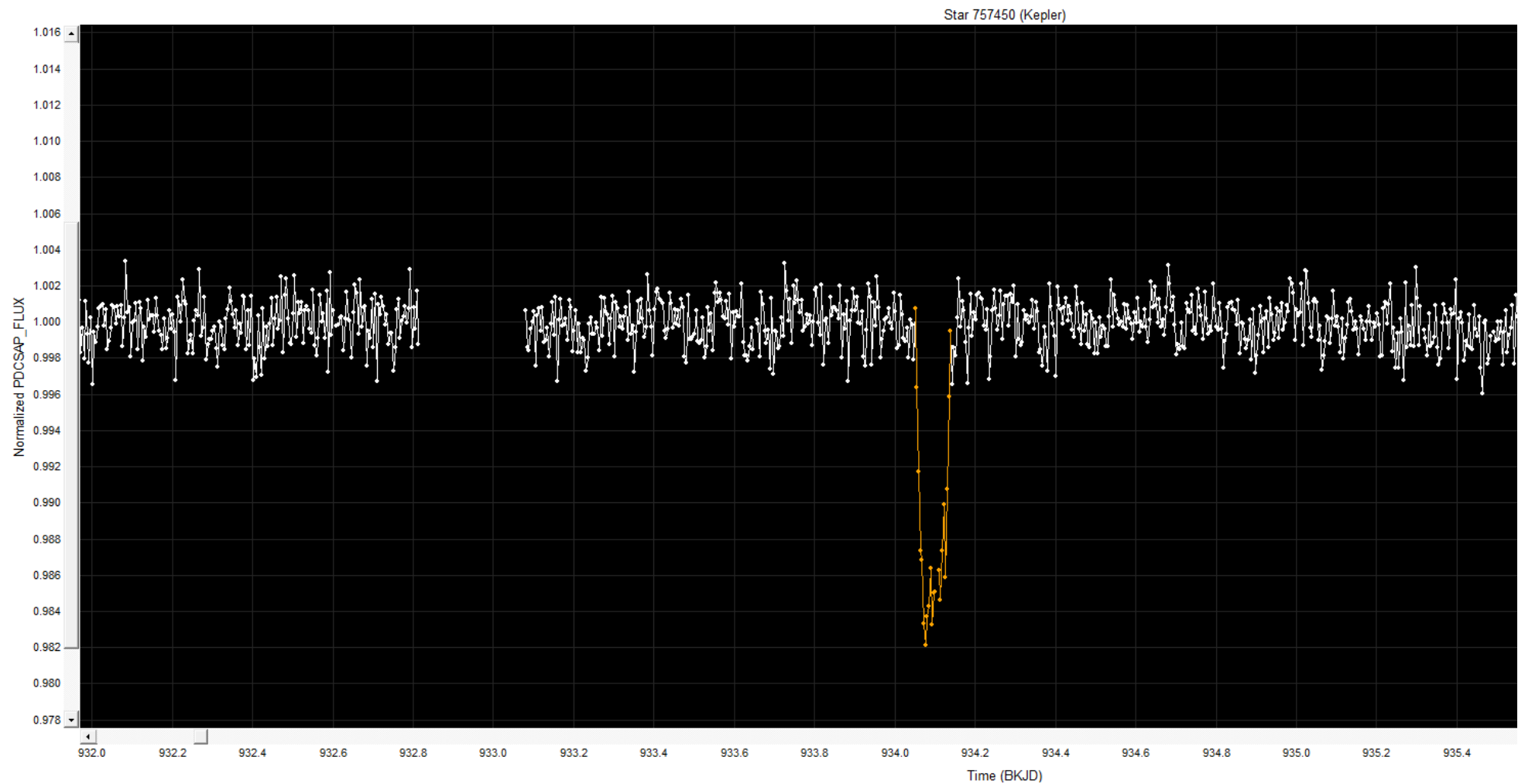


Figure 6.7: Phase fold complete, instance generated, and candidate curve highlighted.

Now that the raw data for Kepler 75 had been detrended and processed, it became possible to analyse individual data points more closely. Once these steps had been completed it became abundantly clear that a candidate planet was indeed present in the light curve and this was clear evidence that the software selected was viable. It also confirmed that a known exoplanet could indeed be found by following the method set out above. In this particular instance, the dip in the light curve is caused by the transit of Kepler 75b, a hot gas giant, sized at $10.1 (\pm 0.4) M_{Jup}$, $1.05 (\pm 0.03) R_{Jup}$, and with a known density of $11.0 (+0.8/-0.9) g cm^{-3}$ (*Bonomo et al., 2015*). To ensure absolute viability of the software, it was further used to confirm the presence of two other known exoplanets; Kepler 93b (*Marcy et al., 2014*), and Kepler 984b (*Sun et al., 2024*). The light curves for these exoplanets can be found in Appendix A. It was also useful to try and identify a ‘False positive’ signal, in which the light curve appears to show the transit of an exoplanet, but the dip in flux is actually created through other mechanisms, such as the movement of the spacecraft, or other cosmic phenomena passing between the observed star and the observer. Initially, one such false positive had been detected around KIC 3439031 which showed regular, extreme dips in the flux (almost a 50% decrease), and it was thought to be the movement of KST creating these extreme episodes. These extreme fluctuations are also shown in Appendix A. However, further research appears to highlight this as actually being two “nearly identical F-type stars” (*Helminiak et al., 2019*) in a binary star system as opposed to a false positive. This highlights how results can be misinterpreted, and the care in which data needs to be analysed. What may on the face of it might appear to be a highly unusual and uncharacteristic event which can be readily disregarded, may actually be data which contains great substance and requires further analysis.

7. Selection of Main Data Set

Once LcTools functionality was validated, and its results matched those of confirmed Kepler Objects of Interest (KOI), the next step was to run more recently packaged data through LcSignalFinder, and then through LcReporter, in order to select a subsample of data to analyse. However, it remained to select the actual data that was to be interrogated. To do this, criteria for selection were established.

Firstly, the data should be readily available to access, with minimal processing required in order to prepare it for interrogation. Secondly, it should not be of a size that would be deemed impractical for analysis by containing too many files or being too large a download size, and thirdly, it should be of a determinable source so that the data's origin could be verified. It was determined that "Lightcurves_Kepler_Bonus_B01" ('*lctools - Kepler Bonus Light Curve Directories*', 2024) fulfilled these criteria, and was selected for further analysis. It was readily accessible through the LcTools main site and involved an extremely simple set up, which was completed by downloading the file into an appropriate C:/ drive location, and selecting it as the work group in LcSignalFinder. It also possessed only 10,000 data files, which, while a large number to be initially presented with, further processing (discussed below in Section 7.1) would allow this to be refined into a highly manageable size. Further, the data's origin was easily determinable, and found to come directly from a MAST data release (*Martinez-Palomera et al.*, 2023), which provided further confirmation that the data was valid for selection.

7.1. Selection of Data Subsample

With an appropriate data set now selected, it became critical to break it down into a manageable subsample that could be analysed more efficiently than the original group of 10,000 data points. To help simplify this task, it was a prudent step to utilise the LcSignalFinder tool. By loading in a particular directory (in this instance "Lightcurves_Kepler_Bonus_B01"), it becomes possible to amend the search parameters with which LcSignalFinder will look for signals. For the purpose of this research, it was decided that a wide search angle should be set, but keeping a minimum Signal-to-Noise (S/N) ratio to maintain a level of data robustness. To achieve this, the search parameters were set to a minimum of: **Transit Duration** - 1.5 Hrs, **Transit Period** - 0.25 Days, **Transit Object Size** - 1 R_{Earth}, **S/N Ratio** - 12. This can be seen below in Figure 7.1.1, which shows the interface available.

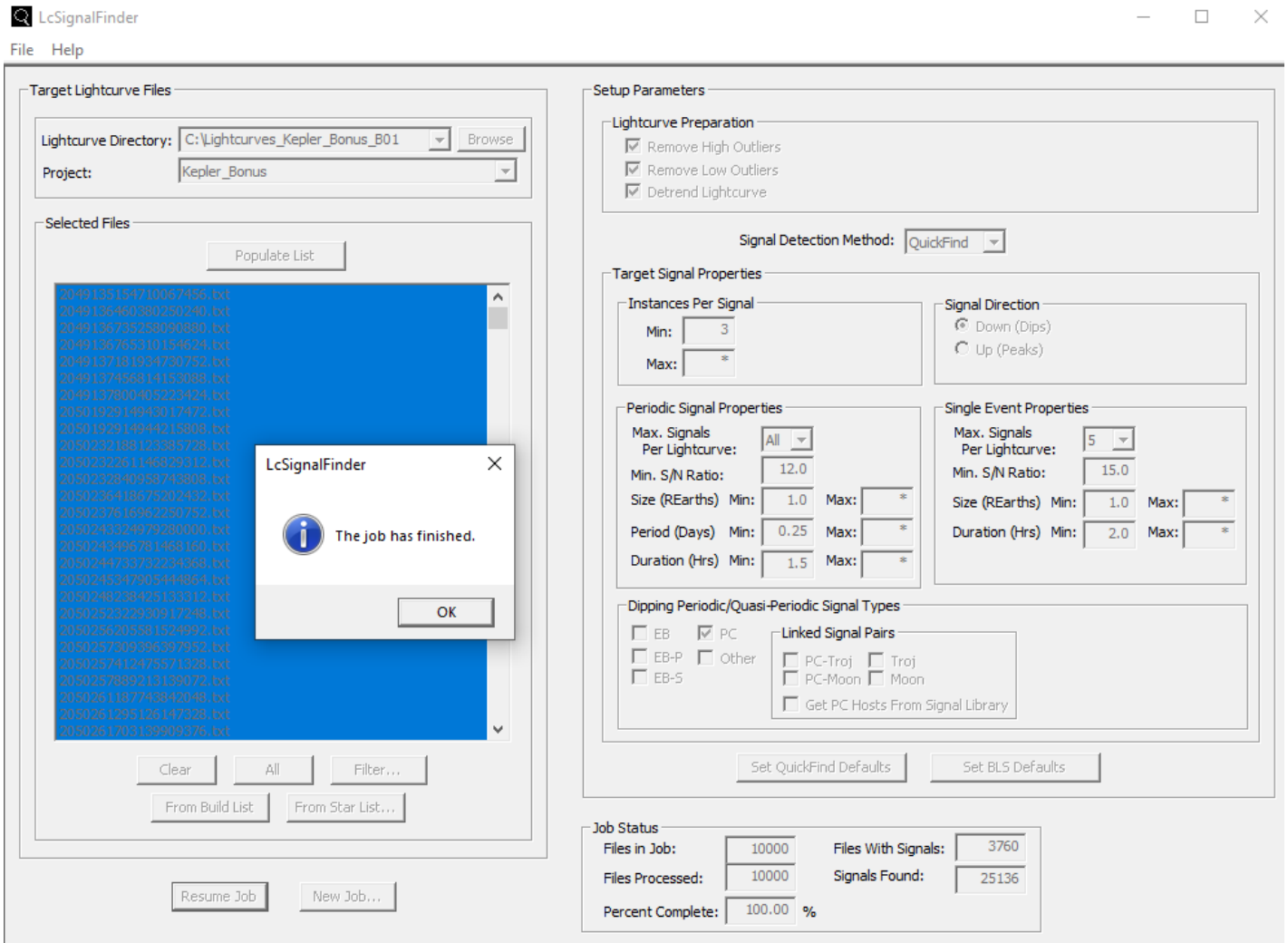


Figure 7.1.1: The interface of LcSignalFinder, after the data set had been analysed.

The analysis of this data set with the given parameters took some 12 hours to complete, and produced the following metrics; **Files with signals** - 3760, **Signals Found** - 25136. This result was then plotted for Object Size (R_{Earth}) vs Instances, to help visualise key areas of the data, shown through Figure 7.1.2. This highlighted that the majority of data was contained within the specific search window (1 - 2 R_{Earth}) that was desired and that exoplanets with fewer instances (0 - 20) were more prevalent.

Kepler_Bonus_B01 Full Report

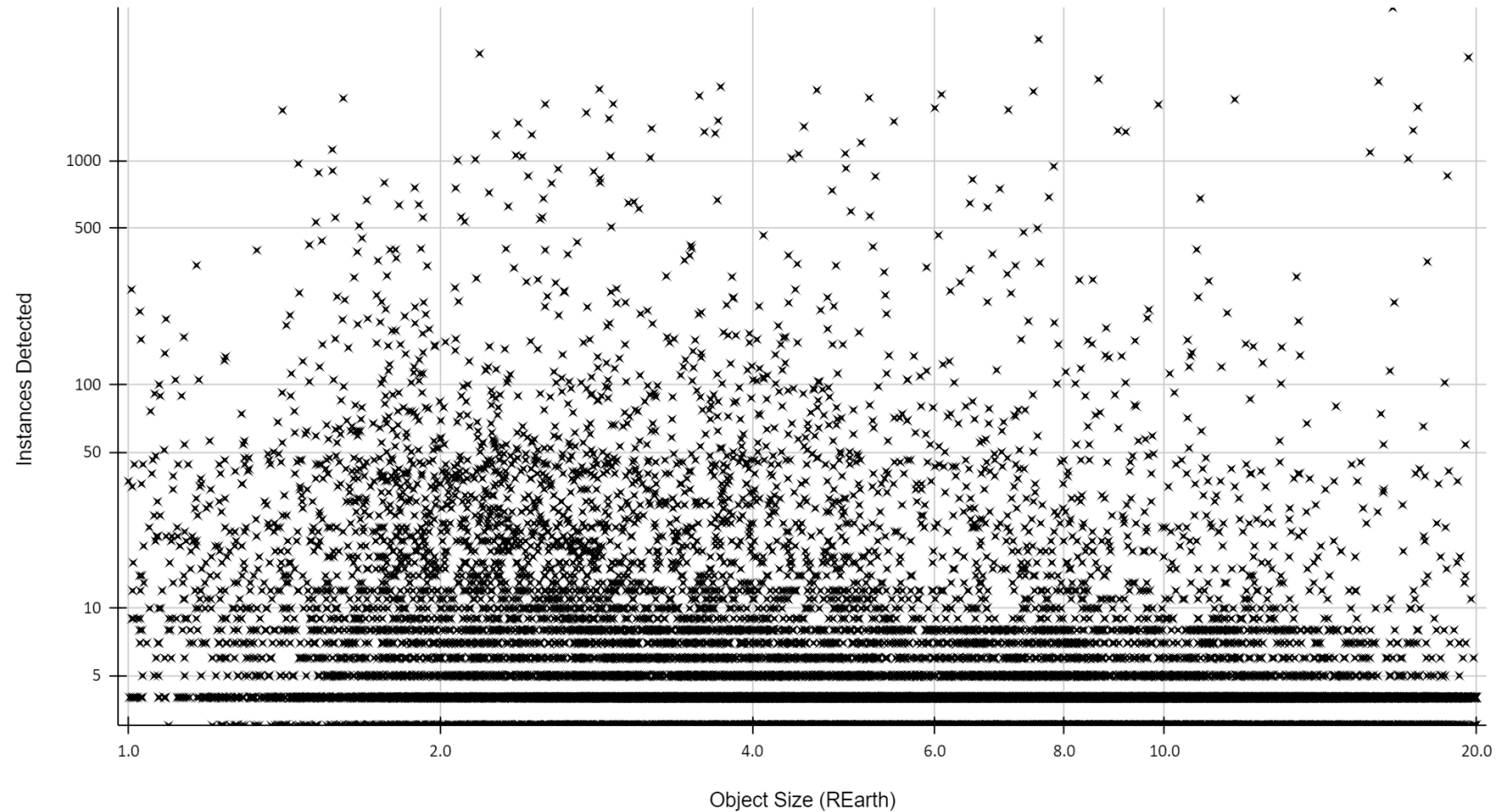


Figure 7.1.2: All 25136 signals found, plotted for Object Size (R_{Earth}) vs Instances.

Whilst the overall number of data files had been decreased, the volume of signals detected would require further reduction. This became possible through the use of LcReporter. This takes the results of LcSignalFinder and plots them into a report compatible with Microsoft Excel. This allows for great customisation of the parameters held by the found signals, through basic filtering methods, shown below in Figure 7.1.3.

As a result, it became possible to narrow down the data group for interrogation from 25,136 files, to just 114 files. This was achieved by filtering for the following parameters:

Transit Instances: Minimum 3 Instances, Maximum 5 Instances

Transiting Object Size: Between 1 - 2 R_{Earth}

S/N Ratio: Minimum value of 12, Maximum value of 13.

Transit Timing Variations : 0 - 3 TTVs (Split between 0, and 1 - 3 TTVs)

These parameters were specifically chosen, as they would highlight any short-period candidates through the use of a high number of minimum instances. A strict S/N ratio was chosen to try and eliminate as much background noise from the light curves as possible, making it easier to identify any exoplanet candidates. It would also cover the current ‘radius valley’ in exoplanet finds between 1.5 R_{Earth} and 2 R_{Earth} (*Gupta and Schlichting, 2019*). This is an area where relatively few exoplanets are found, with most exoplanets being either smaller, or larger than this particular radial size. There appears to be a physical constraint as to why few exoplanets of this size are found, although the mechanisms behind this are yet to be fully understood. For convenience, the overall subsample of 114 files was further split into two groups, that will henceforth be referred to as ‘Subsample A’ and ‘Subsample B’. Subsample A consists of 18 files, and Subsample B consists of the remaining 96 files. This split was necessary due to the TTV parameters which had been selected. It was necessary to divide the entire subsample between those files which contained a TTV trace (Subsample B), and those files which did not contain a TTV trace (Subsample A). This allowed for a greatly reduced

possibility of confusion between results and which filtering parameters the individual file had been subjected to. TTVs are the recorded differences between the expected orbital period of exoplanets, and the observed true orbital period. This could be an exoplanet transiting a short period (possibly as short as a few minutes) either earlier or later than anticipated should its orbital period have maintained perpetual stability. They are particularly useful because they help to add constraints onto the masses and eccentricities of exoplanets, or in some cases, even help to constrain the existence of non-transiting companions (*Leleu et al., 2021*).

Candidate Signals & TTVs Detected by LcSignalFinder in Lightcurve Directory 'C:\Lightcurves_Kepler_Bonus_B01'																
Host Star		Signal Properties							TTV Properties							
Star ID	Stellar Magnitude	Sign al Type	Epoch (BKJD)	Durati on (Hrs)	Period (Days)	Instanc es	Object Size (REarths)	Dept h (PP)	SNR Vs	TT Vs	Significa nt TTVs %	Significa nt TTVs %	Min TTV (Hrs)	Max TTV (Hrs)	Av TTV Mag (Hrs)	Lightcurve File
2051747663046115584	18.7	PC	895.975	4.904	287.558	3	1.6	3074	12.3	0	0.0%	0.0%	0.0	0.0	0.0	2051747663046115584.txt
2052683003834919680	18.8	PC	134.921	8.828	263.166	5	1.7	976	12.9	0	0.0%	0.0%	0.0	0.0	0.0	2052683003834919680.txt

Figure 7.1.3: Filters available for data files from initial analysis.

With highly condensed, manageable, and specified subsamples now ready, data interrogation could begin. LcTools enables the user to set up a specific work group, consisting of chosen files from LcReporter. This means that the subsamples selected could be specifically reviewed from the entire data set. It should be noted however, that the Star ID system used in LcTools follows the Gaia naming convention, as opposed to a specific KOI/KIC naming convention. For example, in Subsample A, the first file to be loaded was ‘Star 2051747663046115584’. This follows the Gaia convention, where it is labelled under ‘Gaia DR3 2051747663046115584’. Where possible, star ID’s have been cross referenced, and will be referred to through either their Kepler ID’s, Gaia ID’s, or their Two Micron All Sky Survey (2MASS) ID’s depending on the availability of stellar data.

8. Data Interrogation of Subsample A

Subsample A, consisting of 18 files, was analysed first, primarily due to its smaller size. This subsample contained those files which did not flag as having a TTV trace, as discussed above in Section 7.1. Figure 8.1 presents the files contained within Subsample A in relation to the detected object size vs the apparent signal duration in hours. It shows that within the dataset there was a trend of the smaller detected objects ($1.5 - 1.7 R_{\text{Earths}}$) having an average transit duration of 3 - 5 hours. This reflects well against the aim to search for short period exoplanets, that will typically be transiting at greater speeds due to their closer orbit, and greater gravitational interaction with their host star. The quicker an exoplanet is orbiting its host star, the less time it will spend (from the point of the observer) in front of the face of the star, and thus have a decreased transit signal duration. Notably though, whilst there are 18 files contained in Subsample A, there are only 16 unique files. This is because the files for Star 2052683003834919680, and Star 2082110397465409792 are duplicated. At first, it was believed this was due to an error in the way the search parameters had been set up, but it was revealed to be that the signals contained within them were so different from one another, that the software had automatically divided these results into two separate lines for convenience. Whilst Star 2052683003834919680 contained no signals of note, Star 2082110397465409792 will be discussed further in Section 9.

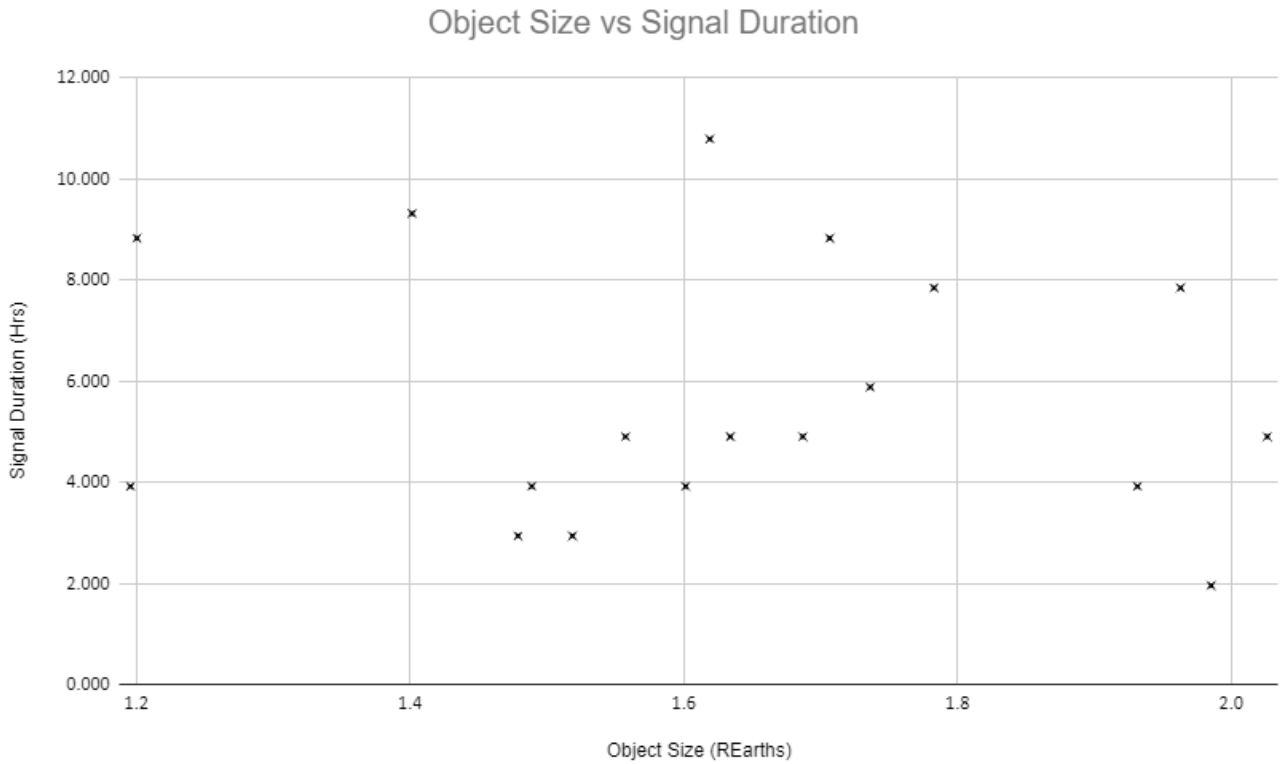


Figure 8.1: Data files from Subsample A plotted for *Object Size (R_{Earth})* vs *Signal Duration*.

All of the data files contained within Subsample A, aside from the two already mentioned above, contained no data that would be indicative of the presence of one or more exoplanets. All files here contained either false signals that had been marked by the search criteria, or a normal stellar flux line. The repeated false signals did raise an issue that was previously unknown until this point. By setting the parameters of search as they were (as discussed in Section 7.1), the search area was wide enough that any particularly substantial change in flux was being recorded as a potential transit event. This added a level of complexity to the data interrogation, as every event would now need to be manually verified. Whilst this was not a critical issue in how it would affect the running of the search, it did greatly increase the workload surrounding the data points.

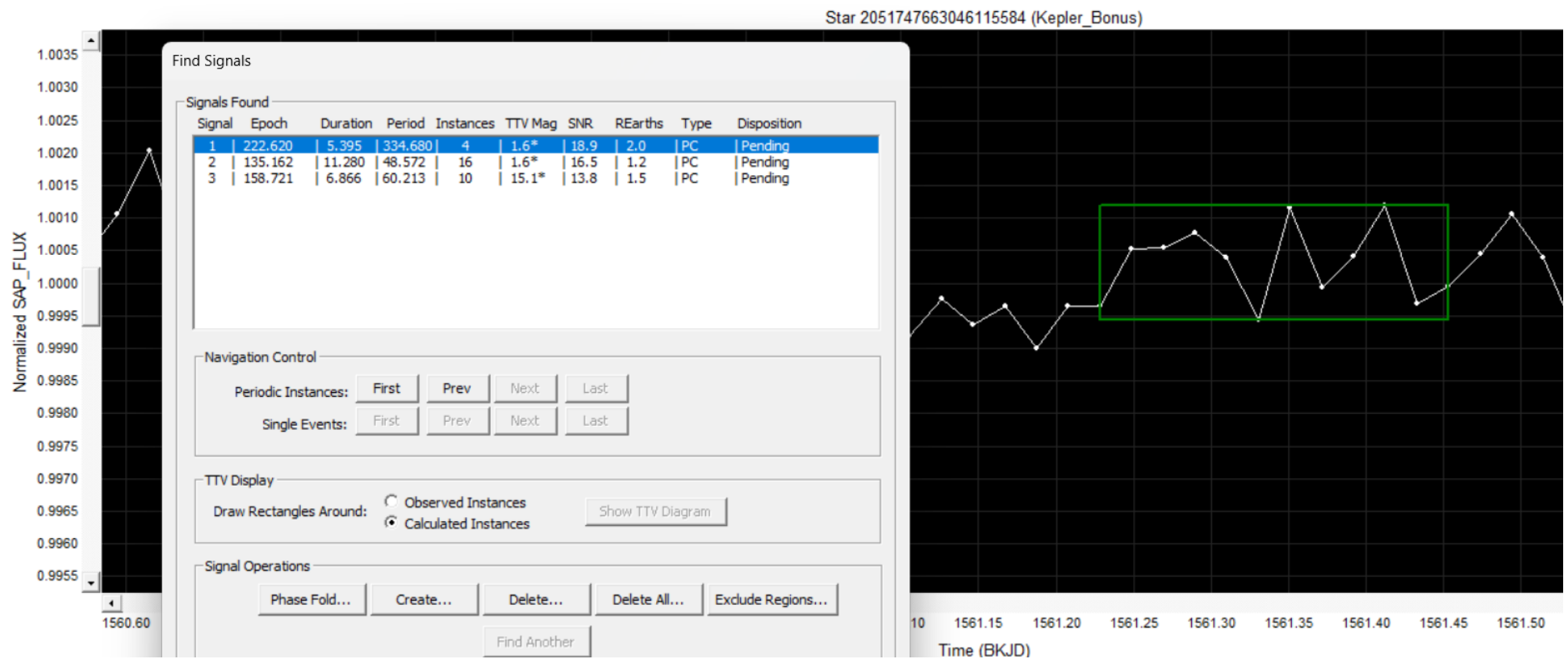


Figure 8.2: False positive event highlighted by software.

All star files contained within Subsample A, and their signal properties, can be found in Appendix E, Table E.1.

As an example of this, Figure 8.2 above shows how the software has recognised a potential transit event, but manual checking and verification clearly shows this as just a normal variation in the flux, but one that just so happened to meet the original search parameters, in this case due to the duration of the event. This would be a common theme throughout all the data files of Subsample A, and also those of Subsample B, so that even those individual files that did actually possess events of interest contained numerous false positive events. This does however, show the type of false positive event that was being initially searched for in Section 6.

8.1. Data Interrogation of Subsample B

Subsample B, was larger than Subsample A, and original thinking was that there would be greater potential to find a transit event of an exoplanet, due to the greater number of files available to contain such an event. The process of data interrogation was identical to that of Subsample A, with the search parameters kept constant. Figure 8.1.1 below shows the data set against object size vs the apparent signal duration, with a similar trend to Subsample A, in that $1.5 - 1.7 R_{\text{Earth}}$ sized objects have an average transit duration of 3 - 6 hours. Again, this fits well with the project's aims to look for short-period exoplanets.

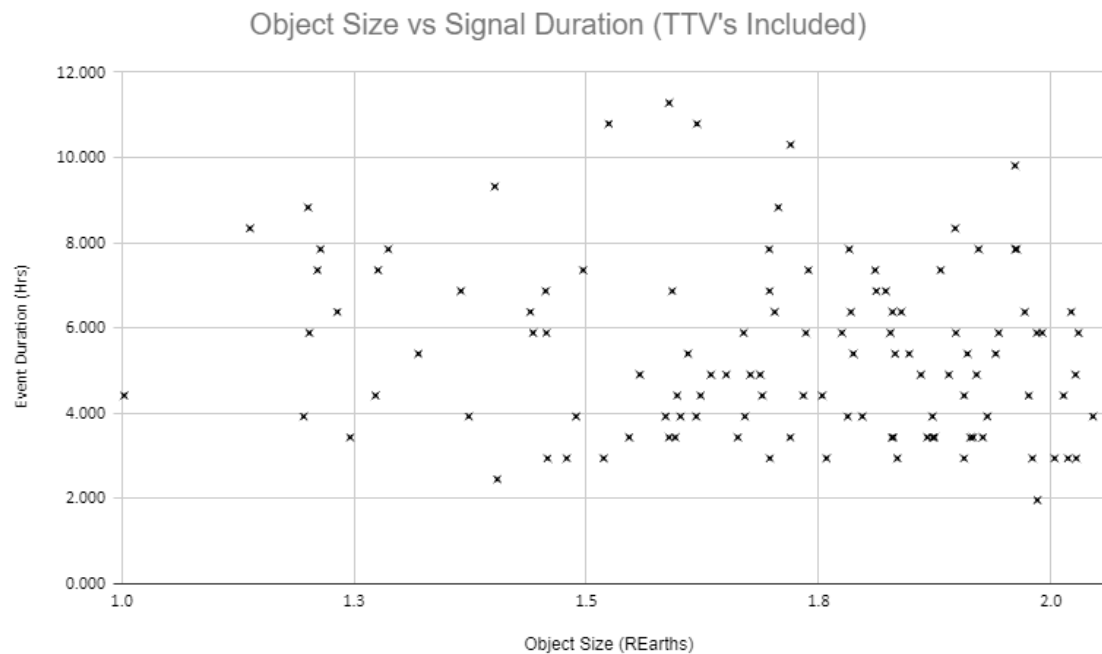


Figure 8.1.1: Data files from Subsample B plotted for Object Size (R_{Earth}) vs Signal Duration.

All star files contained within Subsample B, and their signal properties, can be found in Appendix F, Table F.1. It should be noted that for Figures 7.1.2, 8.1, and 8.1.1, these plots contain all the data available in the various sample sizes, including false positive signals. Each mark does not necessarily denote the presence of an exoplanetary signal, but without extensive manual verification of each file, it is difficult to differentiate which marks relate to potential candidates or false positives.

Subsample B consisted of 96 files, with 73 of these being unique. Again, this divide was caused by duplicate files being created from the way in which the software split different signals in each file. However, much in the same way that Subsample A had more blank results than positives, only one of the data files in Subsample B actually contained a verifiable single, and this will be discussed later, in Section 11. All files contained at least one false positive result, with most containing between 10 and 100 false positive signals. These were primarily from normal flux variations meeting the wide set criteria of the signal search, with duration of flux variation being the most common factor. The light curve for one such example of this (Star 2079536131512017024), is contained within Appendix B. During the analysis of Subsample B, an example of a typical flux line was encountered, that visualised well a typical result once false positives were disregarded. This was Star 2077594982383871488, and its light curves can also be found in Appendix B. One file was found with an anomalous light curve that had regularly repeating flux variations, but with an upwards trend. Typically, any transit would create a decrease in the flux levels reaching the observer, but this particular star (2085565548335557504), had periodic increases in flux of between +0.015 and +0.04, as shown below in Figure 8.1.2. Whilst the actual level of flux increase is not particularly extreme, the periodicity of the increase is unusual. The period between each increase of flux at a level of +0.015 is 5.2 days (\pm 0.1 days), and the period between each increase of flux and a level of +0.04 is 5.4 days (\pm 0.2 days). The pattern loosely resembles that of a binary star system, which typically has one small spike, and one large spike, but these are always in a flux decrease, not increase. The exact mechanism behind the pattern is not known, and Section 12 will look to suggest ways in which the mechanism can be determined.

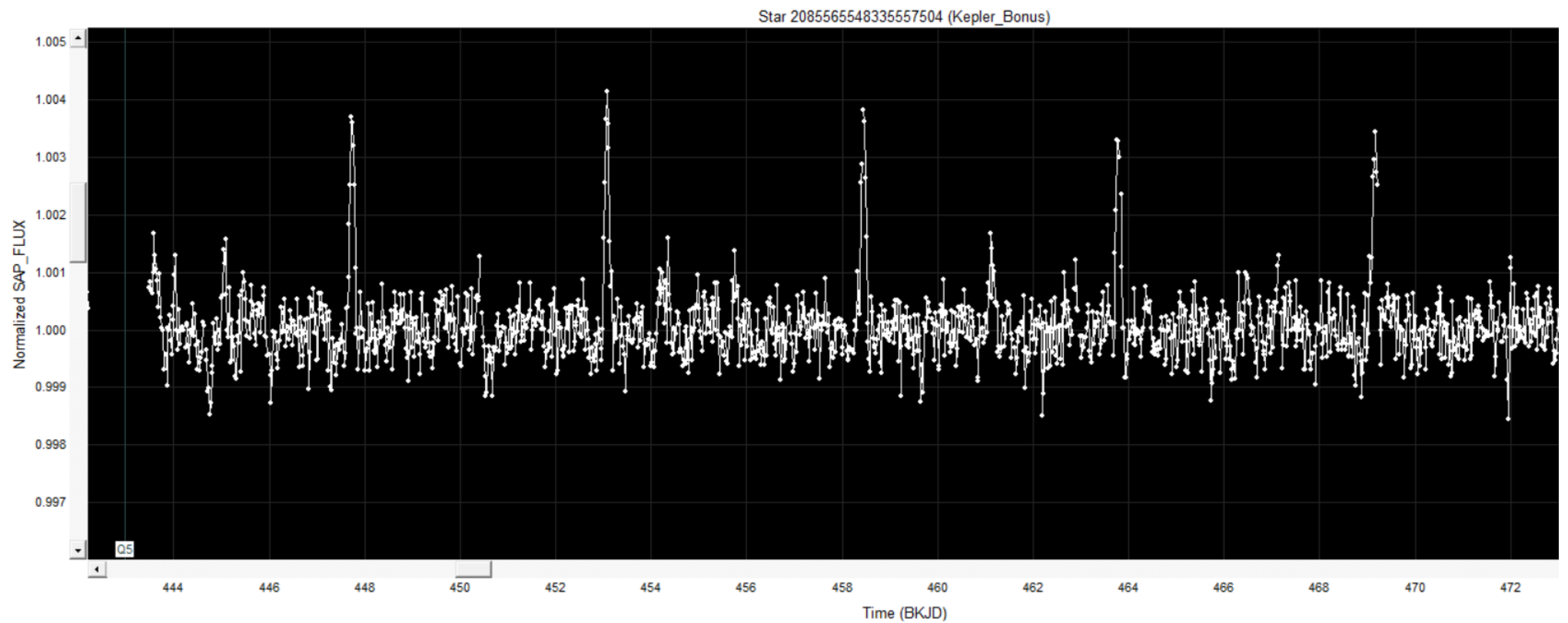


Figure 8.1.2: Unusual periodic flux increases in the light curve of Star 2085565548335557504

9. Presentation of New Binary Star System

Subsample A did contain one file of considerable note. Analysis of the light curve for Star 2082110397465409792 clearly showed that it is a binary star system, which appears to not have been previously documented. Given that the data file for this light curve followed the Gaia naming convention, the first step to corroborate the find was to try and cross-reference the ID of the star. By accessing the Gaia archive ('*Gaia ESA Archive*', 2024), and entering the star number, it becomes possible to determine the coordinates of the star submitted. These coordinates can then be entered into the IRSA catalogue ('*IRSA: WISE*', 2024) to determine the star's location in the night sky, and what imagery, and spectral analysis is available. IRSA will also provide any alternative ID's, should the star be identifiable. With the star's coordinates entered into IRSA, the location is revealed as highlighted below in Figure 9.1:

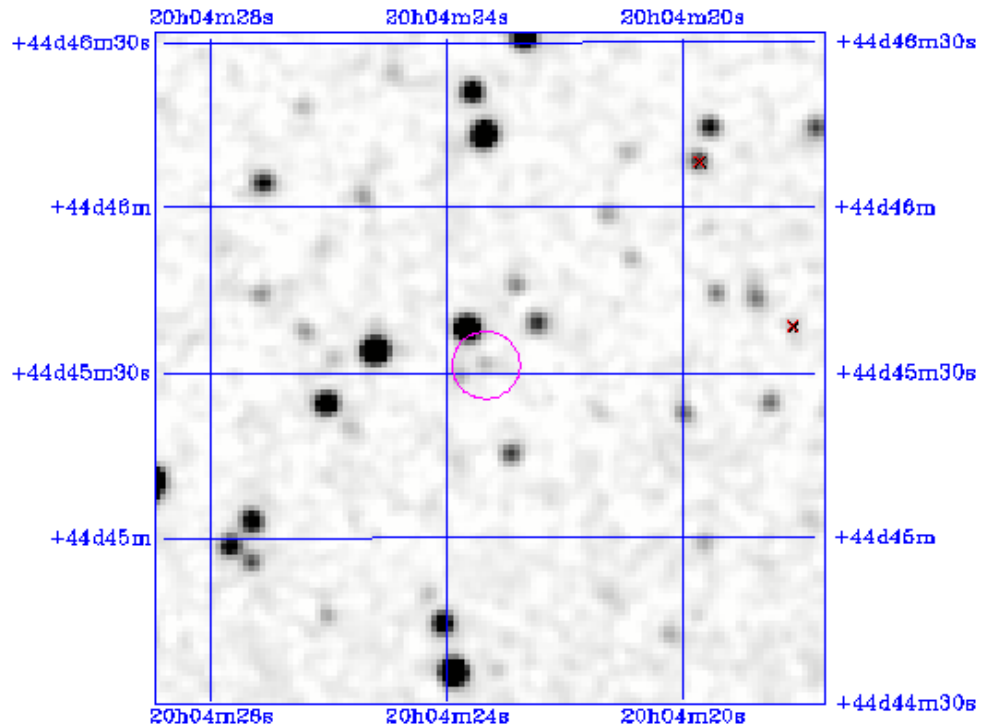


Figure 9.1: Map denoting the position of Star 2082110397465409792

As demarcated by the crosshair in Figure 9.2 ('*WorldWide Telescope*', 2024), this places the star within the Cygnus constellation, which is highlighted via the red lines. This means that the star was first observed by the original KST mission, rather than when it was in its K2 extension phase, as discussed in Section 3. IRSA also revealed that the star is filed in the 2MASS catalogue, under the ID '2MASS 20042333+4445313'. With the stars ID revealed, further imagery could be sourced on IRSA, resulting in J, H, K and 3 Colour band images all being available, and shown below in Figure 9.3.

Again, the crosshair determines the position of 2MASS 20042333+4445313 in relation to its stellar neighbours.



Figure 9.2: The position of Star 2082110397465409792 in the Cygnus constellation

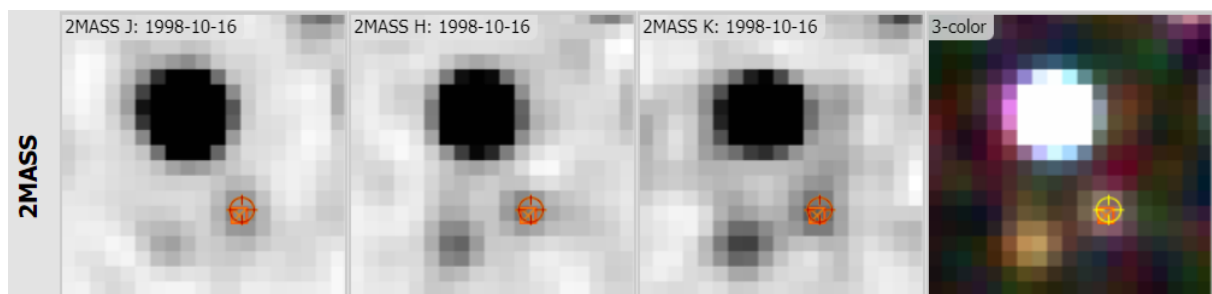


Figure 9.3: J/H/K and 3-Colour band imagery of 2MASS 20042333+4445313. (2MASS Image Results, 2024)

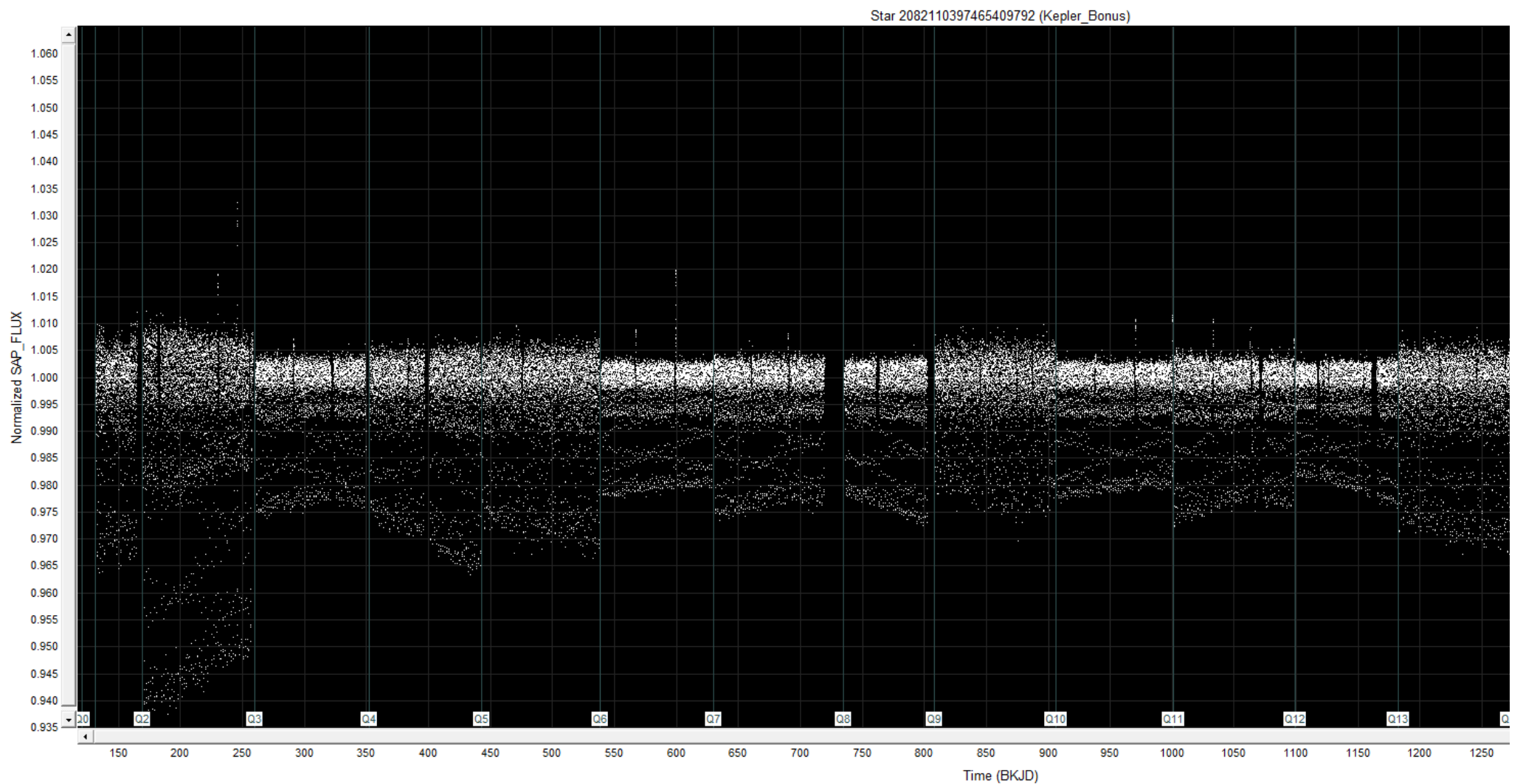


Figure 9.4: Detrended light curve of 2MASS 20042333+4445313.

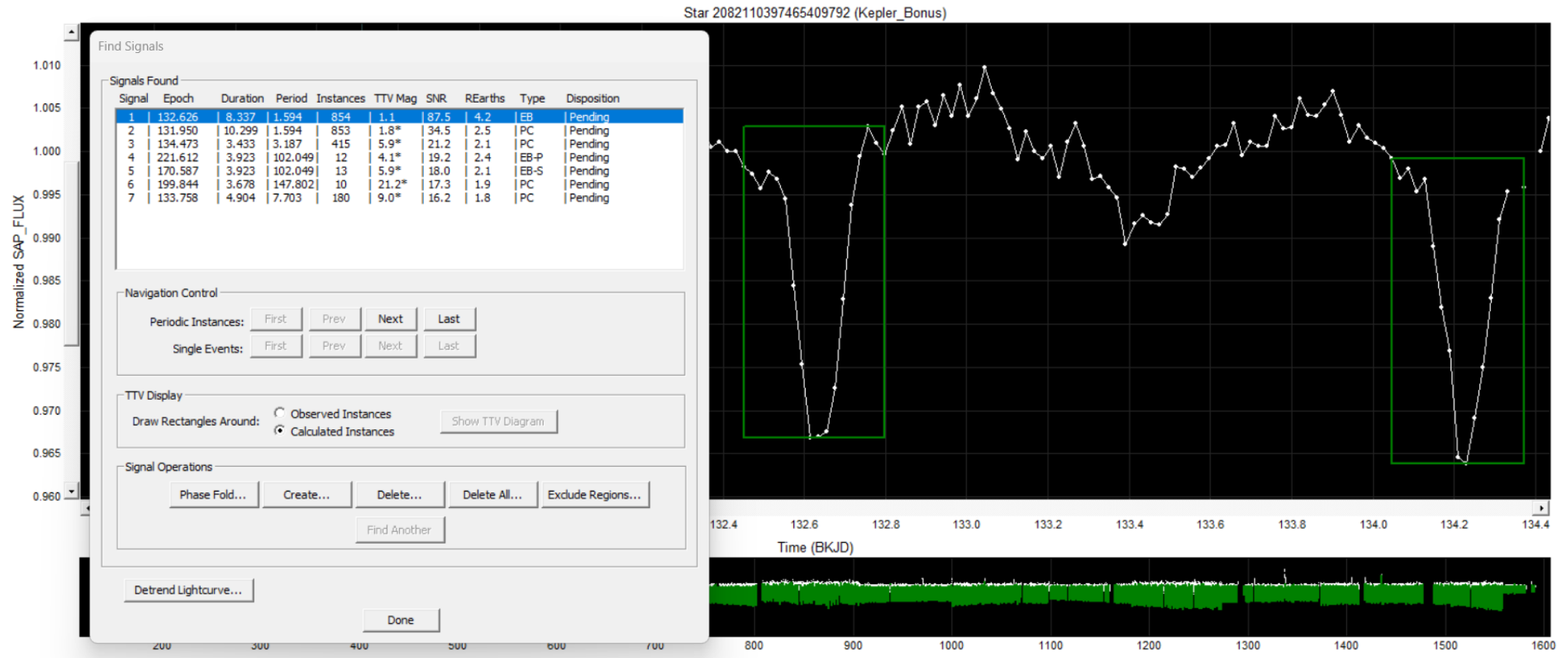


Figure 9.5: Signal search in the light curve of 2MASS 20042333+4445313.

Next, it became advantageous to see if additional research material could be found for 2MASS 20042333+4445313, to determine if the star has previously been documented in relation to the KST. The simplest way to achieve this, is to enter the Star ID into the Exoplanet Archive (*'NASA Exoplanet Archive'*, 2024). This site contains an entire breakdown of all Kepler candidates, and stellar data from where the candidates are located. As shown in Figure C.7 and Figure C.8 in Appendix C, whilst the Star ID was recognised, (in both Gaia and 2MASS convention), no data was possessed by the archive as shown by Figure C.9, also in Appendix C. Appendix C further contains precise positional data for 2MASS 20042333+4445313.

With the binary star system now located in the night sky, the reasoning for the decision to label it as such a star system will be presented. The detrended light curve for 2MASS 20042333+4445313 is shown above in Figure 9.4, with the raw file available in Appendix C (Figure C.1). It is immediately apparent that there are consistent, periodic dips in the flux. Planned procedure was followed, and even with visual clues that strong transit events were to be found, a signal search was still performed, as shown in Figure 9.5.

Unlike the rest of the files contained within Subsample A, none of the signals detected were labelled as false positives, and thus manual checking and verification was primarily used to confirm the presence of these flux dips along the entire length of the light curve. All signals had a uniform shape, and there were two distinct flux decreases on show. These shall now be referred to as ‘Transit Event A’, and ‘Transit Event B’ for clarity. Transit Event A was the largest event and saw a flux decrease of -0.037% at its greatest, and -0.022% at its least extreme, from a baseline of 100% flux. Transit Event B saw decreases in the flux ranging from -0.012% to -0.007%. From these variations in flux, it can be determined that Transit Event A is caused by the largest of the two stars, and that Transit Event B was caused by the smaller of the two stars. Being larger, Transit Event A will cause greater eclipses in the light curve as it passes between the star of Transit Event B and the observer, and vice versa. Transit Event A occurred every 1.6 days (\pm 0.035 days), and Transit Event B occurred every 1.6 days (\pm

0.030 days). This can be seen in Figure C.5 and Figure C.6 in Appendix C. Figure 9.6 below, shows the stellar properties of 2MASS 20042333+4445313, however it is unclear if these properties relate to the stars in Transit Event A or in Transit Event B. Whilst the data is limited, a radius of $0.256 R_{\odot}$ and a temperature of 3327K, would propose a preliminary description of these stars (or at least one of these stars) being an M Dwarf. These are the most common type of star in the universe, and are known to be of lower mass than our own Sun, and much less luminous ('M-dwarf mirage – Exoplanet Exploration: Planets Beyond our Solar System', 2014).

Stellar Properties	
Star ID:	2082110397465409792
Mag:	18.9
Temp:	3327 K
Radius:	0.256 Sols
Mass:	N/A Sols
Distance:	421.67 Parsecs
RA:	301.097164 Degrees
Dec:	44.758822 Degrees
Metallicity:	N/A
OK	

Figure 9.6: Stellar properties of 2MASS 20042333+4445313

With minimal data available, narrowing the classification band of these M Dwarfs was not possible within the confines of this paper, with Section 12 outlining possible future research avenues to rectify this. As discussed previously in Section 6, a phase fold would highlight any subtleties in the light curve, whilst providing confidence in the data, as it would allow any anomalies to be highlighted. Figure 9.7 Below is the phase fold curve of Transit Event A, and Figure 9.8 is the phase fold of Transit Event B, with both curves being measured in a period of days.

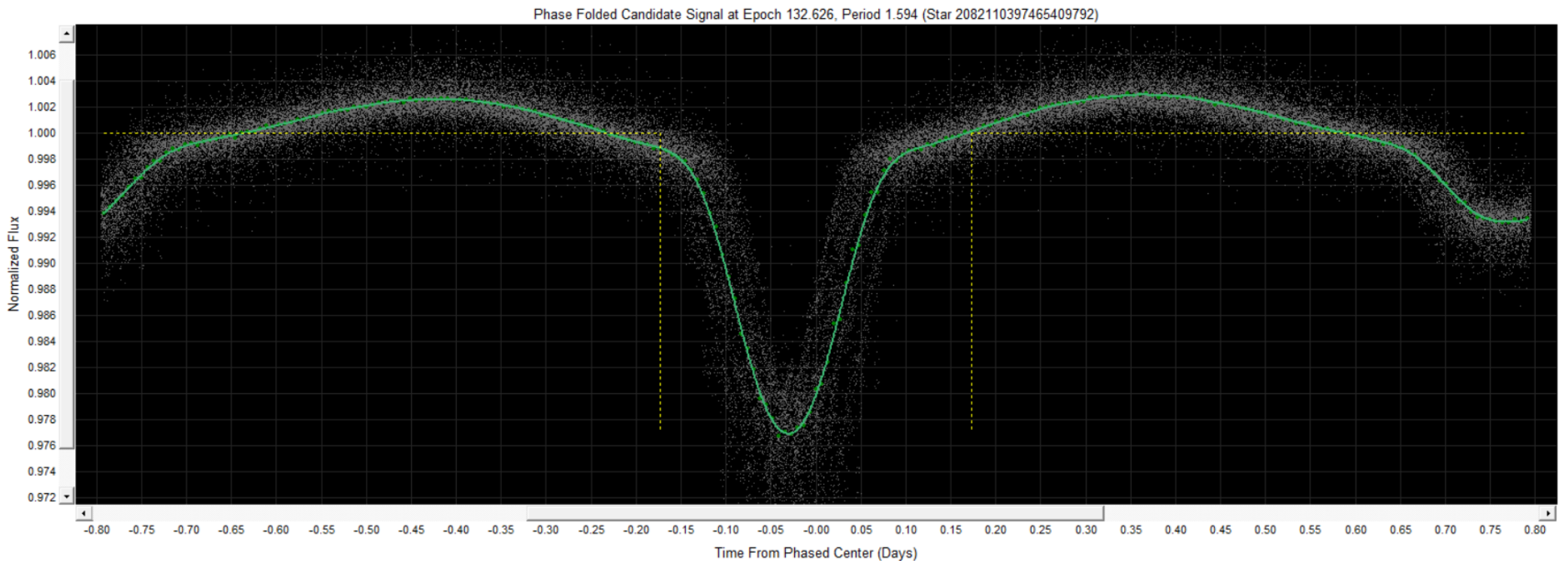


Figure 9.7: Phase fold curve of Transit Event A

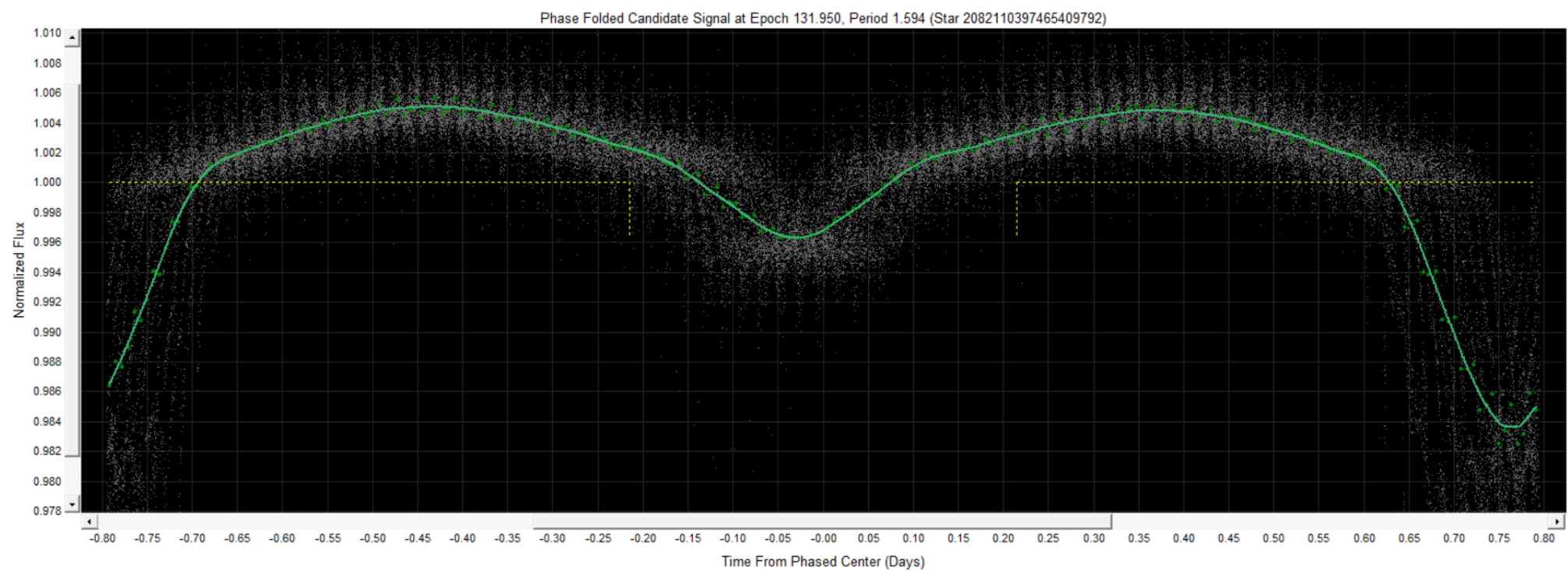


Figure 9.8: Phase fold curve of Transit Event B

It is clear to see from these curves, that there is a high level of data robustness, with no discernable data points being anomalous outliers. Both flux decreases are clearly visible, and highlight well the strength of these decreases, despite their relatively small percentage at a baseline of 100% flux. These curves provide a high level of confidence that these decreases are caused by the repeating transits of a binary star system, and not external phenomena such as exozodiacal or interstellar dust, comets, or exoplanets, nor from the tracking, pointing or reorienting of the KST itself.

10. Presentation of New Exoplanet Candidates

As described in Section 8.1, due to the larger number of files available to analyse in Subsample B, original thinking was that there was greater opportunity to detect exoplanet signatures in at least one light curve. This came to fruition in the file for Star 2077415590199401728. However, there were immediate difficulties with trying to locate this star in order to be able to determine any cross-ID's that were available. Whilst IRSA ('IRSA: WISE', 2024) was able to provide a positional image based on the coordinates provided by LcTools stellar data (Figure 10.1), closer inspection of this region highlighted an issue.

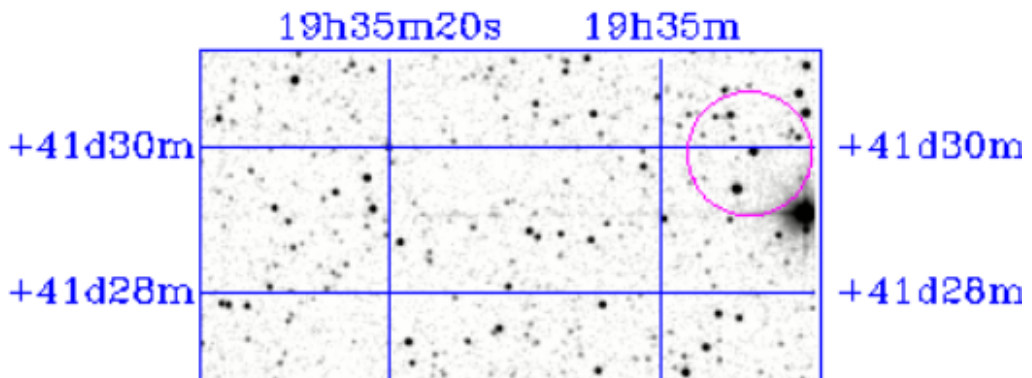


Figure 10.1: Map denoting the position of Star 2077415590199401728.

As seen in the 2MASS imagery in Figure 10.2, the coordinates correspond to an area to the left (rounded crosshair) of 2MASS 19345313+4129556, which is marked by the crossed square. The

extremely close proximity of these two marks made it initially difficult to determine whether the coordinates relate to this main foreground star, or a separate object.

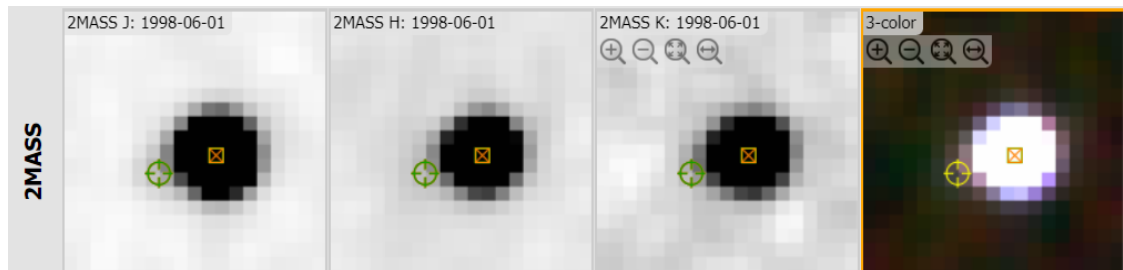


Figure 10.2: *J/H/K and 3-Colour band imagery of Star 2077415590199401728. (2MASS Image Results, 2024)*

Gaia imagery however, clearly shows a distended area to the background and left hand side of 2MASS 19345313+4129556, as marked by the pink crosshair in Figure 10.3. Therefore, whilst no cross-referencing of ID is available due to Gaia and IRSA recognising only 2MASS 19345313+4129556, it can be maintained that Star 2077415590199401728 is indeed a separate object. This is further confirmed by the Gaia archive having separate, and more complete data for 2MASS 19345313+4129556, as shown by Figure 10.4 and Figure 10.5.

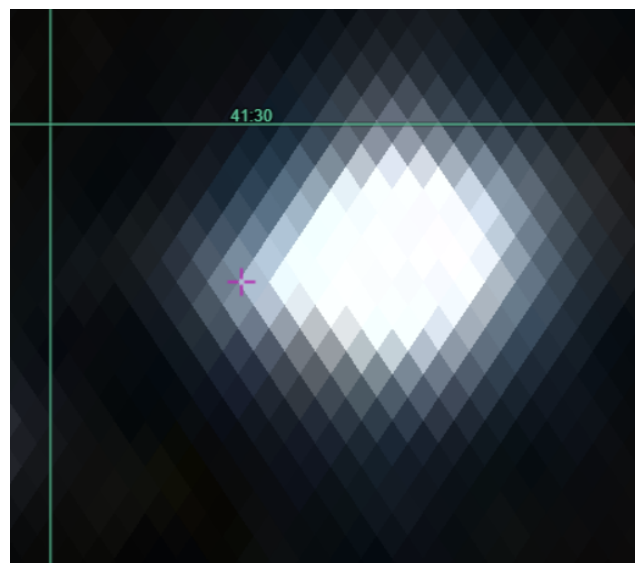


Figure 10.3: *Gaia imagery of Star 2077415590199401728 at a FOV of 28" x 23" ('Gaia ESA Archive', 2024)*

Gaia DR3 2077415590199401088

Astrometry	Photometry	Spectroscopy	Astrophysical parameters
Description	Value		Unit
Object type	star with 99.97% probability		
T _{eff}	5663 [5659, 5672]		K
log(g)	4.335 [4.329, 4.341]		log(cm s ⁻²)
[M/H]	-0.079 [-0.085, -0.070]		dex
A _G	0.0652 [0.0623, 0.0699]		mag
E(BP-RP)	0.0348 [0.0333, 0.0374]		mag
d(GSP-Phot)	539 [535, 542]		pc

Figure 10.4: Gaia data for 2MASS 19345313+4129556. ('Gaia ESA Archive', 2024)

Gaia DR3 2077415590199401728

Astrometry	Photometry	Astrophysical parameters
Description	Value	Unit
Object type	star with 100.00% probability	
T _{eff}	5247 [5227, 5267]	K
log(g)	4.769 [4.750, 4.785]	log(cm s ⁻²)
[M/H]	-3.601 [-3.780, -3.260]	dex
A _G	0.0357 [0.0175, 0.0474]	mag
E(BP-RP)	0.0197 [0.0096, 0.0262]	mag
d(GSP-Phot)	1733 [1715, 1749]	pc

Figure 10.5: Gaia data for Star 2077415590199401728. ('Gaia ESA Archive', 2024)

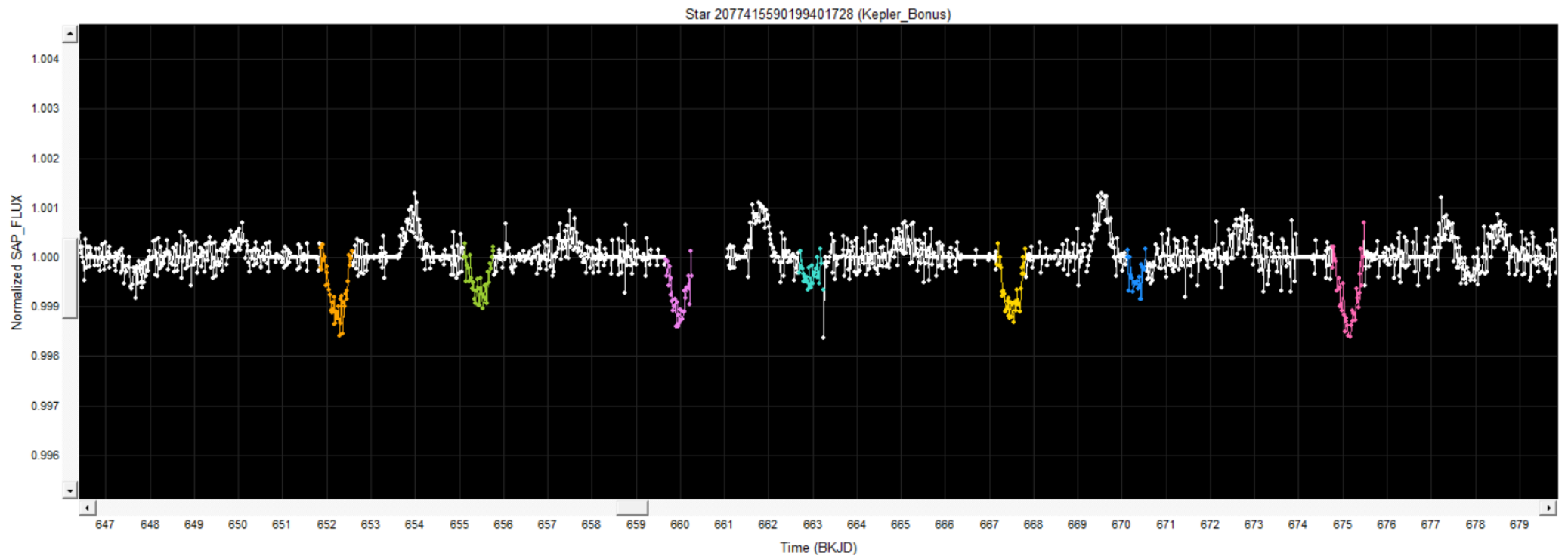


Figure 10.6: Exoplanet transits in the light curve of Star 2077415590199401728.

With Star 2077415590199401728 now confirmed as a separate object, it becomes possible to freely present the case for new exoplanet candidates found orbiting around this star. As with all other data files, the process of analysis was as follows: Opening of light curve, detrending of data, signal search performed and manual verification of signal search results. Figures D1 through D5 can be found in Appendix D, to highlight that these steps were undertaken with Star 2077415590199401728. With these steps concluded, the light curve for Star 2077415590199401728 suggests that it is orbited by two exoplanets. The first of these, hereby referred to as 1728a, is measured by LcViewer as being approximately $2.2 (\pm 0.2) R_{\text{Earth}}$, and the second, hereby referred to as 1728b, is measured at $1.6 (\pm 0.2) R_{\text{Earth}}$. These sizes are at the higher end of the radius valley, as described previously in Section 7.1. The orbital period was determined to be 7.66 days for 1728a, and 7.35 days for 1728b. Figure 10.6 below clearly shows these transit events within the light curve, but colour has been added to further highlight them, for convenience and ease of viewing. Using data from LcTools, determination of other properties of these exoplanets and their host star has been possible, as well as confirming some data (namely planetary radius) from LcTools. These are laid out in Section 11.

However, whilst the light curve of Star 2077415590199401728 does show two clear transit events, it also possesses unusual upward trending events. These occur most prevalently immediately prior to the transit of 1728b, and after the transit of 1728a. Two such examples are contained below, in Figure 10.7 and Figure 10.8.

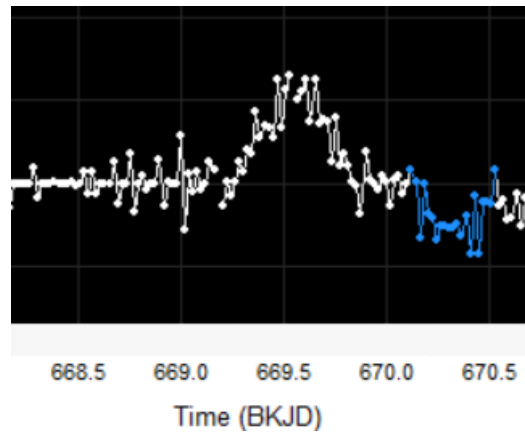


Figure 10.7: Flux increase in the light curve of Star 2077415590199401728.

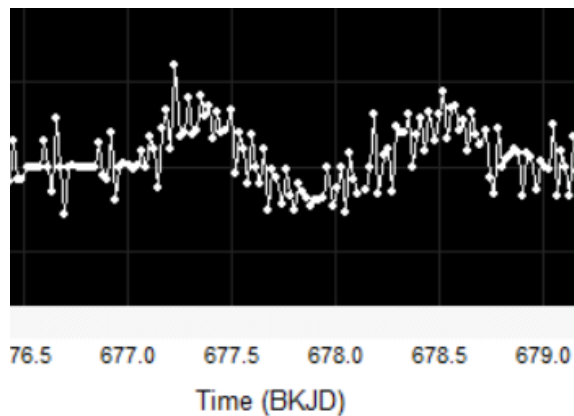


Figure 10.8: Secondary flux increase in the light curve of Star 2077415590199401728.

Given how unusual these upward trending curves are, it was an immediate priority to try and determine the mechanism behind them. It is Figure 10.8 that provides the largest clue. The dip in flux, followed by a routine increase, is something that the work of (*Van Kooten et al., 2020*) looked to determine. Their findings show that these patterns are caused by the forward scattering of light, as a result of the transiting of dust particles around a host star. This concept is visualised below in Figure 10.9.

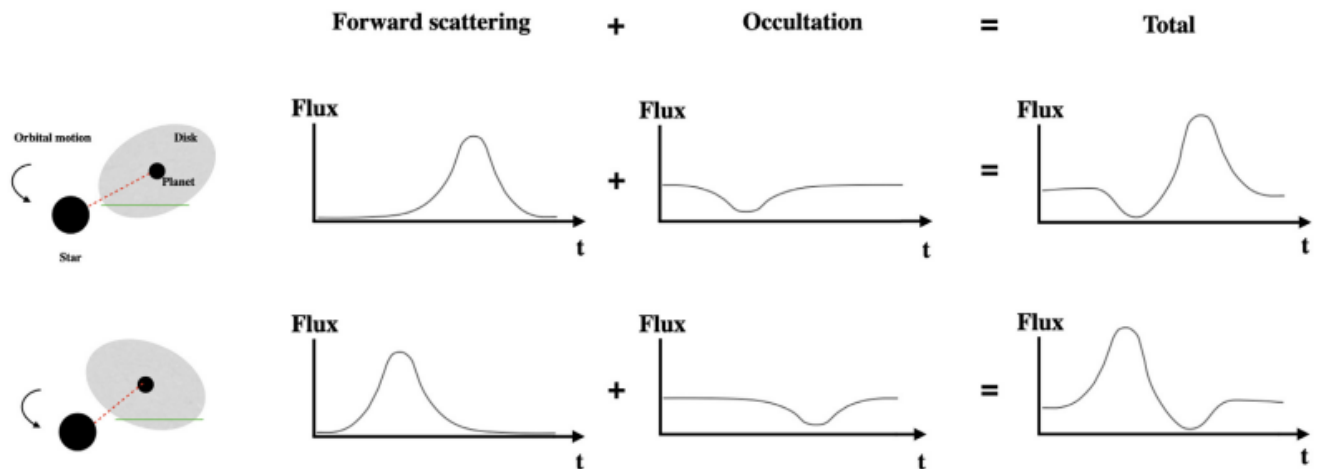


Figure 10.9: Forward scattering of light due to dust, in a light curve. (*Van Kooten et al., 2020*)

Further, the work of (*Wheeler and Kipping, 2019*), suggests that periodic increases in flux may be a result of exoplanetary rings, or exoplanets that are disintegrating or having their atmospheres evaporated, causing a similar scattering in starlight. Their findings also suggested that some of these flux increases were a result of processing artefacts in the light curve, and not actually due to any of the factors listed above. A visualisation of one such flux increase is shown below in Figure 10.10.

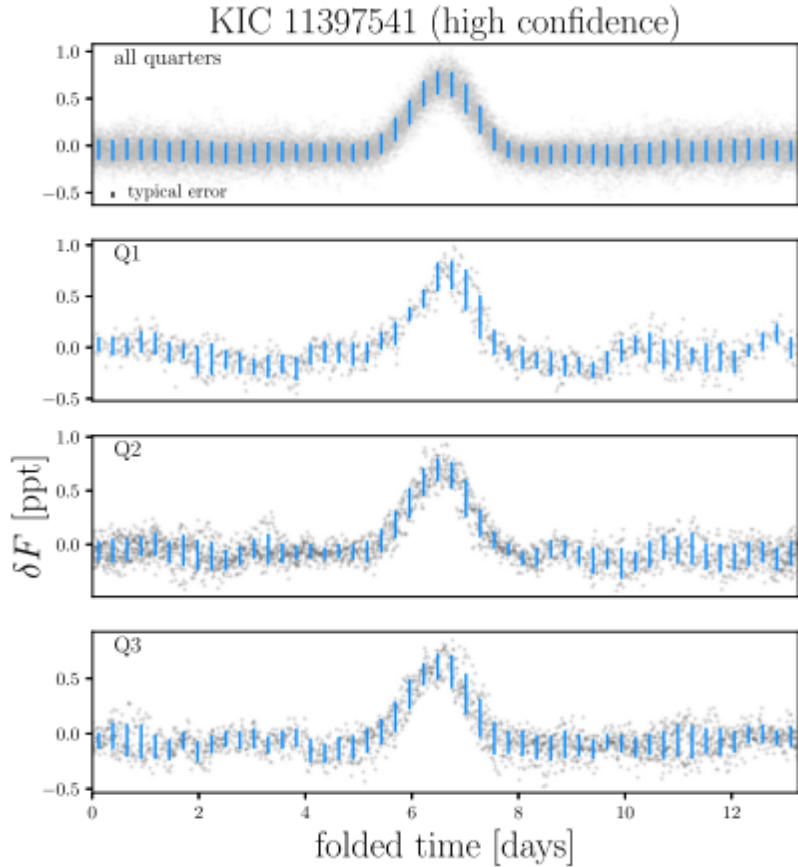


Figure 10.10: Flux increase in the light curve of KIC 11397541. (*Wheeler and Kipping, 2019*)

It would seem likely then, that these flux increases are either as a result of processing issues in the raw data of the light curve, or some form of interaction between the light of Star 2077415590199401728 and dust particles. What form these dast particles are in, whether that be in a dense cloud, or scattered rings, is not yet possible to determine. It was not possible to determine the true cause of these increases within the confines of this paper, and as such, further research is proposed in Section 12.

11. Calculations of Stellar and Planetary Characteristics

This section focuses on the calculations done to try and determine both the robustness of the measurements and data provided by LcViewer, as well as new characteristics about the exoplanet candidates and Star 2077415590199401728.

Candidate 1728a Radius:

$$R_p = \sqrt{R_s^2 \times \frac{\text{Transit Depth}}{100}} = R_p = \sqrt{0.526^2 \times \frac{0.1572}{100}} = R_p = 0.0208 R_\odot$$

$$R_\odot = 109 R_{\text{Earth}} = R_p = 0.0208 \times 109 = R_p = 2.267 R_{\text{Earth}}$$

Candidate 1728b Radius:

$$R_p = \sqrt{R_s^2 \times \frac{\text{Transit Depth}}{100}} = R_p = \sqrt{0.526^2 \times \frac{0.1035}{100}} = R_p = 0.0016 R_\odot$$

$$R_\odot = 109 R_{\text{Earth}} = R_p = 0.0016 \times 109 = R_p = 1.744 R_{\text{Earth}}$$

These calculations compare favourably to the figures of LcTools, which showed 1728a as having a radius of $2.2 (\pm 0.2) R_{\text{Earth}}$, and 1728b as having a radius of $1.6 (\pm 0.2) R_{\text{Earth}}$. To determine the orbital distances of these exoplanets, a derivation of Kepler's Third Law was required, as shown below:

$$T^2 = \left(\frac{4\pi^2}{GM_s}\right)d^3 = d = \sqrt[3]{\frac{GM_s}{4\pi^2} \times T^2}$$

‘T’ was already known through LcViewer measurements as being 7.66 days for 1728a, and 7.35 days for 1728b, and thus it was possible to convert this into seconds as part of the determination of the orbital period.

Candidate 1728a Orbital Distance:

$$d = \sqrt[3]{\frac{GM_S}{4\pi^2} x T^2} = d = \sqrt[3]{\frac{(6.67 \times 10^{-11}) x (1.23 \times 10^{30})}{4\pi^2} x (661824)^2}$$

$$d = 9691375276 \text{ m} = \textcolor{blue}{d = 0.064 \text{ AU}}$$

Candidate 1728a Orbital Distance:

$$d = \sqrt[3]{\frac{GM_S}{4\pi^2} x T^2} = d = \sqrt[3]{\frac{(6.67 \times 10^{-11}) x (1.23 \times 10^{30})}{4\pi^2} x (635040)^2}$$

$$d = 9428106013 \text{ m} = \textcolor{blue}{d = 0.063 \text{ AU}}$$

These orbital distances seem somewhat anomalous, as aside from the slight separation in the actual timing of these transits, it would imply that these exoplanet candidates are on an almost identical orbital plane. Further, given that the orbital period for 1728b is shorter than that of 1728a, at some point in the future they would actually begin to affect one another's orbits, possibly to the extent of degradation and then destruction when the Roche limit is approached. Further work needs to be conducted in order to determine the true orbital distances of these candidates, and this is suggested in Section 12. The above calculations uses the mass of Star 2077415590199401728, which was calculated as below:

Mass of Star 2077415590199401728

$$L_{\odot} = 3.846 \times 10^{26} \text{ W}$$

$$L_{Star} = 7.105 \times 10^{25} \text{ W}$$

$$M_{Star} = L \frac{1}{3.5}$$

$$M_{Star} = 0.1847 L_{\odot} \times \frac{1}{3.5}$$

$$\textcolor{blue}{M_{Star} = 0.617 M_{\odot}}$$

This calculation made use of the luminosity and magnitudes of Star 2077415590199401728, which were calculated below, and made use of the stellar data within LcViewer. Apparent and Absolute Magnitudes were calculated from the given apparent magnitude of 17.8 (see Figure D7 of Appendix D), and the given stellar distance of 1733.39 parsecs (pc), also in Figure D7 of Appendix D.

Apparent and Absolute Magnitudes of Star 2077415590199401728

$$m - M = 5 \times \log\left(\frac{d}{10}\right)$$

$$m = 17.8$$

$$M = m - 2.5 \log\left(\frac{d}{10}\right)^2$$

$$M = 17.8 - 2.5 \log\left(\frac{1733.39}{10}\right)^2$$

$$\textcolor{blue}{M_{Absolute} = 6.6}$$

Luminosity of Star 2077415590199401728

$$M = -2.512 \log_{10}\left(\frac{L}{L_\odot}\right)$$

$$\frac{M}{-2.512} = \log_{10}\left(\frac{L}{L_\odot}\right)$$

$$L_{Star} = L_\odot \left[10^{\frac{-M}{2.512}} \right]$$

$$L_{Star} = (3.0128 \times 10^{28}) \times \left(10^{\frac{-6.6}{2.512}}\right)$$

$$\textcolor{blue}{L_{Star} = 7.105 \times 10^{25} W}$$

$$\textcolor{blue}{L_{Star} = 18.47\% L_\odot}$$

12. Conclusion and Future Research Avenues

To conclude, this paper has presented the case for both a new binary star system, and new exoplanet candidates, and met the aims laid out in Section 4 well. With the detected exoplanet candidates being $2.267R_{\text{Earth}}$ and $1.744R_{\text{Earth}}$, in size, they fit well within the radius valley, although future research will be crucial to determine the accuracy of these findings, as well as reveal further information. The binary star system comprises at least one M Dwarf star, with its light curve giving rise to high confidence in the detection, due to its characteristic shape of one large, one small flux decrease.

Referring to Star 2077415590199401728, future research should focus on follow up observations to determine whether these truly are exoplanet transits, or are false positive events. If they are found to be false positives, they can then be used as reference points for future research projects, and be listed appropriately in the Exoplanet Archive (*'NASA Exoplanet Archive'*, 2024). However, in the case where they are confirmed to be exoplanets, through using other detection methods such as Direct Imaging or Radial Velocity (see Section 1.1.2), then those same methods can be used to determine their true masses, radii, and orbital periods. Particular interest should be applied to the determination of these candidates' orbital periods, as the findings in Section 11, imply that these candidates are essentially next to each other in their orbital plane, and would be in danger of future collision given the slight variation in orbital times. Spectrographic measurements should then be taken to determine if any atmosphere is present on either candidate. Regardless of secondary research confirming (or otherwise), the presence of exoplanets around Star 2077415590199401728, they and the star itself should be given proper identification (KOI number) in the Kepler catalogue. Further, as noted in Section 10, this paper was not able to determine whether the cause of the flux increases seen in the light curve of Star 2077415590199401728 were as a result of processing errors in the light curve, or through the interaction of the starlight with exozodiacal or interstellar dust particles. Therefore, this paper recommends that this too is explored as a future avenue of research.

In the case of 2MASS 20042333+4445313, further research should focus on better understanding the delineation between both of the stars present in this binary system. Whilst some data is already available, such as effective temperature, which star this data pertains to in the system is currently unclear, and should be explored readily. Particularly, focus should be given to try and confirm the spectral classes of these binary stars, and calculating their true masses and radii.

In the case of Star 2085565548335557504 (see Section 8.1), further research is recommended to determine the cause of these periodic flux increases. Whilst the flux increase could loosely be determined to be a result of the forward scattering of light due to interactions with dust, or a potential gravitational microlensing event, the periodicity is highly unusual and unlike anything else reviewed within the confines of this paper. Secondary observations of this star are recommended, with a focus on determining if these flux increases are caused by external phenomena, or by an unusual periodic flaring event.

Research Acknowledgments

This research has made use of the NASA/IPAC Infrared Science Archive, which is funded by the National Aeronautics and Space Administration and operated by the California Institute of Technology.

This work has made use of data from the European Space Agency (ESA) mission Gaia (<https://www.cosmos.esa.int/gaia>), processed by the Gaia Data Processing and Analysis Consortium (DPAC, <https://www.cosmos.esa.int/web/gaia/dpac/consortium>). Funding for the DPAC has been provided by national institutions, in particular the institutions participating in the Gaia Multilateral Agreement.

Whilst proper citation is provided throughout, the author would like to extend a personal thanks to Allan Schmitt, for without the LcTools package, none of this research would have been possible.

BIBLIOGRAPHY

Anon (n.d.) *2MASS Interactive Image Service Results* [online]. Available from:

https://irsa.ipac.caltech.edu/cgi-bin/2MASS/IM/nph-im_pos?type=at&ds=asky&date=&scan=&coadd=&band=A&subsz=120&POS=301.097233+44.758720%20EquJ2000 (Accessed 21 April 2024).

Anon (2020) *Color-Shifting Stars: The Radial-Velocity...* | The Planetary Society [online].

Available from:

<https://www.planetary.org/articles/color-shifting-stars-the-radial-velocity-method> (Accessed 21 April 2024).

Anon (n.d.) *ESA - Ariel* [online]. Available from:

https://www.esa.int/Science_Exploration/Space_Science/Ariel (Accessed 21 April 2024).

Anon (n.d.) *ESA - Cheops* [online]. Available from:

https://www.esa.int/Science_Exploration/Space_Science/Cheops (Accessed 21 April 2024).

Anon (n.d.) *ESA - COROT overview* [online]. Available from:

https://www.esa.int/Science_Exploration/Space_Science/COROT_overview (Accessed 21 April 2024).

Anon (n.d.) *ESA - Plato* [online]. Available from:

https://www.esa.int/Science_Exploration/Space_Science/Plato (Accessed 21 April 2024).

Anon (2021) *ESO - Instrument Description* [online]. Available from:

<https://www.eso.org/sci/facilities/paranal/instruments/sphere/inst.html> (Accessed 21 April 2024).

Anon (2015) *Exoplanet Diagrams: The transit method* [online]. Available from:

<https://exoplanet-diagrams.blogspot.com/2015/07/the-transit-method.html> (Accessed 21 April 2024).

Anon (n.d.) *Exoplanet Exploration: Planets Beyond our Solar System* [online]. Available from:

<https://exoplanets.nasa.gov/> (Accessed 21 April 2024).

Anon (n.d.) *Exoplanet-catalog – Exoplanet Exploration: Planets Beyond our Solar System CoRoT-7 b* [online]. Available from:

<https://exoplanets.nasa.gov/exoplanet-catalog/1242/corot-7-b/> (Accessed 21 April 2024).

Anon (n.d.) *Gaia ESA Archive* [online]. Available from: <https://gea.esac.esa.int/archive/> (Accessed 21 April 2024).

Anon (n.d.) *Historic Timeline | Explore – Exoplanet Exploration: Planets Beyond our Solar System* [online]. Available from:

<https://exoplanets.nasa.gov/alien-worlds/historic-timeline/#first-exoplanets-discovered> (Accessed 21 April 2024).

- Anon (n.d.) *IRSA: WISE* [online].** Available from:
https://irsa.ipac.caltech.edu/applications/wise/?__action=layout.showDropDown& (Accessed 21 April 2024).
- Anon (n.d.) *lctools - Kepler Bonus Light Curve Directories* [online].** Available from:
<https://sites.google.com/a/lctools.net/lctools/data-sources/kepler-bonus-light-curve-directories> (Accessed 21 April 2024a).
- Anon (n.d.) *lctools - Kepler Bonus Star List Files* [online].** Available from:
<https://sites.google.com/a/lctools.net/lctools/data-sources/kepler-bonus-star-list-files> (Accessed 21 April 2024).
- Anon (n.d.) *Light Curves, Periods, and Phase* [online].** Available from:
<http://astro.wku.edu/labs/m100/phase.html> (Accessed 21 April 2024).
- Anon (2024) *Mercury: Facts - NASA Science* [online].** Available from:
<https://science.nasa.gov/mercury/facts/> (Accessed 21 April 2024).
- Anon (n.d.) *TESS Mission Overview* [online].** Available from: <https://tess.mit.edu/science/> (Accessed 21 April 2024).
- Anon (2022) *NASA's Webb Takes Its First-Ever Direct Image of Distant World – James Webb Space Telescope* [online].** Available from:
<https://blogs.nasa.gov/webb/2022/09/01/nasas-webb-takes-its-first-ever-direct-image-of-distant-world/> (Accessed 21 April 2024).
- Anon (n.d.) *Open Exoplanet Catalogue - Kepler-75 b* [online].** Available from:
<https://www.openexoplanetcatalogue.com/planet/Kepler-75%20b/> (Accessed 21 April 2024).
- Anon (n.d.) *Other Worlds - Webb/NASA* [online].** Available from:
<https://webb.nasa.gov/content/science/origins.html> (Accessed 21 April 2024).
- Anon (n.d.) *RELATED SOFTWARE | MAST* [online].** Available from:
<https://archive.stsci.edu/missions-and-data/kepler/mission-related-software> (Accessed 21 April 2024).
- Anon (n.d.) *Roman Space Telescope/NASA* [online].** Available from: <https://roman.gsfc.nasa.gov/> (Accessed 21 April 2024).
- Anon (n.d.) *Space-Warping Planets: The Microlensing Method | The Planetary Society* [online].** Available from:
<https://www.planetary.org/articles/space-warping-planets-the-microlensing-method> (Accessed 21 April 2024).
- Anon (n.d.) *The Nancy Grace Roman Space Telescope* [online].** Available from:
<https://www.jpl.nasa.gov/missions/the-nancy-grace-roman-space-telescope> (Accessed 21 April 2024).

Anon (2017) *The Orbit of Pluto. How Long is a Year on Pluto? - Universe Today* [online]. Available from: <https://www.universetoday.com/14344/how-long-is-a-year-on-pluto/> (Accessed 21 April 2024).

Anon (2020) *What Is a Barycenter? | NASA Space Place – NASA Science for Kids* [online]. Available from: <https://spaceplace.nasa.gov/barycenter/en/> (Accessed 21 April 2024).

Anon (n.d.) *What's a transit? – Exoplanet Exploration: Planets Beyond our Solar System* [online]. Available from: <https://exoplanets.nasa.gov/faq/31/whats-a-transit/> (Accessed 21 April 2024).

Anon (n.d.) *Wobbly Stars: The Astrometry Method | The Planetary Society* [online]. Available from: <https://www.planetary.org/articles/wobbly-stars-the-astrometry-method> (Accessed 21 April 2024).

Anon (n.d.) *WorldWide Telescope — Web Client* [online]. Available from: <https://www.worldwidetelescope.org/webclient> (Accessed 21 April 2024).

Anon (n.d.) *NASA Exoplanet Archive* [online] Available from: <https://exoplanetarchive.ipac.caltech.edu/> (Accessed 21 April 2024)

Beaulieu, J. et al. (2006) Juliane Maries Vej 30, 2100 København Ø, Denmark. 10 European Southern Observatory, Casilla 19001. Australia. 13 South African Astronomical Observatory, PO Box. [Online] 1914. [online]. Available from: <http://www.astro.livjm.ac.uk/RoboNet/> (Accessed 21 April 2024).

Bonomo, A. S. et al. (2015) Improved parameters of seven Kepler giant companions characterized with SOPHIE and HARPS-N. *A&A*. [Online] 57585. [online]. Available from: <http://www.aanda.org> (Accessed 21 April 2024).

Borucki, W. J. et al. (2011) CHARACTERISTICS OF KEPLER PLANETARY CANDIDATES BASED ON THE FIRST DATA SET. *The Astrophysical Journal*. [Online] 728 (2), 117. [online]. Available from: <https://iopscience.iop.org/article/10.1088/0004-637X/728/2/117> (Accessed 21 April 2024).

Chauvin, G. et al. (2004) A giant planet candidate near a young brown dwarf Direct VLT/NACO observations using IR wavefront sensing. *A&A*. [Online] 42529–32. [online]. Available from: <http://dx.doi.org/10.1051/0004-6361:200400056> (Accessed 21 April 2024).

Curiel, S. et al. (2022) 3D orbital architecture of a dwarf binary system and its planetary companion. Available from: <https://arxiv.org/pdf/2208.14553.pdf> (Accessed 21 April 2024)

Currie, T. et al. (2023) Direct imaging and astrometric detection of a gas giant planet orbiting an accelerating star. *Science*. [Online] 380 (6641), 198–203. [online]. Available from: <https://www.science.org> (Accessed 21 April 2024).

Fischer, D. A. et al. (2015) Exoplanet Detection Techniques. Available from: <https://arxiv.org/abs/1505.06869> (Accessed 21 April 2024).

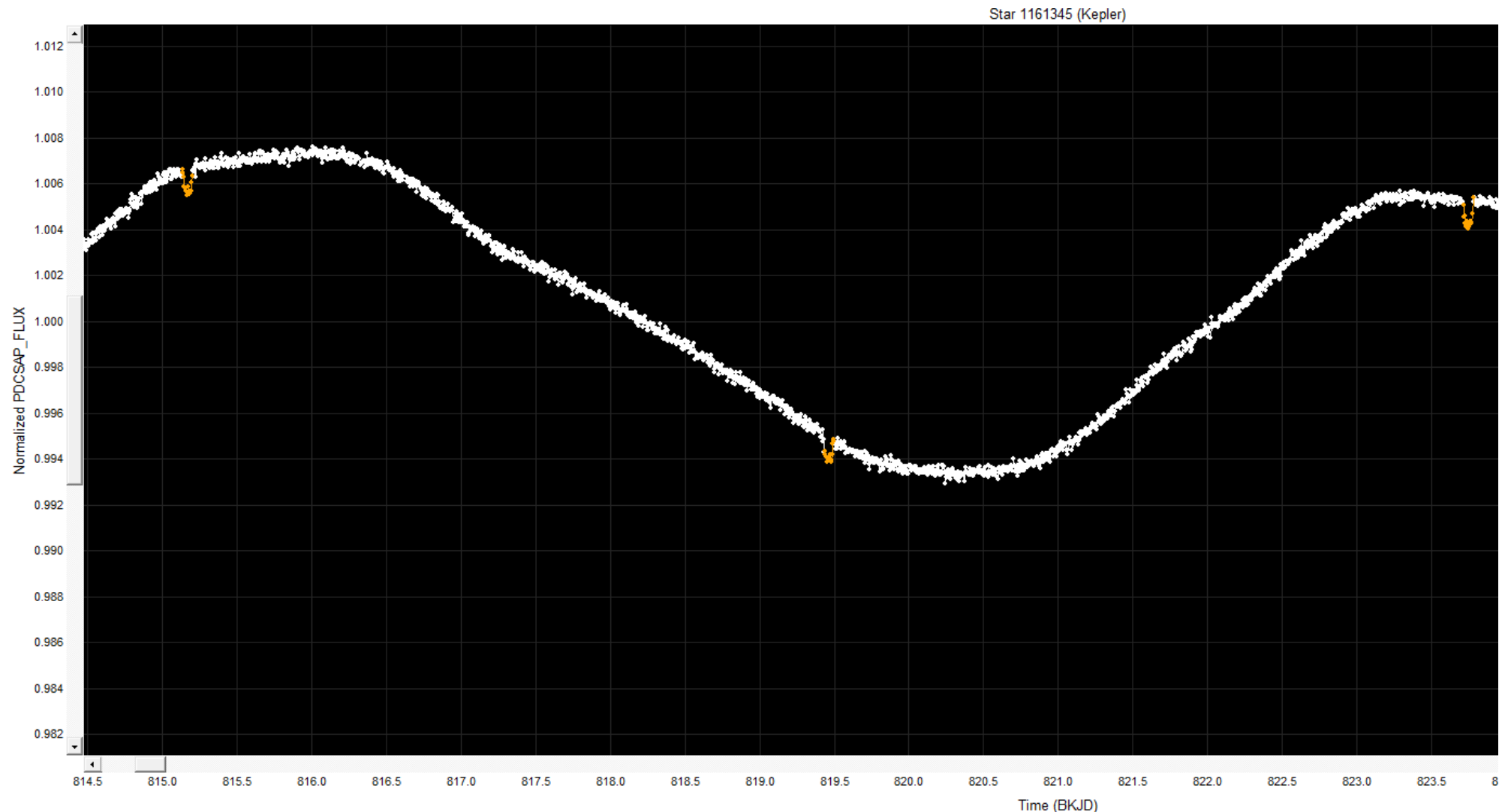
- Gupta, A. & Schlichting, H. E. (2019) Sculpting the valley in the radius distribution of small exoplanets as a by-product of planet formation: the core-powered mass-loss mechanism.**
Owen & Wu. [Online] 48724–33. [online]. Available from:
<https://academic.oup.com/mnras/article/487/1/24/5484904> (Accessed 21 April 2024).
- Haas, M. R. et al. (2010) KEPLER SCIENCE OPERATIONS.** *The Astrophysical Journal Letters.* [Online] 713115–119. [online]. Available from:
<https://iopscience.iop.org/article/10.1088/2041-8205/713/2/L115/pdf> (Accessed 21 April 2024).
- Hébrard, G. et al. (2013) Astrophysics KOI-200 b and KOI-889 b: Two transiting exoplanets detected and characterized with Kepler, SOPHIE, and HARPS-N.** *A&A.* [Online] 554114. [online]. Available from: <https://www.aanda.org/articles/aa/pdf/2013/06/aa21394-13.pdf> (Accessed 21 April 2024).
- Helminiak, K. G. et al. (2019) HIDES spectroscopy of bright detached eclipsing binaries from the Kepler field – III. Spectral analysis, updated parameters and new systems.** *Monthly Notices of the Royal Astronomical Society.* [Online] 484 (1), 451–475. [online]. Available from: <https://dx.doi.org/10.1093/mnras/sty3528> (Accessed 21 April 2024).
- Howell, S. B. et al. (2014) The K2 Mission: Characterization and Early Results.** Available from:
<https://iopscience.iop.org/article/10.1086/676406> (Accessed 21 April 2024).
- Jurgenson, C. et al. (2016) EXPRES: A Next Generation RV Spectrograph in the Search for Earth-like Worlds.** 1203–432. [online]. Available from:
<https://arxiv.org/ftp/arxiv/papers/1606/1606.04413.pdf> (Accessed 21 April 2024).
- Van Kooten, M. A. M. et al. (2020) Periodic brightening of Kepler light curves: investigating the possibility of forward scattering due to dust clouds.** *Monthly Notices of the Royal Astronomical Society.* [Online] 499 (2), 2817–2825. [online]. Available from:
<https://dx.doi.org/10.1093/mnras/staa3048> (Accessed 21 April 2024).
- Léger, A. et al. (2009) Transiting exoplanets from the CoRoT space mission VIII. CoRoT-7b: the first super-Earth with measured radius.** *A&A.* [Online] 506287–302. [online]. Available from: <https://www.aanda.org/articles/aa/pdf/2009/40/aa11933-09.pdf> (Accessed 21 April 2024).
- Leleu, A. et al. (2021) Astronomy Alleviating the transit timing variation bias in transit surveys I. RIVERS: Method and detection of a pair of resonant super-Earths around Kepler-1705.** [online]. Available from: <https://doi.org/10.1051/0004-6361/202141471> (Accessed 21 April 2024).
- Marcy, G. W. et al. (2014) Masses, radii, and orbits of small Kepler planets: The transition from gaseous to rocky planets.** *Astrophysical Journal, Supplement Series.* [Online] 210 (2), 20. [online]. Available from: <https://ui.adsabs.harvard.edu/abs/2014ApJS..210...20M/abstract> (Accessed 21 April 2024).
- Martínez-Palomera, J. et al. (2023) Kepler Bonus: Light Curves of Kepler Background Sources.** *The Astronomical Journal.* [Online] 166 (6), 265. [online]. Available from:
<https://ui.adsabs.harvard.edu/abs/2023AJ....166..265M/abstract> (Accessed 21 April 2024).

- Collaboration, Prusti. et al. (2016) The Gaia Mission.** [Online] 595. [online]. Available from: <https://www.aanda.org/articles/aa/pdf/2016/11/aa29272-16.pdf> (Accessed 21 April 2024).
- Sahlmann, J. et al. (2013) Astronomy Astrophysics Astrometric orbit of a low-mass companion to an ultracool dwarf.** *A&A*. [Online] 556133. [online]. Available from: <http://www.aanda.org> (Accessed 21 April 2024).
- Sahu, K. C. et al. (2008) Transiting planets in the galactic bulge from SWEEPS survey and implications.** *Proceedings of the International Astronomical Union*. [Online] 4 (S253), 45–53. [online]. Available from: https://www.researchgate.net/publication/231841705_Transiting_Plans_in_the_Galactic_Bulge_from_SWEEPS_Survey_and_Implications (Accessed 21 April 2024).
- Schmitt, A. R. & Vanderburg, A. (2021) LcTools II: The QuickFind Method for Finding Signals and Associated TTVs in Light Curves from NASA Space Missions.** [online]. Available from: <https://archive.stsci.edu/hlsp/qlp> (Accessed 21 April 2024).
- Skrutskie, M. F. et al. (2006) The Two Micron All Sky Survey (2MASS).** *AJ*. [Online] 131 (2), 1163–1183. [online]. Available from: <https://ui.adsabs.harvard.edu/abs/2006AJ....131.1163S/abstract> (Accessed 21 April 2024).
- Sozzetti, A. et al. (2023) The GAPS Programme at TNG XLVII. A conundrum resolved: HIP 66074b/Gaia-3b characterised as a massive giant planet on a quasi-face-on and extremely elongated orbit.** *A&A*. [Online] 67715. [online]. Available from: <https://doi.org/10.1051/0004-6361/202347329> (Accessed 21 April 2024).
- Sun, L. et al. (2022) A highly mutually inclined compact warm-Jupiter system KOI-984?** *Monthly Notices of the Royal Astronomical Society*. [Online] 512 (3), 4604–4617. [online]. Available from: <https://ui.adsabs.harvard.edu/abs/2022MNRAS.512.4604S/abstract> (Accessed 21 April 2024).
- Vanderburg, A. & Johnson, J. A. (2014) A TECHNIQUE FOR EXTRACTING HIGHLY PRECISE PHOTOMETRY FOR THE TWO-WHEELED Kepler MISSION.** Available from: <https://arxiv.org/abs/1408.3853> (Accessed 21 April 2024).
- Wheeler, A. & Kipping, D. (2019) The weird detector: flagging periodic, coherent signals of arbitrary shape in time-series photometry.** *Monthly Notices of the Royal Astronomical Society*. [Online] 485 (4), 5498–5510. [online]. Available from: <https://dx.doi.org/10.1093/mnras/stz775> (Accessed 21 April 2024).

Appendix A - Software Viability Confirmation

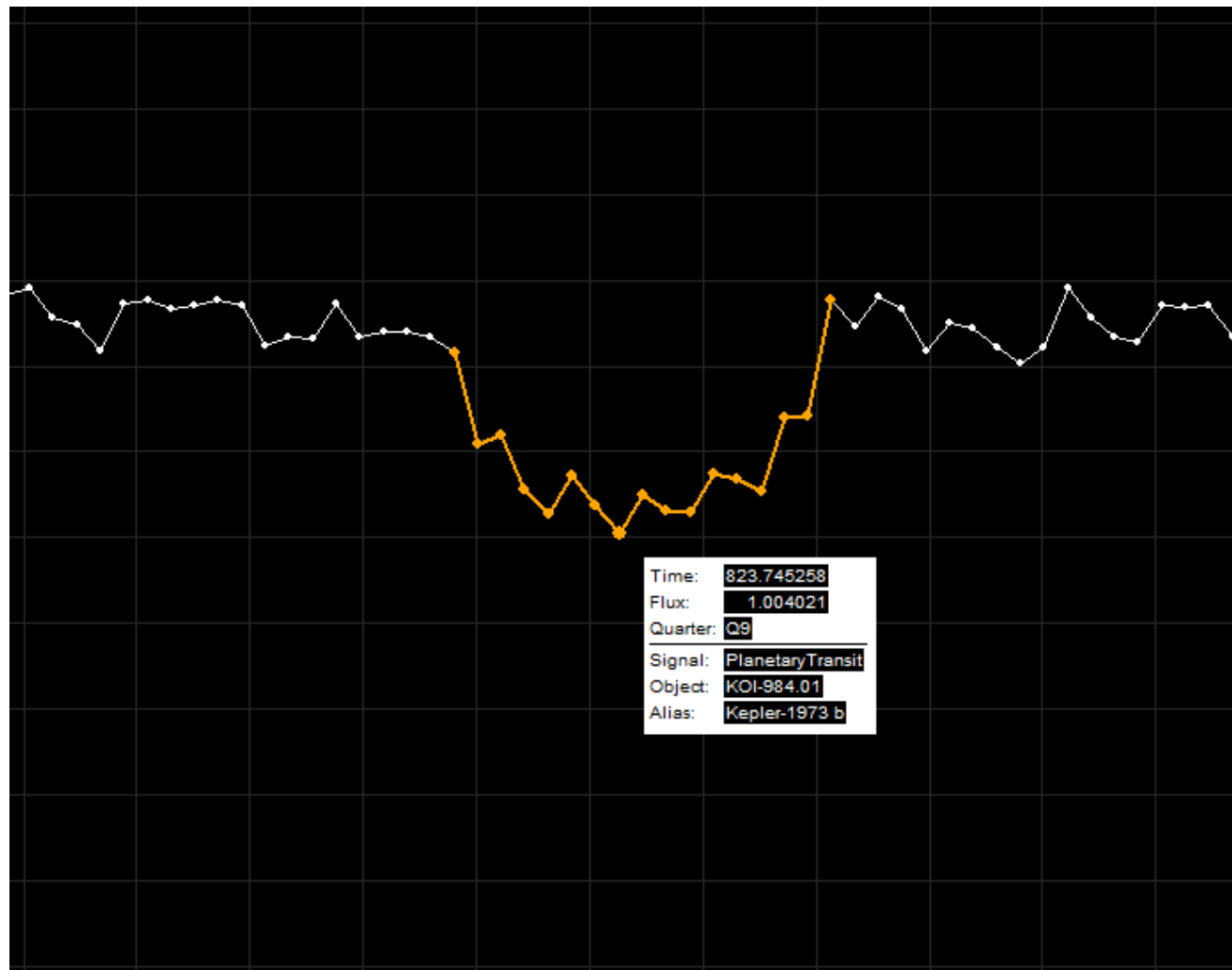
1. Figure A1.

- a. Light curve of known exoplanet Kepler 1973b, used to confirm the viability of LcTools software. Three flux dips are clearly present.



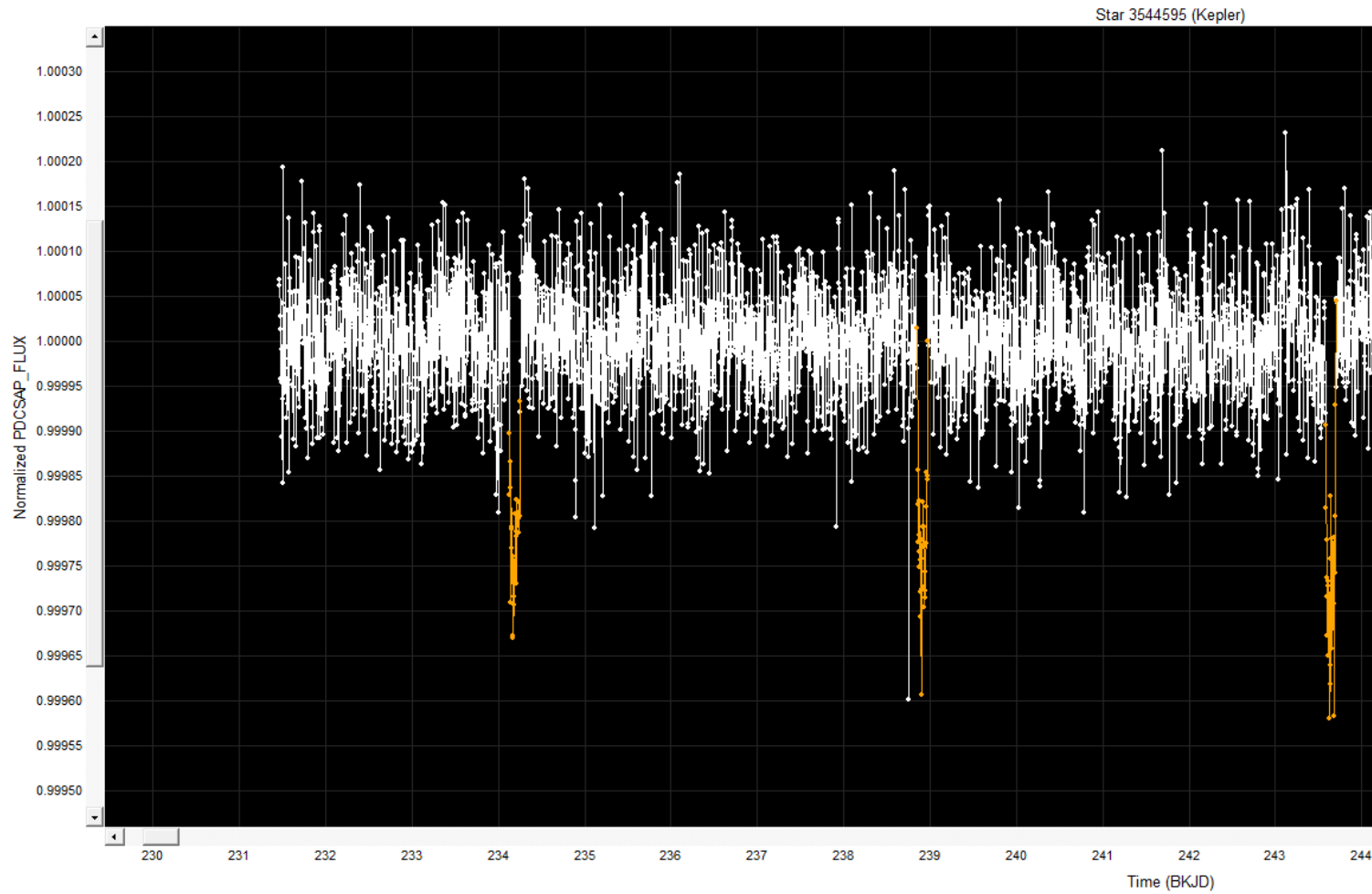
2. Figure A2.

- a. A closer view of one flux decrease from Figure A1 above, caused by known exoplanet Kepler 1973b.



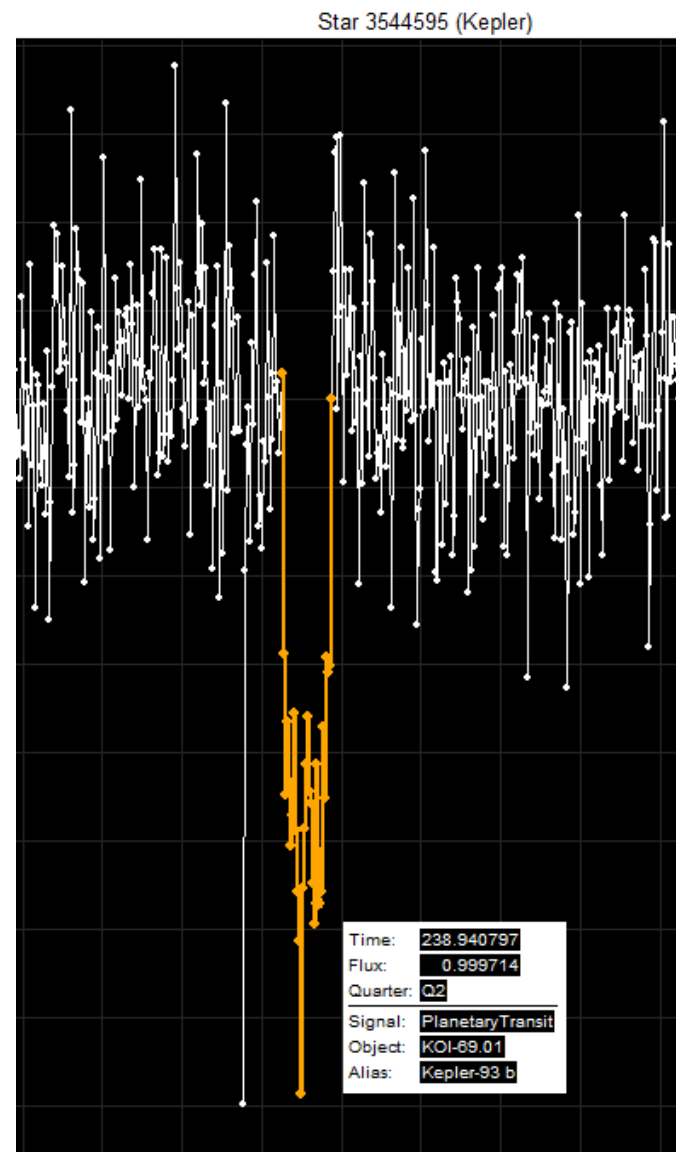
3. Figure A3.

- a. Light curve of known exoplanet Kepler 93b, orbiting Kepler 93, also used to confirm the viability of the LcTools software package. Again, three flux dips are shown.



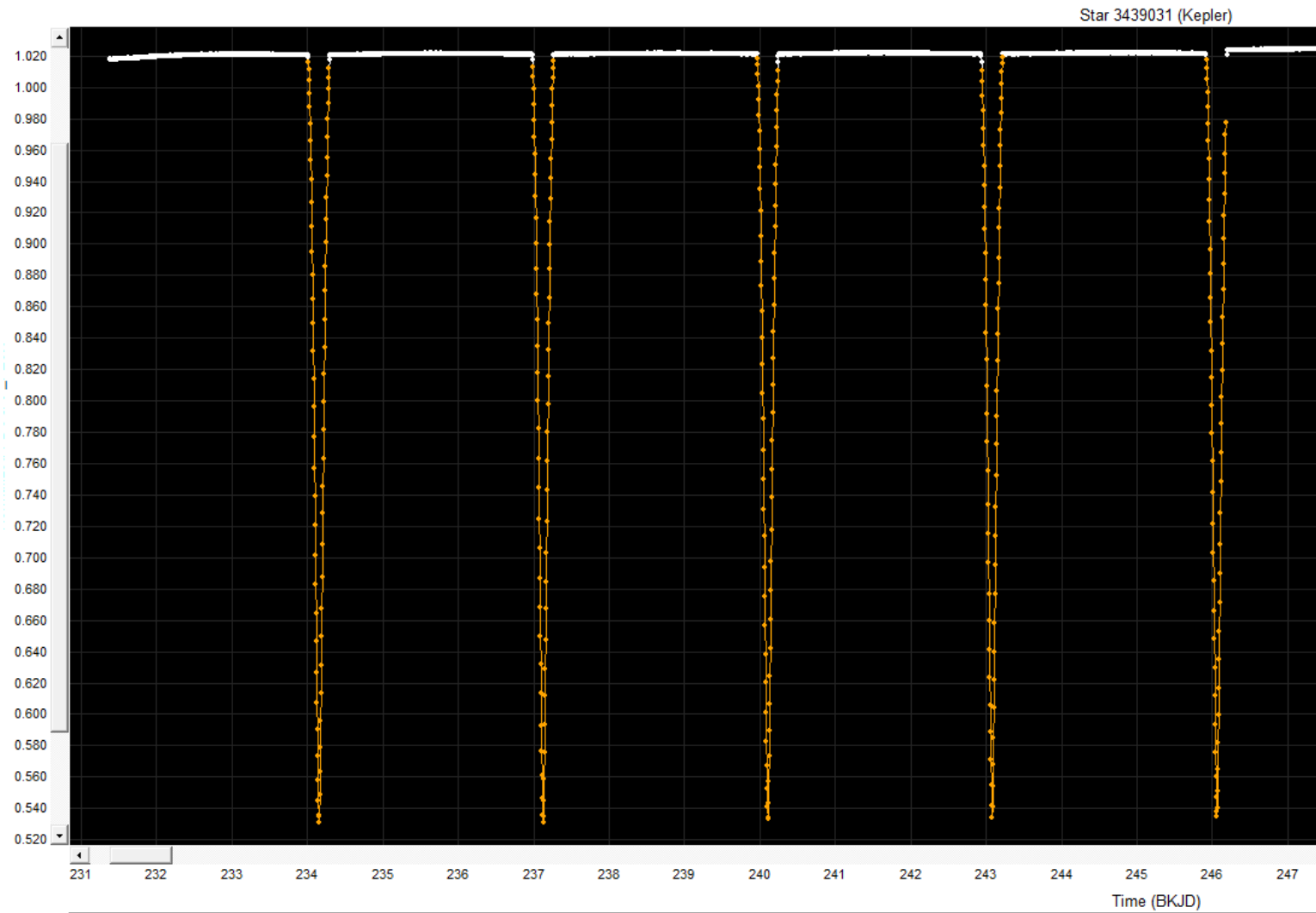
4. Figure A4.

- a. A closer view of one flux decrease from Figure A3 above, caused by known exoplanet Kepler 93b.



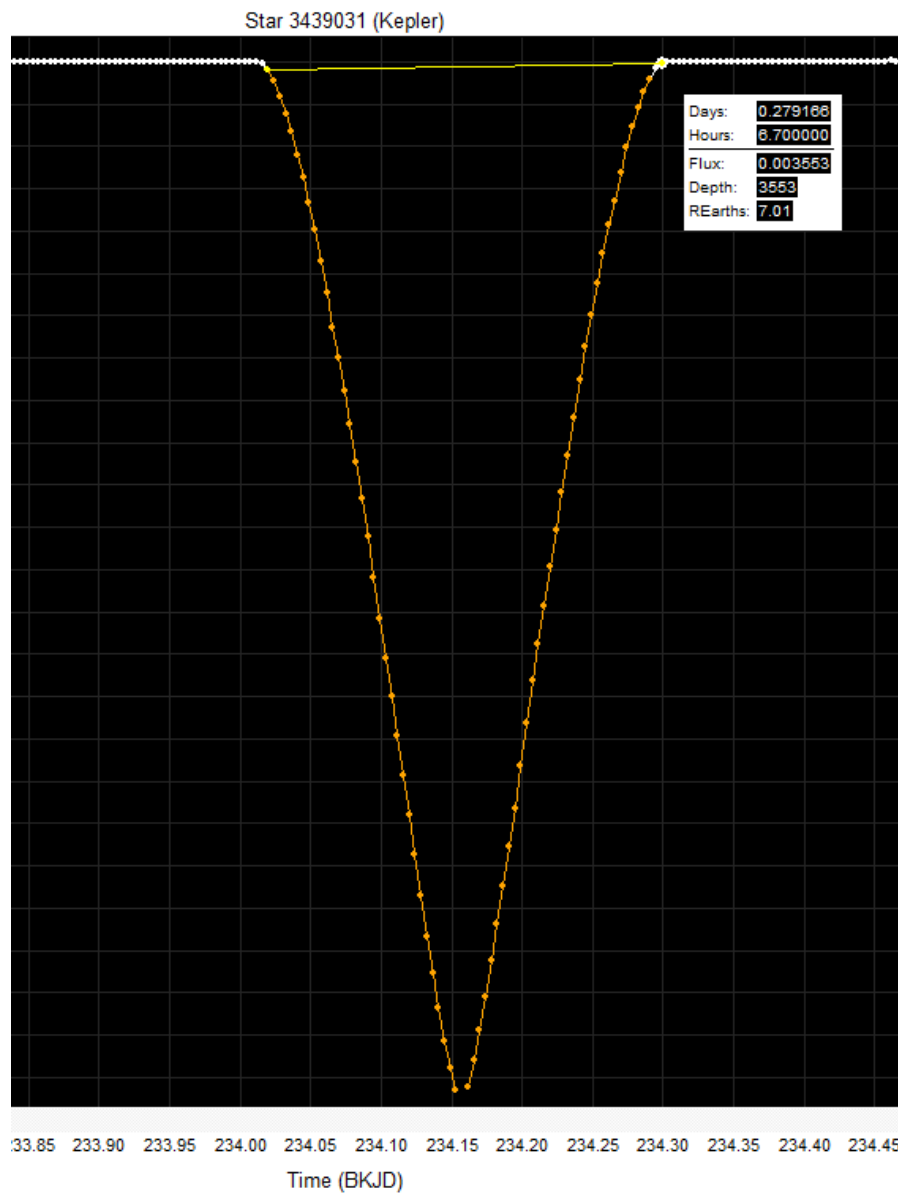
5. Figure A5.

- a. The light curve of KOI 4980, with periodic, near identical flux dips. Further research [Helminiak et al] presents the case that this is actually a binary star system.



6. Figure A6.

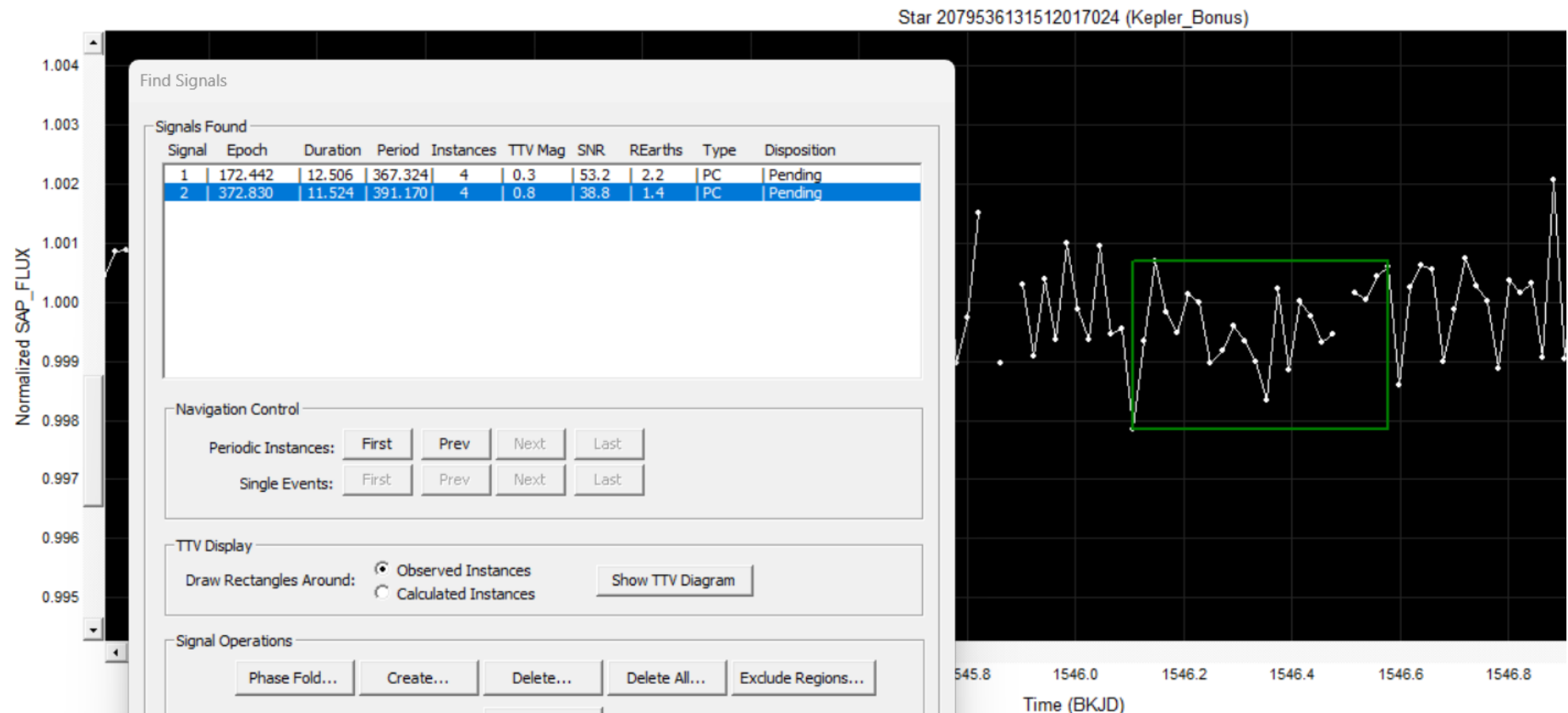
- a. A closer view on one of the flux decreases of KOI 4980.



Appendix B - Example Light Curves

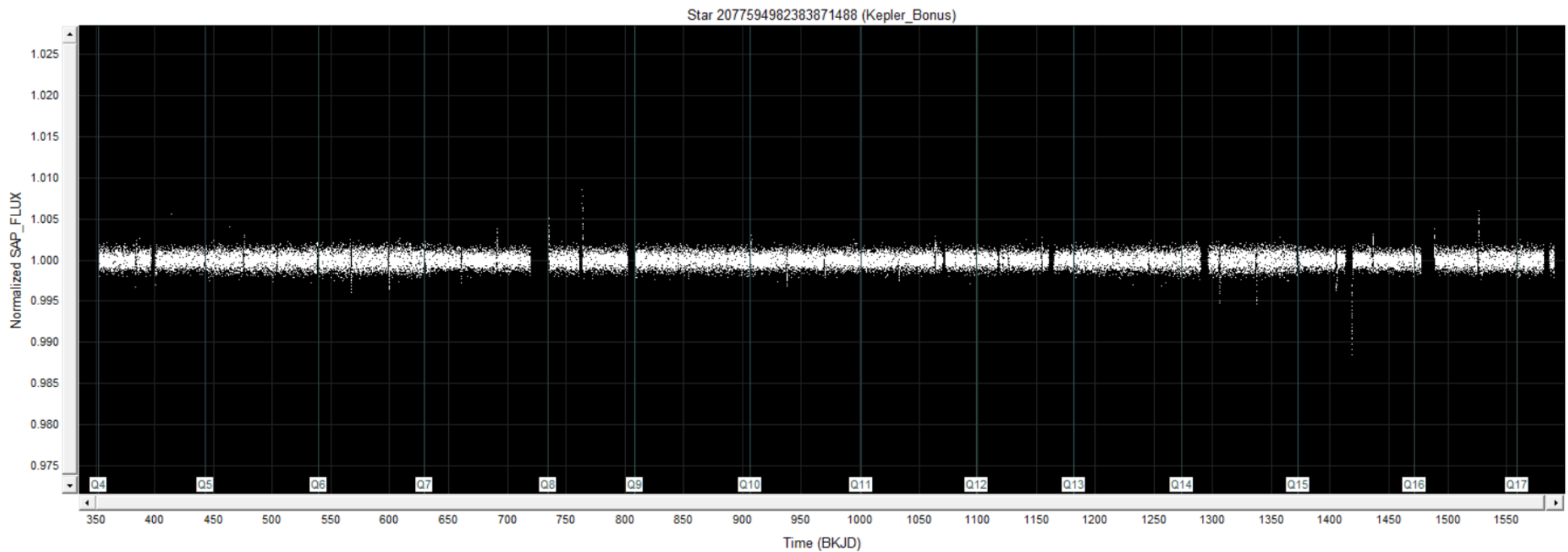
1. Figure B1

- a. An example of a light curve (Star 2079536131512017024) containing only false positives, due to the search parameters selected.



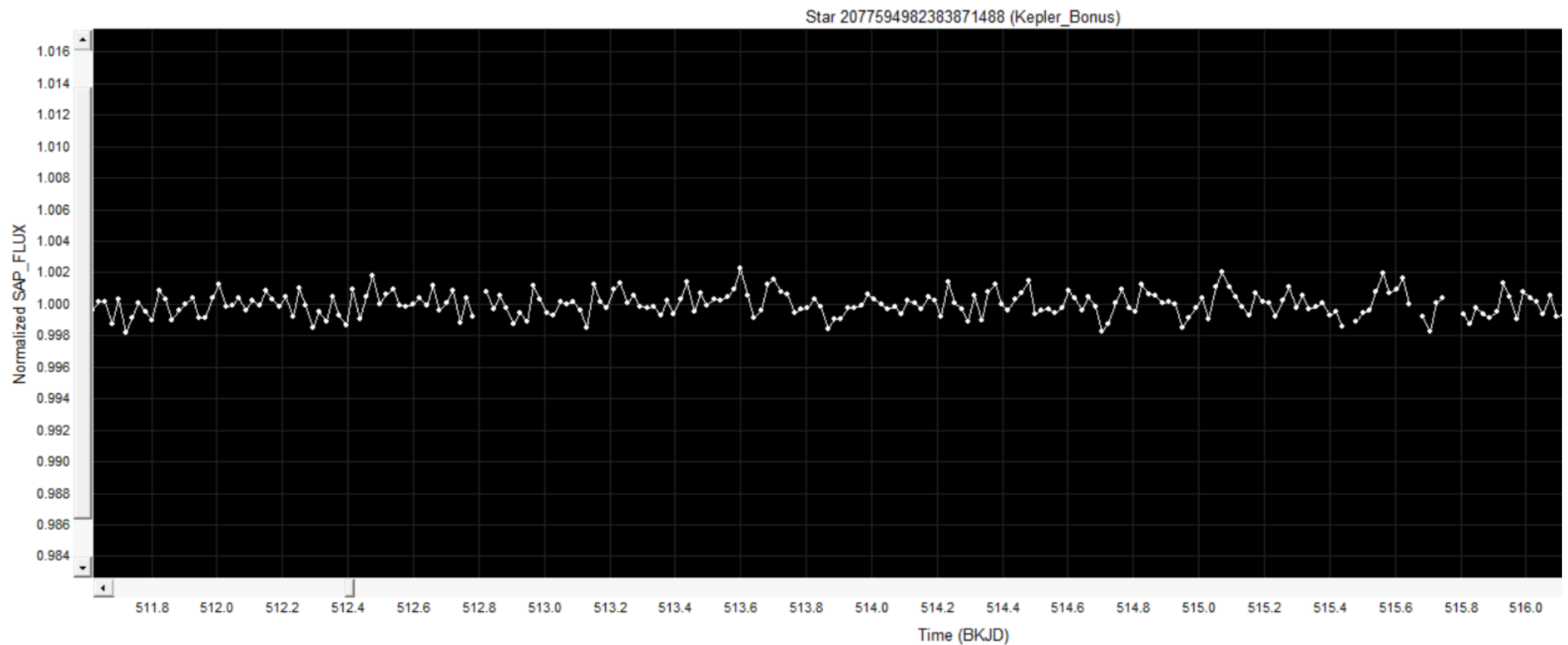
2. Figure B2.

- a. The detrended light curve of Star 2077594982383871488 exhibited typical flux line patterns, and was an excellent example of a star with no exoplanet activity, but also with no interference from either KST movements, or other cosmic phenomena.



3. Figure B3.

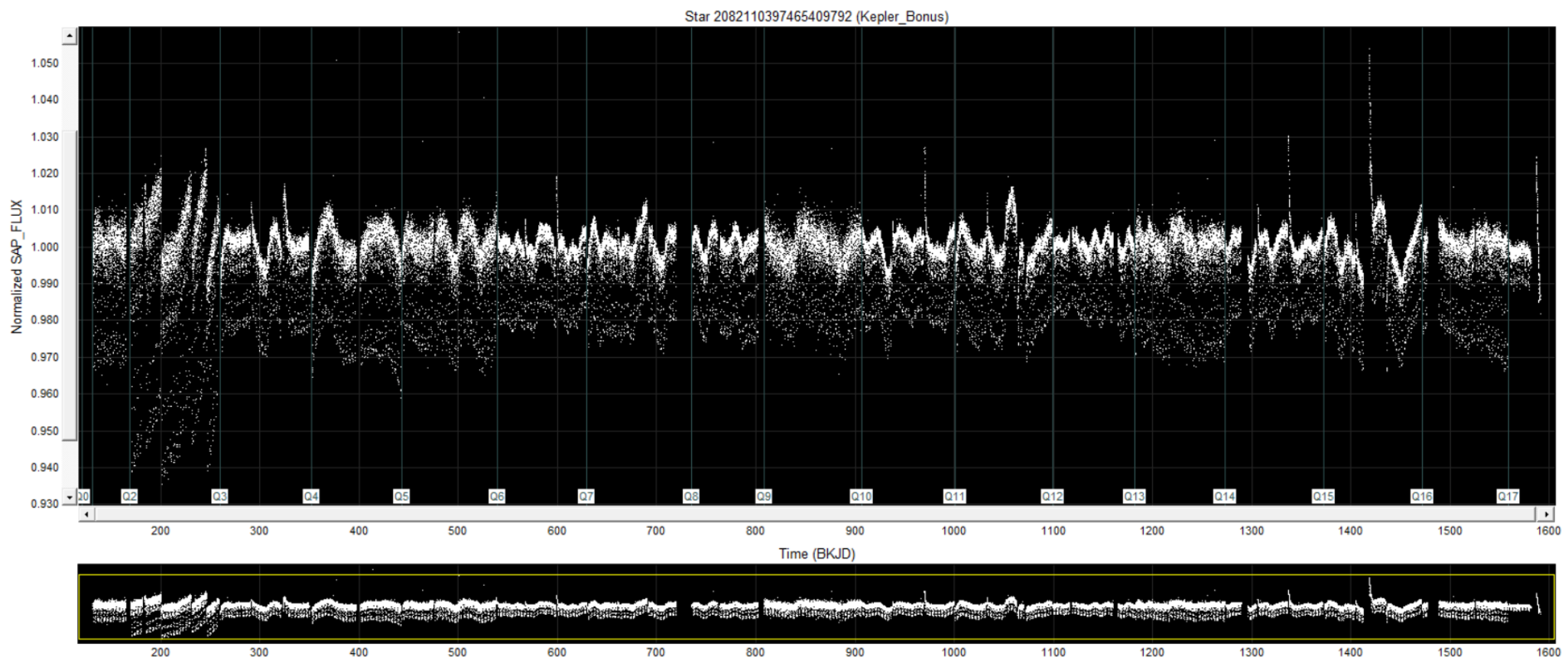
- a. A closer inspection of the light curve of Star 2077594982383871488, showing typical variation in flux.



Appendix C - *Binary Star Light Curves*

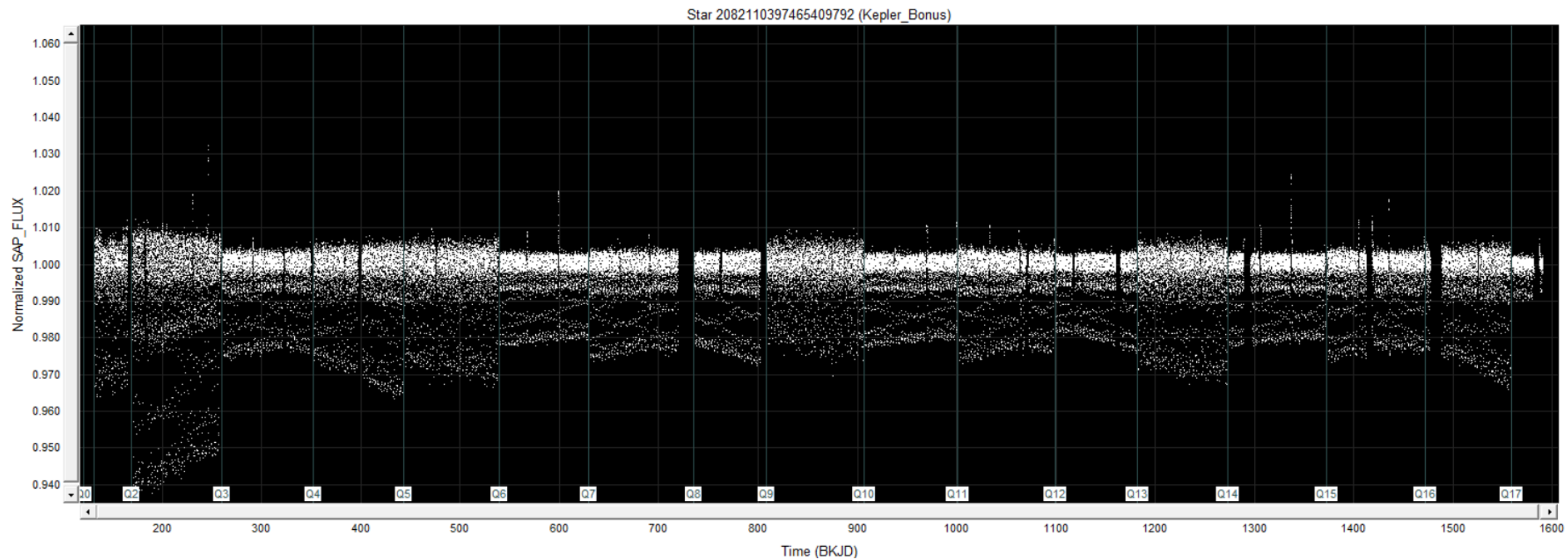
1. Figure C1.

- a. The raw file for Star 2082110397465409792, as seen when loaded into the LcViewer software.



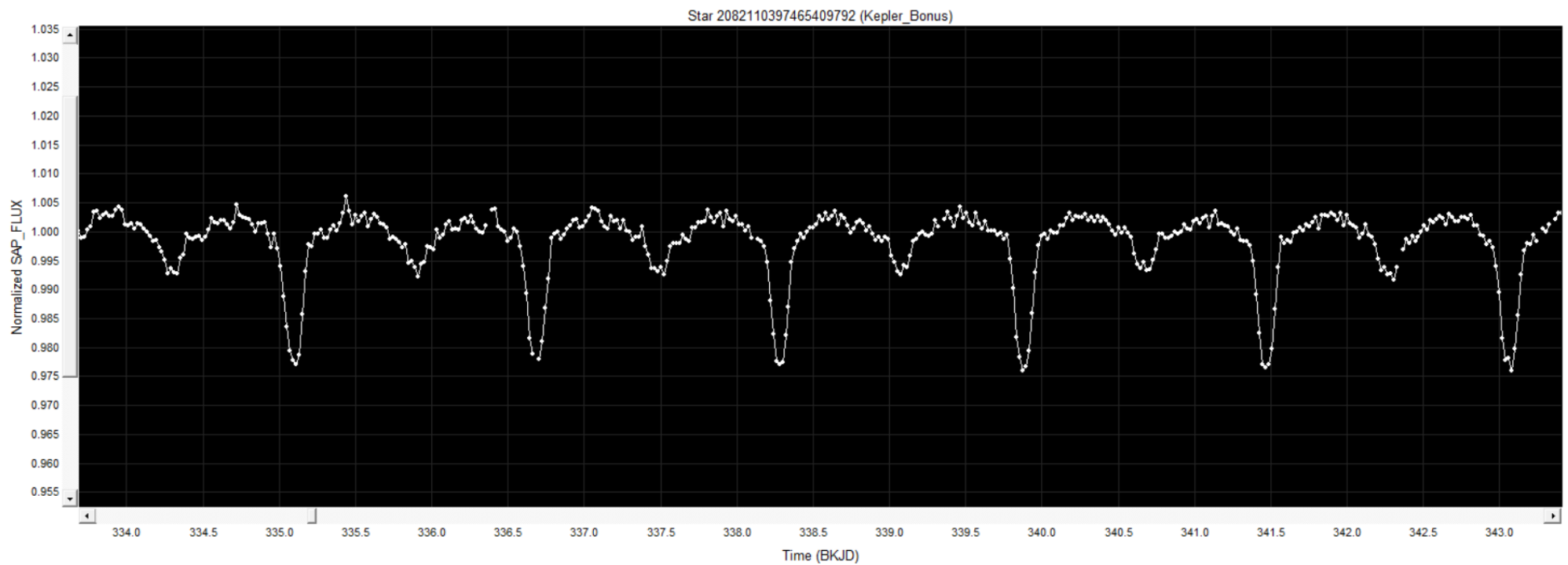
2. Figure C2.

a. The detrended file for Star 2082110397465409792.



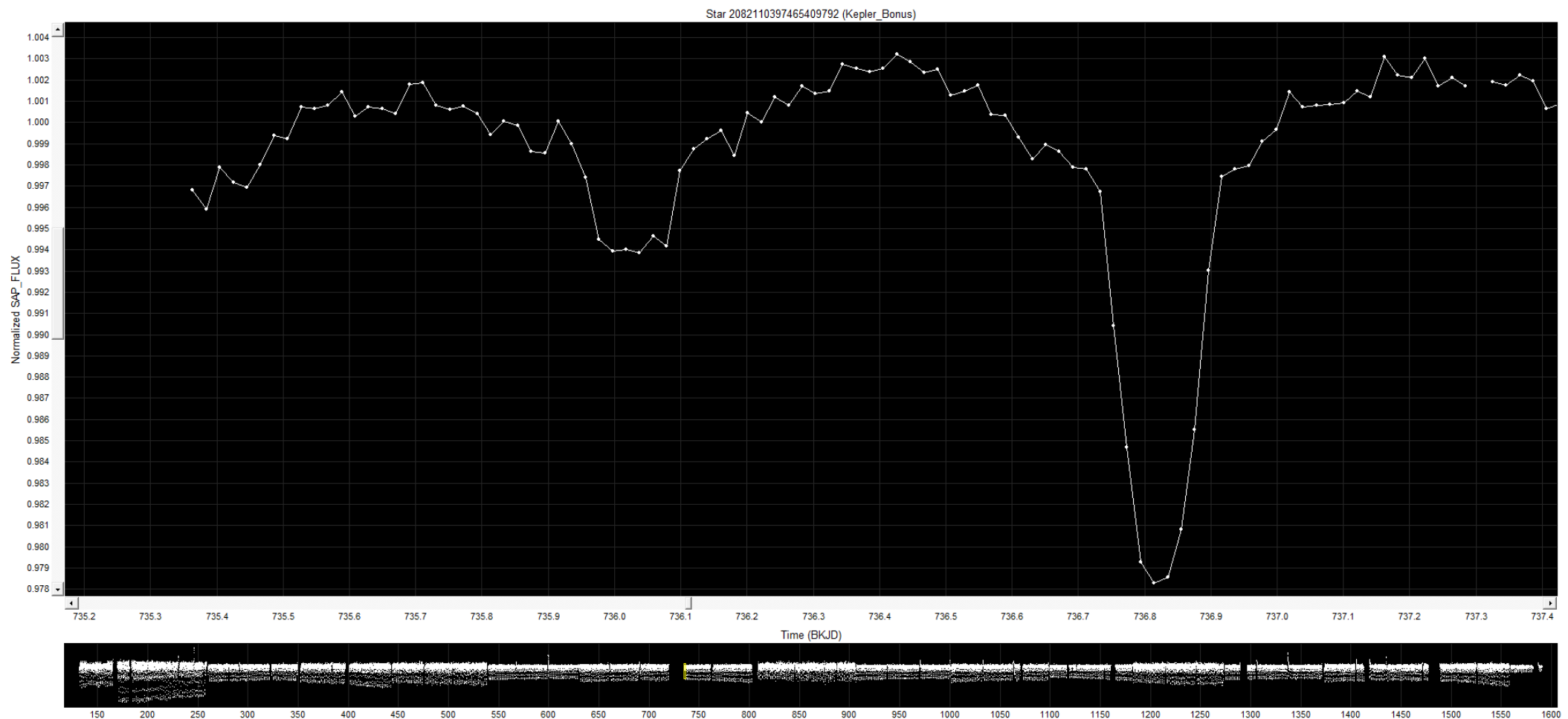
3. Figure C3.

a. Closer inspection of the flux line. There are two clear dimming events present.



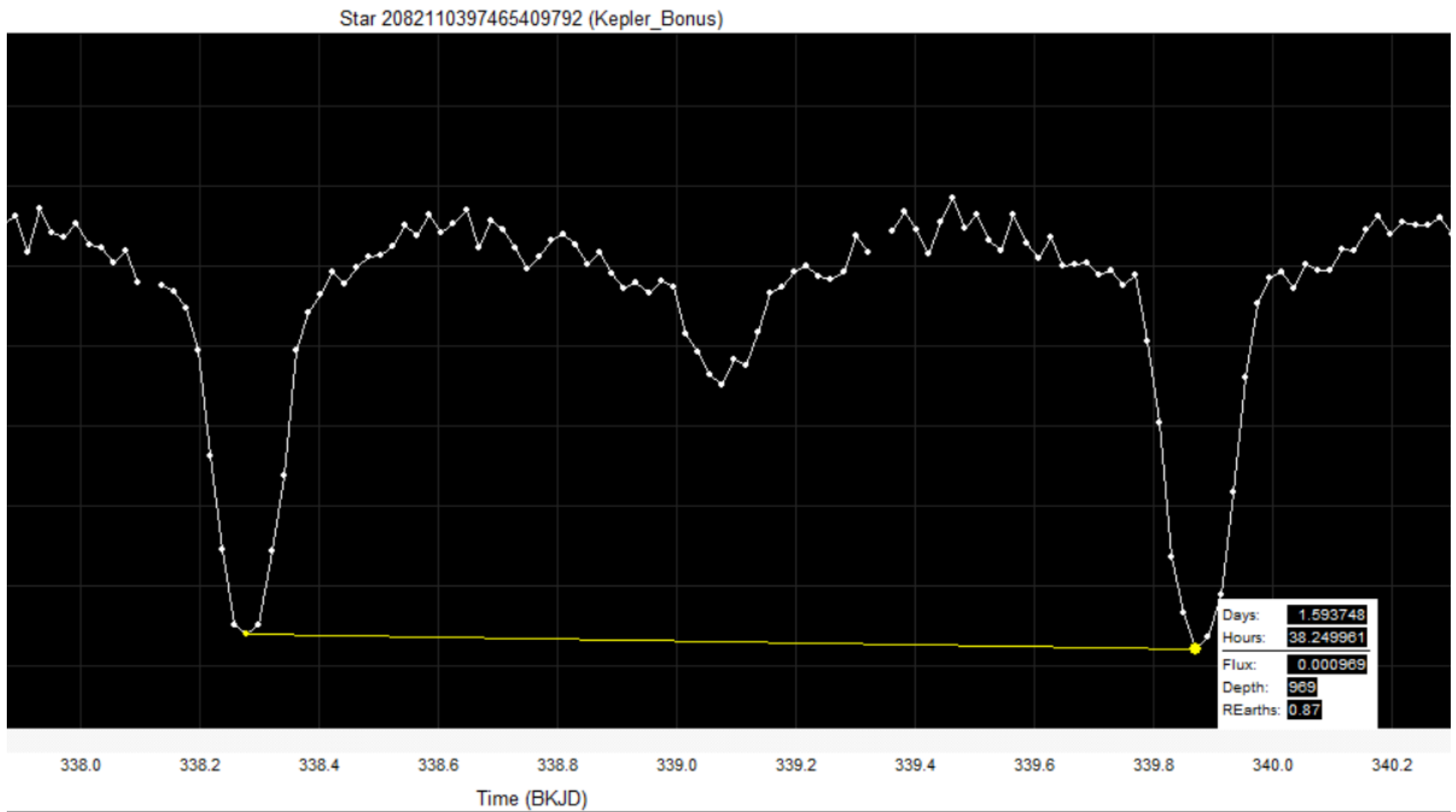
4. Figure C4.

a. A closer view of each flux dip.



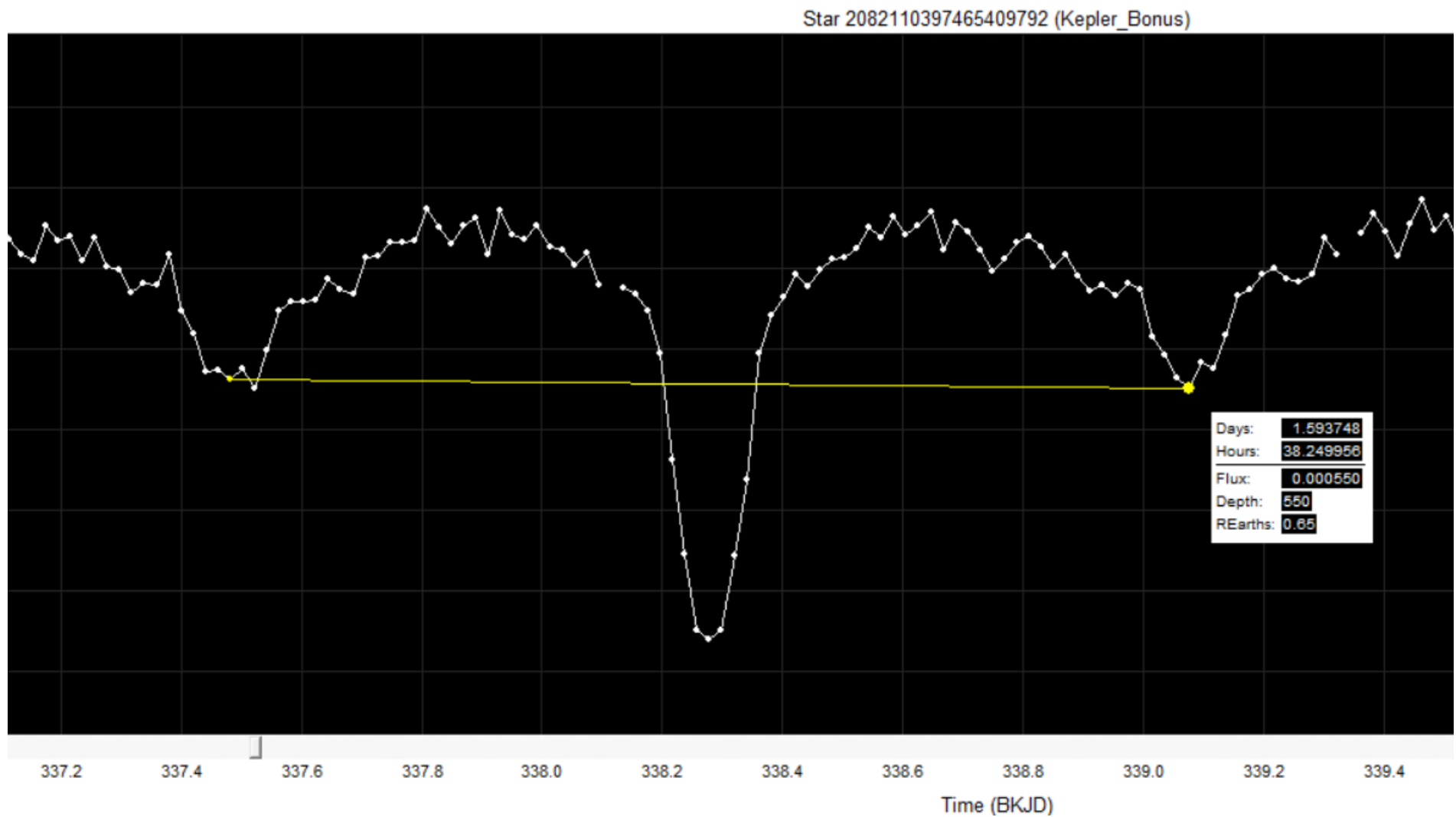
5. Figure C5.

- a. Orbital period measurement of the largest dimming event. Orbital periods are measured at the centrepoint of each dimming event.



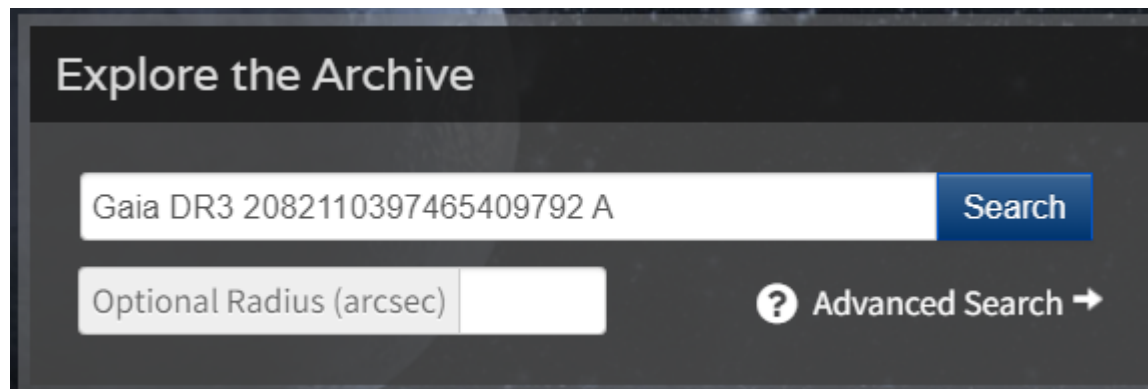
6. Figure C6.

a. Orbital period measurement of the smaller dimming event. Orbital periods are measured at the centrepoint of each dimming event.



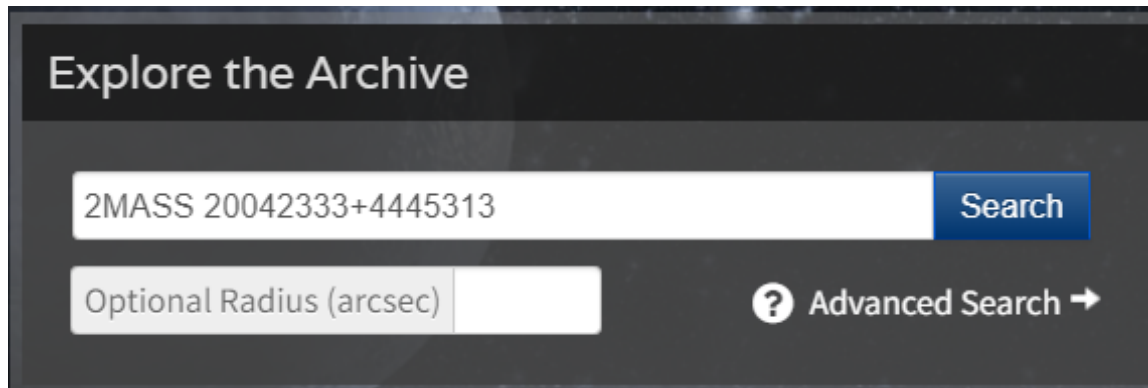
7. [Figure C7.](#)

- a. Exoplanet Archive search with the Gaia DR3 naming convention.



8. [Figure C8.](#)

- a. Exoplanet Archive search with the 2MASS naming convention.



9. Figure C9.

- a. Results of the search terms in both Figures 7 and 8. Whilst the terms are both recognised, no data is currently held on the Exoplanet Archive.

The screenshot shows the homepage of the NASA Exoplanet Archive. At the top, it displays the text "NASA EXOPLANET ARCHIVE" and "NASA EXOPLANET SCIENCE INSTITUTE". Below this is a navigation bar with links for "Home", "About Us", "Data", "Tools", "Support", and "Login". The main content area contains two messages: "The object name you submitted is recognized by the Exoplanet Archive, but we currently do not have any data on it." and "If the planet or star you are querying for is part of a binary or multiple system, the component letter should also be included. Examples include alpha Cen B, 16 Cyg B and GJ 676 A." Below these messages are logos for NASA, ipac, NExSci, and Caltech. At the bottom is another navigation bar with links for "Home", "About Us", "Data", "Tools", and "Support".

10. Figure C10.

- a. Precise positional data of the star.

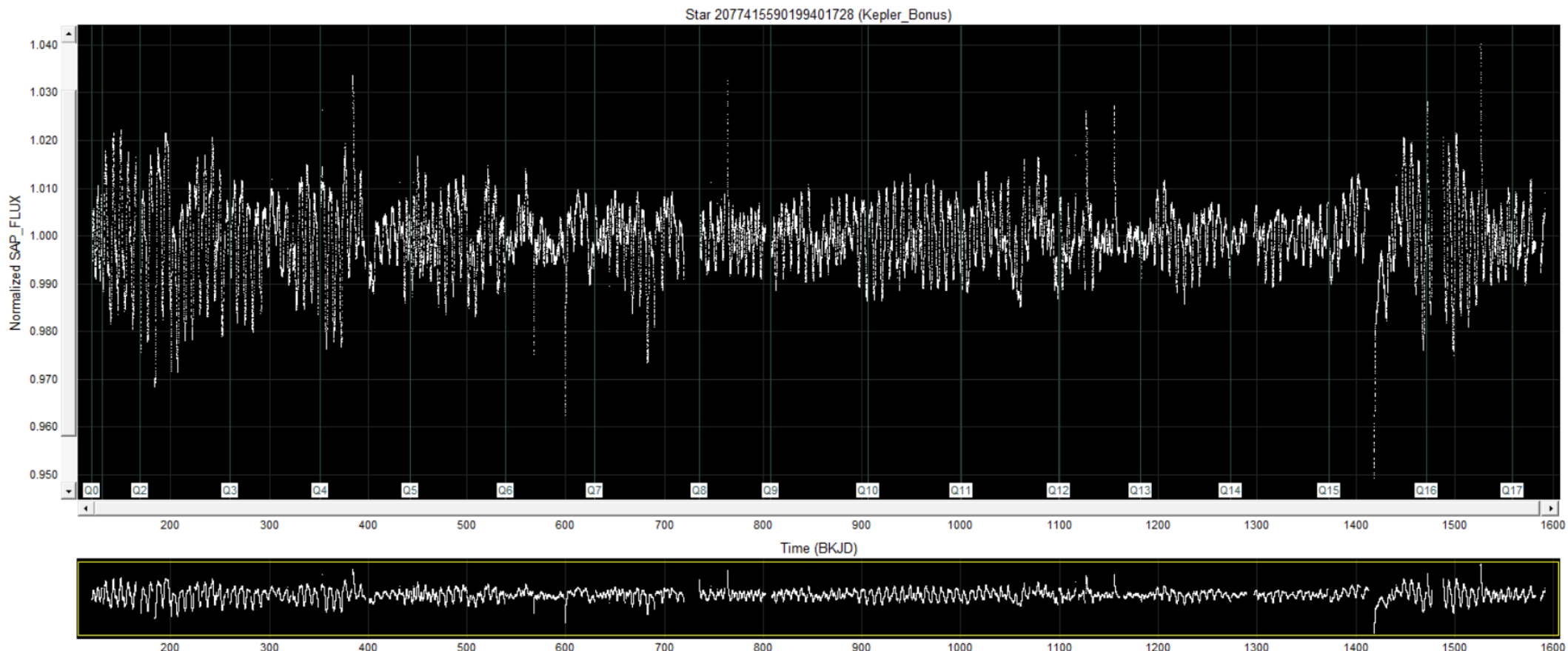
2MASS 20042333+4445313		
20h 04m 23.34s	+44d 45m 31.4s	Equatorial J2000
301.09723	+44.75872	Equatorial J2000 (deg)
20h 02m 46.26s	+44d 36m 56.8s	Equatorial B1950
300.69275	+44.61579	Equatorial B1950 (deg)
80.12004	+7.08207	Galactic (deg)
322.85967	+62.60832	Ecliptic J2000 (deg)

Appendix D - Exoplanet Candidate Figures

I

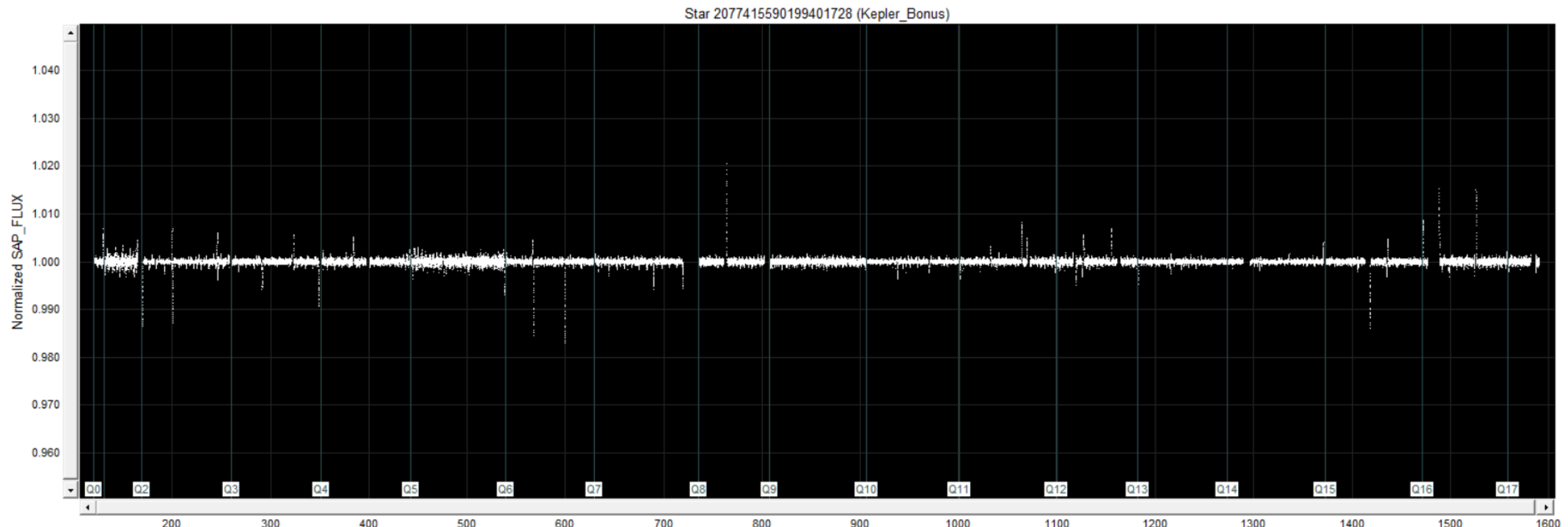
1. Figure D1.

- a. The raw file for Star 2077415590199401728, as seen when loaded into the LcViewer software.



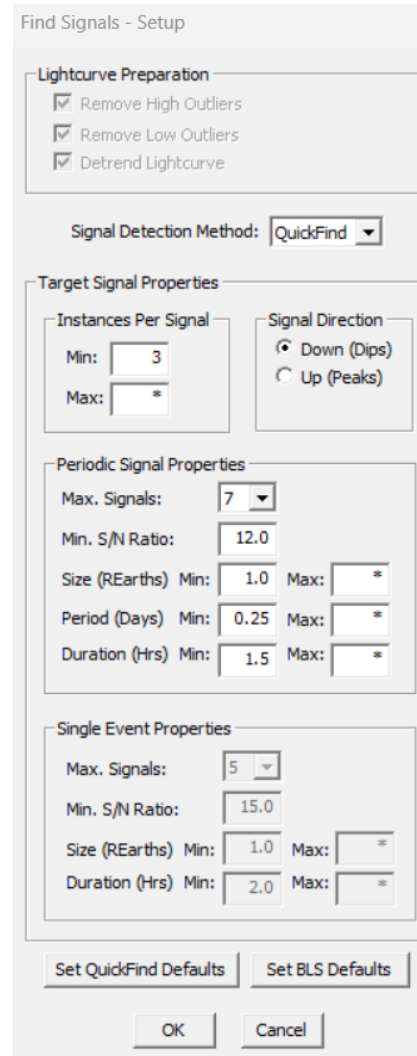
2. **Figure D2.**

- a. Star 2077415590199401728 with its raw file now detrended.



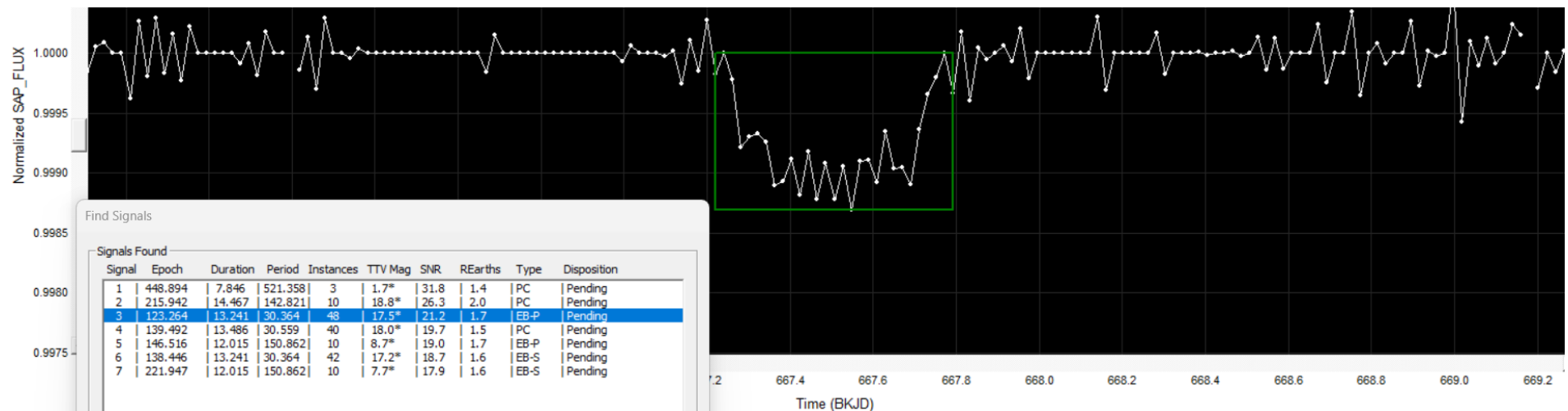
3. **Figure D3.**

a. Signal search parameters



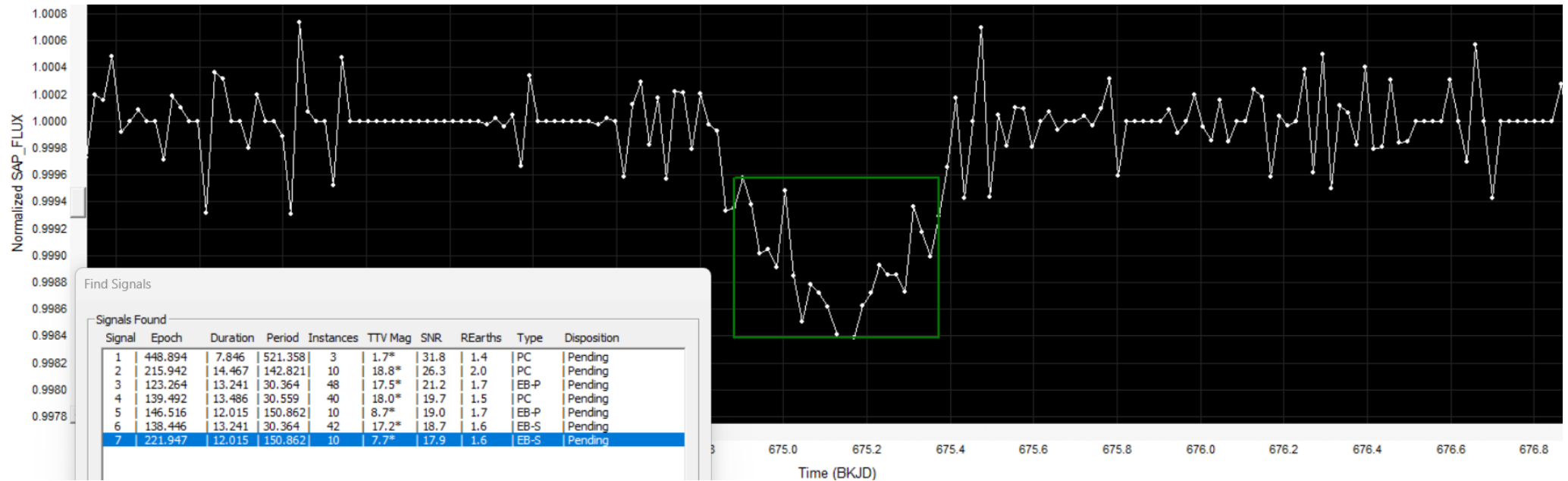
4. **Figure D4.**

a. Manual verification of first transit event



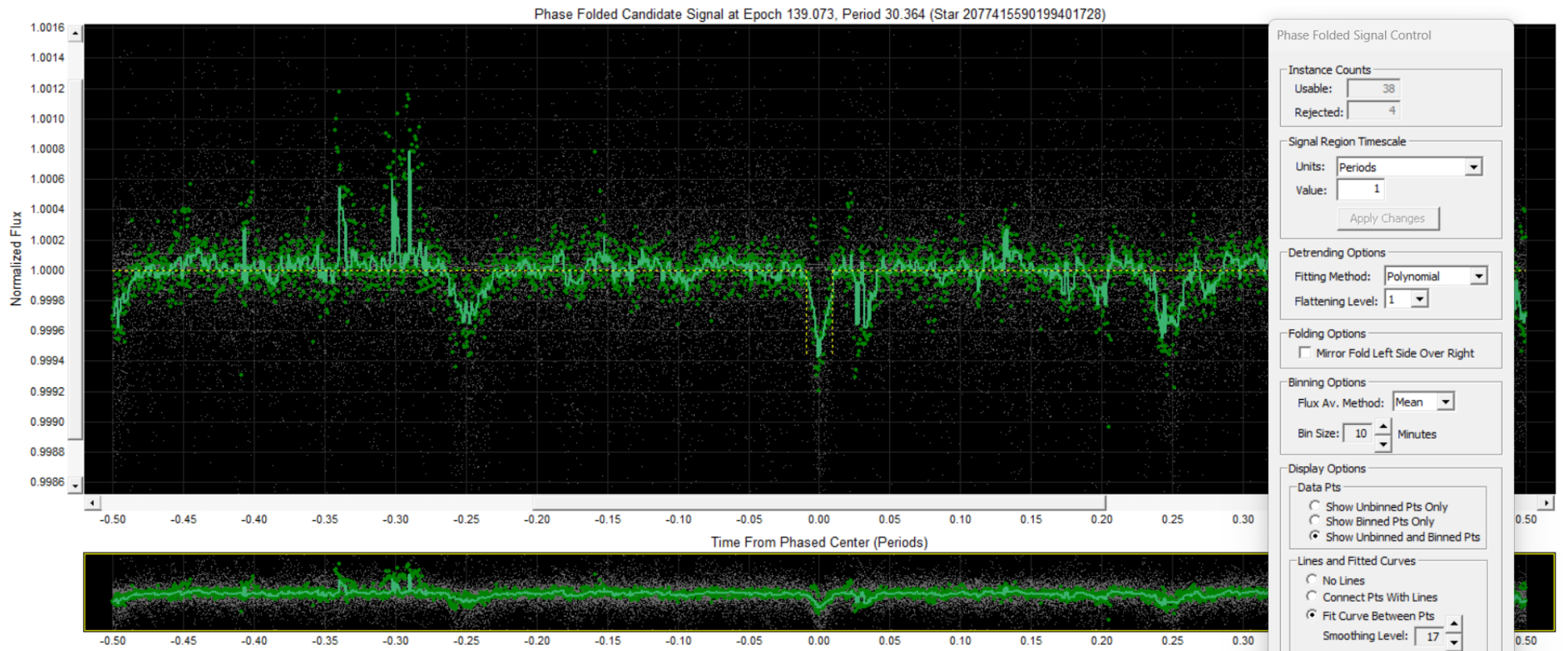
5. **Figure D5.**

a. Manual verification of second transit event



6. Figure D6.

- a. Phase fold diagram which clearly records the dipping events of transiting exoplanets. It also highlights the anomalous flux increases which are present in the light curve.



7. **Figure D7.**

- a. Stellar Data for Star 2077415590199401728.

Stellar Properties

Star ID:	2077415590199401728
Mag:	17.8
Temp:	5246 K
Radius:	0.526 Sols
Mass:	N/A Sols
Distance:	1733.39 Parsecs
RA:	293.722945 Degrees
Dec:	41.498423 Degrees
Metallicity:	N/A

8. Figure D.8.

- a. The location of Star 2077415590199401728 in the Cygnus Constellation, as marked by the grey crosshair.

(‘WorldWide Telescope’, 2024)



Appendix E - Star Files Included in Subsample A

1. Table E.1

a. Star files contained within Subsample A, with the files pertaining to the new binary star system highlighted in blue.

<u>Star ID</u>	<u>Stellar Magnitude</u>	<u>Instances</u>	<u>Object Size (R_{Earths})</u>	<u>TTVs</u>	<u>Significant TTVs</u>
2051747663046115584	18.7	3	1.6	0	0
2052683003834919680	18.8	5	1.7	0	0
2052683003834919680	18.8	4	2.0	0	0
2073555376672401920	18.4	4	1.5	0	0
2073581318288923904	18.7	5	1.8	0	0
2075318061311422208	18.0	4	1.6	0	0
2076220111816774528	17.5	4	1.9	0	0
2077823027971101184	19.0	4	1.5	0	0
2078741154540050432	18.4	4	1.2	0	0
2079087152804910336	18.8	3	2.0	0	0
2079189892721063680	17.8	5	1.4	0	0
2082110397465409792	19.0	4	1.5	0	0
2082110397465409792	19.0	4	2.0	0	0
2085216384674630144	17.5	4	1.6	0	0
2086633517720818816	17.9	4	1.7	0	0
2101097009073808512	17.6	4	1.6	0	0
2101563442520594944	18.6	4	1.7	0	0
2102969992769708032	16.7	4	1.2	0	0

Appendix F - *Star Files Included in Subsample B*

1. Table F.1

a. Star files contained within Subsample B, with the file pertaining to the new exoplanet candidates highlighted in blue.

Star ID	Stellar Magnitude	Instances	Object Size (R_{Earths})	TTVs	Significant TTVs
2050256205581524992	18.9	3	1.7	1	1
2051105376451577600	18.1	4	2.0	1	0
2051293083704793728	18.0	3	1.9	1	1
2051293083704793728	18.0	3	1.8	1	1
2051728799548846720	17.8	3	1.8	1	1
2051747663046115584	18.7	3	1.6	0	0
2051930040237947136	18.5	5	2.0	2	2
2052683003834919680	18.8	5	1.7	0	0
2052683003834919680	18.8	4	2.0	0	0
2052697331846873984	18.8	5	1.8	3	3
2052697331846873984	18.8	4	1.7	1	1
2052704543095371008	18.3	4	2.0	1	0
2052727980741552000	16.9	5	1.7	2	2
2052727980741552000	16.9	4	2.0	1	1
2052727980741552000	16.9	4	1.9	1	1
2052743442620729472	18.6	4	2.0	1	1
2052812157803402496	18.5	3	1.9	1	1
2053556050428114304	18.3	4	2.0	1	1
2073293521104524416	18.8	4	1.6	1	1
2073475696446584704	18.7	3	1.9	1	1
2073482396602579968	17.5	3	2.0	1	1
2073511739798909824	18.4	4	1.5	1	1
2073555376672401920	18.4	4	1.5	0	0
2073555376672401920	18.4	4	1.2	1	1
2073581318288923904	18.7	5	1.8	0	0

2073594065744028416	18.8	4	1.9	1	1
2073597432997975424	18.8	4	2.0	1	1
2073598188912624384	18.6	4	1.4	1	1
2073598188912624384	18.6	4	1.6	1	0
2073739201273151232	18.3	4	1.5	1	1
2073837367054416896	18.9	4	1.3	1	1
2075060573723189376	19.0	4	1.5	1	1
2075060573723189376	19.0	5	1.6	2	2
2075060573723189376	19.0	4	1.7	1	1
2075318061311422208	18.0	4	1.6	0	0
2075438633937085568	18.6	4	1.2	1	1
2076066072811493248	18.8	3	1.9	1	1
2076066072811493248	18.8	4	1.9	1	1
2076104250780691968	18.4	4	2.0	1	1
2076170496362437248	17.6	5	1.9	3	3
2076220111816774528	17.5	4	1.9	0	0
2076392528993229696	18.9	5	1.6	3	3
2076392528993229696	18.9	5	1.4	3	3
2076392528993229696	18.9	3	1.3	1	1
2076392528993229696	18.9	5	1.3	3	3
2076600886431591168	19.0	4	1.9	1	1
2076600886431591168	19.0	4	1.8	1	1
2076610434153982336	18.8	5	1.6	3	3
2076612671824004608	17.5	3	1.9	1	1
2076756398609718016	17.4	4	2.0	2	2
2077219666668373632	18.5	4	1.4	1	1
2077415590199401728	17.8	5	1.9	2	2
2077594982383871488	18.9	3	1.8	1	1
2077764169736569472	18.3	3	1.8	1	1
2077823027971101184	19.0	4	1.5	0	0
2078628175422288256	18.7	5	1.7	3	2
2078741154540050432	18.4	4	1.2	0	0
2078747403718076288	18.4	4	1.8	1	1

2078747403718076288	18.4	4	1.9	1	1
2078762904254878208	18.8	5	1.8	2	0
2078836846406438272	18.9	3	2.0	1	1
2079087152804910336	18.8	3	2.0	0	0
2079189892721063680	17.8	5	1.4	0	0
2079292731415821312	18.4	4	1.7	1	1
2079536131512017024	18.8	3	1.8	1	1
2080267963869371648	17.9	4	1.7	1	1
2081881733405662720	18.6	4	2.0	1	1
2082110397465409792	19.0	4	1.5	0	0
2082110397465409792	19.0	4	2.0	0	0
2082203551022917504	18.0	4	1.5	3	3
2082304736149768960	19.0	4	1.8	2	2
2082304736149768960	19.0	4	1.7	1	1
2085203461116242816	18.1	3	1.7	1	1
2085216384674630144	17.5	4	1.6	0	0
2085232293234235520	19.0	4	1.2	2	1
2085312518923260416	17.6	4	1.5	1	1
2085565548335557504	18.1	4	1.9	1	1
2086086923009582080	16.7	4	1.7	1	1
2086105305469614080	17.8	3	1.8	1	1
2086381454679017216	18.0	4	1.8	2	2
2086562186906662400	18.7	3	1.6	1	1
2086633517720818816	17.9	4	1.9	1	1
2086633517720818816	17.9	4	1.8	2	2
2086633517720818816	17.9	4	1.7	0	0
2086633517720818816	17.9	4	1.7	1	1
2100692487573471872	18.1	4	1.9	1	1
2101097009073808512	17.6	4	1.6	0	0
2101279592425272960	17.8	4	1.2	1	1
2101315055968803584	18.9	4	1.8	1	1
2101335603092609024	18.6	5	1.9	3	3
2101335603092609024	18.6	3	1.9	1	1

2101563442520594944	18.6	4	1.7	0	0
2101576980259559808	16.8	5	1.4	3	3
2102132680304569088	18.0	5	1.7	3	3
2102132680304569088	18.0	3	1.9	1	1
2102132680304569088	18.0	4	1.8	2	2
2102969992769708032	16.7	4	1.2	0	0
2103796791150291456	18.3	4	1.1	1	1
2106781209306988416	17.6	3	1.9	1	1
2125814064823049472	18.4	4	2.0	2	2
2126094818244095872	18.7	3	1.7	1	1
2126135775049237632	18.9	4	1.2	2	2
2126754112907173888	18.3	4	1.3	1	1
2127360734086585344	18.1	5	1.5	3	3
2127403649394847744	17.9	4	2.0	1	1
2127403649394847744	17.9	4	1.6	2	1
2129102287488497024	17.7	4	1.8	1	1
2130037392062267008	18.9	4	1.8	2	2
2130037392062267008	18.9	4	1.7	1	1
2130478742901868032	18.6	4	1.8	1	1
2130478742901868032	18.6	4	1.4	1	1
2135200080194460544	18.0	5	1.6	3	3
2135200080194460544	18.0	4	1.0	1	1
2135239009774644992	18.8	5	1.6	2	0